Roll Damping Prediction of a Free Floating Barge

Mohammad Hajiarab

Thesis submitted for the degree of
Doctor of Philosophy

School of Marine Science and Technology
April 2013

Abstract

Traditionally the problem of calculating the motion responses of a ship in a seaway has been formulated in frequency domain in terms of linear potential theory. By using the potential flow method in roll calculation, the fluid is assumed to be ideal, irrotational and viscous effects are neglected.

Experiments have shown that the roll amplitude responses of rectangular bodies floating in beam waves are overestimated when calculated by potential flow method. This is largely attributable viscous effects [1]. For this reason seakeeping calculation methods introduce empirical factors to account for viscous effects. On the other hand, much of the nonlinear forces and moments experienced by ship in a seaway may be due to the viscous effects leading to flow separation and generation of vortices [2].

One approach to modelling flow separation and vortex shedding is to solve the Navier-Stokes equations. However, for moving bodies in the presence of a free surface at high Reynolds numbers (which implies the use of fine computational meshes) the software and hardware resources required, supposing the problem is even viable, are often so large as to be prohibitive.

Another approach is to use methods based on vortex dynamics for modelling separated flows about bluff bodies. These methods were developed as a means of modelling high Reynolds number flows in which the vorticity is confined to small sub-domains of otherwise irrotational flows [2].

This work concerns development of a purely theoretical model for estimating the roll response of vessels that takes these effects into account. The objective of

this thesis is to develop a model including viscous effects that can be used in seakeeping and survivability calculations.

The idea being proposed is to match a local discrete vortex based method to a global model of a body floating with six degrees of freedom. A software is developed that can be bolted on to conventional seakeeping software so that the motions of sharp edged bodies floating in waves can be calculated without recourse to empirical methods.

The theoretical approach to predict roll damping for a three-dimensional barge shaped floating vessel in the frequency domain is described here. The approach consists of matching a simple discrete vortex method (DVM) describing local separated flow, to an inviscid three-dimensional seakeeping code. Model tests have been carried out to validate the theoretical model and the associated add-on software.

As demonstrated in this report, there is a good agreement between the model test RAO and the damped RAO indicating the theoretical method provides a good estimate of the viscous damping of the vessel due to vortex shedding from its edges.

Although viscous damping in sway and heave motions is not as significant as for the roll for a barge the same methodology can be used to calculate viscous damping for both sway and heave as well.

As tangential relative fluid velocities are used in this method the same final relative velocities can be used to calculate skin friction damping component. In this study skin friction damping is considered to be negligible and is ignored in the final calculated damped RAO.

Acknowledgments

I would like to express my profound gratitude to my supervisor Professor Martin J. Downie from Newcastle University and my advisor Professor J. Michael R. Graham from Imperial College London for their guidance and support throughout this project. Also I would like to express my appreciation of Dr. Peter Wright for acting as my second supervisor.

I would also like to thank my colleagues from Lloyd's Register Group namely Dr. Graham Stewart, Mr. Richard Bamford, Dr. Frank Lin, Dr. Kourosh Parsa, Dr. Karl Mitchell, Dr. Chris Cooper, Dr. Piotr Krawczyk and others for their technical support and encouragement of my work.

Lastly, I would like to offer my best regards to my family and friends for their everlasting support specially my wife Yasaman for her patience with me during these years, my brother Masih for his professional software development assistance in this work and my friend Captain Hossein Enshaei for sharing the same enthusiasm in research work.

Keywords

Roll damping

Viscous effects

Discrete Vortex Method

Floating body

Flow separation

Abbreviations

$\dot{a}$	Angular velocity
$\hat{a}$	Angular velocity amplitude
a_4	Vortex induced added mass coefficient
b	Breadth of the barge
b_4	Vortex induced damping coefficient
c_4	Coefficient representing the lever arm of the vortex roll moment
g	Gravity
h	Draught of the barge
k_j	Wave number
q	Total relative fluid velocity at the shedding edge calculated for the combined six degree of freedom motion
$q(s)$	Source density
q_j	Total relative velocity at the shedding edge calculated in the forced roll motion mode
s	Distance from edge to centre of the facet in which the velocity is calculated
x	Width of the facet along the length
A_j	Wave amplitude
A_{jk}	Added mass matrix component in mode j due to motion in mode k
$(A + iB)$	Vortex force coefficient calculated with the Discrete Vortex Method for an infinite right angle edge, which is equal to 1.566-i0.157

AR	Aspect ratio of the barge cross section
C_D	Drag coefficient
C_m	Inertia coefficient
C_{Fv}	Vortex force coefficient
C_{jk}	Restoring matrix component in mode j due to motion in mode k
F_j	Complex amplitude of exciting force in mode j with the force/moment components given by the real part of $F_j e^{-i\omega t}$
F_v	Vortex force component
F_{v2}	Sway vortex force
F_{v3}	Heave vortex force
F_{v4}	Vortex shedding roll moment
H	Wave height
K_c	Keulegan-Carpenter number
L	Length scale
M_{jk}	Generalized mass matrix component in mode j due to motion in mode k
P_a	Atmospheric pressure
Q	Strength of a source in potential theory
$S(\omega_j)$	Wave spectrum value at the j-th circular frequency
T	Period of oscillation
U	Free stream velocity with amplitude U_0
χ	Damping torque
ε_j	Phase angle of the j-th wave component of the irregular wave
θ	Wave propagation angle of the wave
η_k	Motion in mode k
$\dot{\eta}_k$	Velocity in mode k

$\ddot{\eta}_k$	Acceleration in mode k
μ	Schwartz-Christoffel ratio
ρ	Fluid field density
ϕ	Velocity potential
ϕ_I	Incident wave potential
ϕ_D	Diffracted wave potential
ϕ_R	Radiated wave potential
ϕ_v	Velocity potential at the vertical side of the shedding edge
ϕ_h	Velocity potential at horizontal side of the shedding edge
ω	Wave excitation frequency
ω_j	Wave frequency
$\Delta\zeta^*$	Distance between points in the ζ plane on either side of the edge
$\Psi(t)$	Dimensionless vortex force coefficient

List of Figures

List of Tables

Table of Contents

1 Introduction

Roll motion is oscillatory motion of a vessel along its longitudinal axis. Extreme roll motions compromise the stability of a floating body. It affects structural integrity, crew comfort, machinery operations and ultimately the safety of a vessel. If the roll motion can be predicted the vessel can be designed to cope with the imposed dynamic motions in response to the environmental loads. While underestimation of roll motion can potentially cause disasters, its overestimation results in a commercially unviable design that leads to increase of the steel weight and limits operability of the floating body. Hence accurate estimation of the roll motion is of great importance.

For a vessel rolling due to a single excitation force in calm water the kinematic energy is dissipated until the vessel converges to a stationary state. The dissipation of the cinematic energy is known as damping. Rolling of a vessel in seas is formulated by the mass spring damper equation. The best known method for predicting the roll motion is to include an equivalent linear viscous roll damping coefficient in the motion equation. Accurate estimation of damping directly affects the outcome of this equation.

Roll damping is estimated by model tests and mathematical approaches. Model tests provide a baseline estimation of the roll damping. However, they are expensive, complex and not always feasible. Mathematical approaches provide a reasonable estimation of roll damping at fraction of cost and implementation complexities. Further, mathematical approaches are

particularly useful where model tests are practically impossible such as ad-hoc operational assessment of already existing vessels.

One of mathematical methods makes use of the discrete vortex method which is a technique for analysing two-dimensional separated flows in the time domain. Graham [3] implemented a simple discrete vortex analysis for flow about an infinite wedge in oscillatory flows in which the flow in an infinite half-plane, the ζ-plane, was transformed to flow about an isolated edge. The method enabled him to calculate a generalised vortex force on the infinite wedge from which he inferred the total force on a finite body with flow separation from its edges. The approach was further developed by Downie et al. [4], [5].

In this work the same technique is used to model separated flow from a barge shaped vessel to provide input to an inviscid three dimensional seakeeping program. The roll RAO is then calculated in frequency domain including vortex shedding.

The roll RAOs predicted by this approach are compared with model test results to assess their validity. The comparison shows a good agreement between the model tests and theoretical calculations [6], [7].

1.1. Problem Statement

Accurate estimate of the roll damping especially for floating offshore installations at a fixed location such as FPSOs is becoming more and more important. Roll motion has direct effect on design of topside foundation, risers and their connection to the floating system, turret structure and bearings, efficiency of process equipment, comfort of crew on board, operations such as helicopter landing, loading and unloading of supplies, oil offloading and sloshing in cargo tanks.

Growing price of oil has made it economically desirable to keep the production plant of the FPSOs functional as long as possible. Accurate estimate

of the motions of a floating production system increases the reliability of the topside process machinery and results in more accurate economical estimation of the production. Further, hull structural cracks usually occur due to lack of adequate strength and fatigue capacity of the structural details. Repair of the cracks on station can have a significant effect on the up-time of the floating production facility. Accurate estimate of loads and motions is a key factor to better design of the structure.

Noting the desire in the oil and gas industries to explore deeper seas and in the same time noting the importance of safety and reliability of the structure of the floating systems, accurate estimate of the motions and accelerations of the vessel becomes vital in structural and process machinery design of floating systems.

1.2. Research Objectives

This work aims to provide a procedure to calculate the viscous roll damping of a floating body in waves. This purely mathematical procedure is developed based on [5]. Model test comparisons are conducted to validate results of the procedure.

The method involves calculating potential gradients of the fluid around the floating body in a diffraction-radiation hydrodynamic software and using them as an input to the above referenced methodology to calculate the viscous damping component. Then the viscous damping component is inputted back to the equation of motion to recalculate RAOs of the vessel accounting for viscosity.

The procedure is developed for a simple boxed shape vessel (rectangular bilge) however, it can be developed for general curved ship shaped vessels with rounded bilge.

The viscous roll damping procedure is coded as a black box with potential to be used with any diffraction-radiation hydrodynamic software available as an add-on.

1.3. Main Contributions of the Work

The procedure presented here allows designers to estimate in particular roll and potentially sway and heave motions of a floating body more accurately in early stages of the design and in absence of dedicated expensive model tests. The procedure can be used with any industry standard three dimensional hydrodynamic packages.

The viscous damping calculation procedure is developed and implemented for a box shaped barge in regular waves. Further attempt is made to apply the method to irregular waves.

1.4. Layout of the Thesis

The first chapter of this thesis provides introduction to the researched topic and the general issues surrounding it.

The second chapter aims to provide a background in to the viscous damping of floating bodies and effort of researchers whom have tried to estimate this phenomenon as accurate as possible.

In the third chapter the fundamental methodology which was developed prior to this work is explained.

The newly developed formulations and mathematical model are presented in Chapter 4.

Chapter 5 explains application of the method presented in Chapter 4 and the code developed to calculate the roll viscous damping base on this method. This

chapter also includes the application procedure of the method including flowcharts and step-by-step definition. Further to the method developed to calculate the viscous damping in regular waves an attempt is made to apply the method to calculation of viscous roll damping in irregular waves.

The preliminary validation study and further confirmatory model test conducted during this work is presented in Chapter 6.

Chapter 7 presents the results and discussions related to application of the method explained in Chapter 4 to Chapter 6. This includes comparison of the numerical results with model test data to demonstrate validity of the procedure.

Finally the main conclusions on the results and recommendations for future work are presented in Chapter 8.

2 Literature Survey

Prediction of roll damping has always been a challenging task for naval architects. Accurate estimate of the roll damping for floating offshore installations is important as the transversal loads are governed by roll motion and this has direct impact on design of hull, topside structures and process plant on board. In case of more conventional sea going vessels small amplitude of roll motion can cause discomfort for passengers of a cruise liner or result in structural problems due to sloshing of liquid cargo in cargo tanks of a tanker.

Attempts in managing the roll motion of floating vessels go back to thousands of years ago when Greeks were using flat plate keels on their ships to reduce the roll motion of their vessels. This is considered to be the oldest and simplistic roll damping device. Recent roll damping devices include fin stabilizers, rudders, gyroscopic stabilisers and anti-roll tanks. These devices have different levels of complexity, effectiveness and cost.

The challenge is to develop a reliable method for calculating the equivalent linearized roll damping which enables the required response statistics to be calculated in the frequency domain for operational strength and fatigue analysis. This challenge is recognised recently by leading classification societies and is reflected in their rules and regulations applicable to floating offshore installations at a fixed location. In particular the Lloyd's Register Response Based Analysis (RBA) methodology requires linearized roll damping of a floating system to be calculated and included in the spectral analysis of vessel

motions for given sea states. Det Norske Veritas also requires the effects of neglecting viscous damping to be investigated if this is going to be the case in the design.

Roll damping is estimated by experimental and numerical methods. The experimental methods are usually followed by derivation of empirical formula from experimental data to allow for generalisation of the experiments. The numerical methods require model tests to demonstrate applicability of the method and assess validity of the results.

An overview of experimental and numerical approaches in estimation of the viscous damping is presented in this chapter.

2.1. Experimental Roll Damping Estimation

The most common practice in estimating the roll damping is model test. There are generally two experimental procedures for estimating the roll damping using model test. One experimental procedure is to conduct a decay test of the model in calm water by giving an initial roll to the model and allowing the model to oscillate freely until the roll motion is decayed. The roll time history is recorded during the decay. Using a linearized form of motion equation and assuming the nonlinear damping is of quadratic type, the equivalent linearized damping is estimated. The linearization procedure is based on the assumption that the same quantity of energy dissipates by the nonlinear and equivalent linear damping.

The other experimental procedure is the forced roll oscillation test. In this procedure the dissipated energy is measured during a forced roll oscillation of the model in calm water and the roll damping is then related to these measurements. This method is however more complicated and is used less in the industry.

The two model test practices mentioned above are conducted in calm water. Therefore the calculated linearized roll damping may not be an accurate representation of the roll damping of a floating vessel in waves [8].

Froude [9] was one of the first scholars to provide an overview on the rolling of ships and the roll damping phenomena. Froude formulated the roll damping in a linear plus quadratic velocity dependent form to account for dissipation of energy during roll motion. He studied the effect of wave height and steepness on the rolling of ships and the influence of this phenomenon on the design of ship hull shape. Based on this work he suggested designing the hull in a way to move the roll natural frequency of the ship away from synchronisation with the excitation waves. His work also lead to use of bilge keels for ships in order to stabilize the ship for roll. He was also one of the pioneers in using passive anti rolling tanks in ships.

Vugts [10] conducted several experimental assessments to determine hydrodynamic coefficients of swaying, heaving and rolling cylinders in free fluid surface. His work was used as the basis for numerous research works assessing the roll damping of floating bodies.

Himeno [12] provided a good overview of the roll damping phenomena. His method which is widely used in the industry is based on several decay model tests of ship shaped bodies for which he fitted a formula to the results. He divide the total viscous roll damping into several components such as wave radiation damping, skin friction damping and eddy damping, lift damping and bilge keel damping which itself consists of normal force damping, hull pressure damping and wave damping due to the bilge keels. He concluded that viscous effects are mostly due to flow separation and eddy formation at the shedding edge and the skin friction has a minimal effect in viscous damping.

Since the roll response for traditional ship forms is known to be nonlinear and quadratic, use of cubic models to fit curves through experimental data results in good prediction of the roll damping especially for ships in seaways.

Noting this, Faltinsen [13] developed the equivalent cycle linearization method in which the coefficients where obtained through decay tests.

Souza et al. [14] realised that uniform matching through roll decay time series of a floating system with unusually large bilge keels is not adequate and the matching should be different between large roll angles and smaller roll angles. Later on Oliveira [15] conducted several model tests following a bilinear approach suggested by Fernandes et al. [16] and demonstrated that the Keulegan-Carpenter effects are different between large and small roll angles. His work showed that the strong vortex attracted to the hull bottom in large roll angles result in stronger damping however at small roll angles the vortices are shed.

Model tests were conducted by Standing [17] to investigate the viscous roll damping and effect of sway and heave motions on roll response of a transportation barge. By comparing motions from the computer model with the data collected from model tests in regular and irregular waves, he concluded that the results from numerical studies compare well with data determined for roll damping from forced roll or free decay model tests. His calculation was done in time domain as well as frequency domain.

Noting criticality of correct estimation of roll responses in floating production units, a study was conducted by Choi et al. [18] on roll response of a barge type LNG FPSO in three different loading conditions in which the damping coefficients where determined through decay tests. Choi et al. [18] conducted free roll decay tests to estimate nonlinear roll damping of a barge shaped LNG FPSO in different loading conditions. They determined the roll RAO by conducting model tests with wide banded wave spectrum. The quadratic damping was then assumed in the calculations as an equivalent linear damping. They demonstrated that the theoretical results compare well with the model test data using an appropriate equivalent linear damping.

Full scale measurements of the motions of the Girassol FPSO was carried out off coast of West of Africa over period of a year by Van Dijk et al. [19] in order

to tune their estimates of viscous damping from their numerical models to full scale results.

Series of systematic model tests were performed by Park et al. [20] to estimate roll damping of a tanker FPSO. The experiments were carried out in a two dimensional wave tank. Scale effects where taken in to account in these experiments. Furthermore, effect of bilge keel, bilge radius and forced roll was considered in the tests. The results were then compared with numerical data calculated using commercial software that utilise potential theory. Based on the comparisons empirical viscous damping factors where determined for further use.

Model test experiments conducted for two FPSOs where reported by van't Veer et al. [21]. There work showed that the appendages such as riser balcony at side of the FPSOs contribute to the overall roll damping characteristic of the vessels. The behaviour of the vessel was modelled through a CFD model and the results where compared. This provided a good understanding of the fluid behaviour around the FPSO appendages.

Velocity field around a ship in forced roll motion was investigated by Aloisio et al. [22]. In order to get a better understanding of the fluid dynamics, model tests were carried out. The model test results were used to calibrate a CFD model. The flow field along the bilge keel of the vessel was presented. There work quantified the flow field around the bilge keel and provided understanding of interaction between the generated vortices and the hull.

van Kessel et al. [23] looked in to the effect of nonlinear damping in operation of a pipe lay/heavy lift vessel. They conducted model tests and compared the results with numerical calculation. Interaction between the roll response of the vessel and operational requirements were investigated demonstrating the close relationship between them and the importance of accurate estimation of the roll damping.

Jung et al. [24] conducted several experiments in a two dimensional wave tank to evaluate vortex generation due to regular waves passing a rectangular

barge. The barge was set up in a way to allow for roll motion only. Images were taken from the velocity field around the barge to capture behaviour of the fluid field. They demonstrated that the characteristics of vortices shed from the shedding edge of the barge vary for different incident regular waves. Their work provided better understanding of near field pressure distribution around a flat bottomed vessel. This lead to a better insight of the roll damping simulation.

Effect of large liquid tanks in prediction of roll damping of floating vessels was investigated by Huang et al. [25]. Their work concluded that the roll damping is sensitive to motion of the fluid in cargo tanks. In order to accurately estimate the damping it was suggested to explicitly model the liquid motion in large tanks.

Series of model tests were conducted by Kwang et al. [26] to investigate effect of viscous damping in roll motion of a rectangular barge. The tests were done in a two dimensional wave tank and the waves were applied to the beam of the model. Velocity field in vicinity of the structure was captured by Particle Image Velocimetry (PIV) method. Further they investigated the roll damping for incident waves with periods shorter than the natural period of the model as well as waves with periods longer than natural period of the model.

Model tests were done by Xiaorong et al. [27] to investigate the nonlinear roll damping of a ship in regular and irregular waves. They used the random decrement method to obtain the nonlinear roll damping. Accuracy of this method was shown to be dependent on the values of the threshold and segment number. Decay curves in calm water obtained by Xiaorong et al. [27] were similar to the ones measured by Kwang et al. [26].

The effect of bilge on roll damping of ship shaped Floating Production and Storage Offloading Vessel (FPSO) was investigated by Rae et al. [28]. The wave damping component of the step model as well as the viscous damping component of the step model of the FPSO was shown to be increasing in comparison to the section with bilge.

Douglas [29] showed that increase in forward speed results in increase in roll damping coefficient. In order to determine the influence of vessel forward speed on its roll damping coefficient he conducted series of trials on a bare hull model in the Massachusetts Institute of Technology towing tank. The Froude numbers were varied from zero to 0.40. Further, theoretical calculations were done and the results were compared with the experimental data. Douglas [29] showed that the wave radiation damping of the barge increases from zero speed condition to normal operating speed condition by a factor of 2 to 3. As a result he concluded that the roll damping of a vessel can be increased in seaway by increasing speed of the vessel.

The wave damping component is dominant in the heave, pitch, sway and yaw damping hence the viscous damping components can be usually ignored. Therefore these damping values are usually calculated by a potential flow theory. However, in the roll damping the viscous damping components play an important role because the wave damping component is usually much smaller than other components created by the viscosity of fluid. Therefore in the theoretical calculation it is difficult to predict a realistic roll damping. Due to this experimental results or predicted results by any empirical method are commonly used to predict the roll damping coefficient. Ikeda et al. [30] measured roll damping of high-speed craft by forced oscillation experiments. Comparison with damping values calculated from a linear potential flow theory showed that the experimental dampings were significantly under estimated. They suggested that the cause may be due to the fact that the prediction method does not take in to account the vertical lift force acting on the craft. They devised a method to predict the contributions of the vertical lift force in to the roll damping. They were able to confirm that the predicted results are in fairly good agreement with the measured ones. A prediction method of heave damping of the craft was also deduced on basis of same quasi-static principle assumption.

2.2. Numerical Roll Damping Estimation

Noting the calculation limitations and time constraints for conducting motion analysis of a floating vessel in the time domain, frequency domain calculations have become the norm in the industry. Although most vessel responses can be calculated with acceptable accuracy in the frequency domain, this is more difficult for roll response due to the nonlinear behaviour of roll damping.

Incecik [31] provided a procedure for calculating loads, motions and structural responses of floating offshore platforms. He investigated hydrodynamic characteristics of circular cylindrical members of offshore floating bodies to devise their structural responses due to wave excitation. Further, the method was implemented into computer codes and was verified by comparing the results with model tests including a full scale semi-submersible motion and response measurement.

Theoretically the total roll damping of a floating vessel can be divided into potential and viscous components. The potential component can be predicted accurately since it has a linear characteristic however, the viscous component is nonlinear and prediction of this is more problematic.

Kerwin [32], Haddara [33], Dalzell [34], Haddara [35] and Nayfeh et al. [36] conducted fundamental research work in calculating the roll damping. Analytical models that were based on classical linear plus quadratic form were replaced by Haddara [33] by linear-plus-cubic velocity dependent roll damping moment. This improved the analytical models. Dalzell [34] used the slowly varying parameters method and a least-square technique to study the cubic and quadratic models. Haddara [35] used the same roll decay data to suggest different roll damping models.

Usually the viscous roll damping is predicted using empirical formula. Peyton Jones et al. [37] classified the empirical viscous roll damping methods to perturbation method, asymptotic method, multiple time scaling and the harmonic balance method.

If motion of a floating body in waves can be assumed to be linear, strip theory can be used to calculate wave induced motions of the ship. In the strip theory method hydrodynamic forces and moments are calculated from two dimensional potential solutions of cross sections along the length of the vessel. By integrating these forces and moments the three dimensional hydrodynamic characteristics of the floating body are calculated. Since the strip theory is based on potential flow theory the viscous effects are neglected. This results in unrealistic prediction of vessel responses at resonance frequencies. In motion calculation methods such as strip theory method or potential flow calculation the roll damping should be estimated and accounted for accurately if a reasonable response is expected to be predicted, especially in vicinity of the roll natural frequency. In order to resolve this issue viscous roll damping is estimated using empirical formulations. Journée [38] provided a good overview of empirical formulation used to estimate the damping in surge and roll for strip theory calculations. Journée [39] developed hydrodynamic software based on strip theory which delivers information on ship motions and added resistance within a very short computation time. Further, he conducted comparative validation studies with validated computer programs.

Schmitke [40] developed a theoretical model based on strip theory to predict ship lateral motions in oblique seas. Focusing on the roll characteristic of the ship in beam seas, behaviour of the numerical model in long waves relative to beam of the ship was investigated. Comparison between the results of numerical calculation and model test was done to assess validity of the theoretical model.

A simplified analytical procedure was provided by Lee et al. [41] to estimate the hydrodynamic radiation damping of a rectangular barge using strip theory. Frequency domain calculations were conducted by combining the two dimensional energy conservation principal with Haskind-Newman relation. Results were compared with experimental data to assess validity of the method.

Free surface waves have effect on the vortex generation whereas the shear layers do not have a noticeable influence on the free surface waves. A numerical

method was suggested by Arne et al. [42] to include both the effect of free surface waves and vortex shedding based on a time step integration method. In this potential flow theory a potential flow boundary value problem outside the thin free shear layers was solved in each time step. This method can be applied to any forced body mode. The limitation of this method is that it can only be applied to sharp corner bodies in order for the separation points to be well defined, hence eliminating the need to conduct the calculation for the boundary layer. Both the surface effects which are usually included in any theory based on potential theory and vortex shedding which is usually neglected in theoretical procedure were included in his method. The results from this potential theory showed that roll damping due to eddy making and wave generation cannot be separated.

Chakrabarti [43] investigated the possible roll damping components and their empirical contributions. He showed that radiation damping is adequate for the accurate prediction of the rigid body motions of an offshore structure in waves however, this prediction was not true for the roll motion of a long floating structure. This is because for a ship, barge and similar long offshore structures the roll damping is highly nonlinear and the radiation damping is generally quite small compared to the total damping in the system. Chakrabarti [43] identified five roll damping components namely hull friction damping, hull eddy damping, free surface wave damping, lift force damping and barge keel damping. He also took in to account the scale effects.

An inappropriate selection of damping and restoring terms may lead to serious discrepancies with reality especially in peak roll amplitudes. A form of nonlinear equation governing the motion of a rolling ship subjected to beam waves was presented by Taylan [44]. He utilized the generalized Duffing method to investigate effect of roll motion in capsizing of a ship. The Duffing method is one of the several approximation methods for solving nonlinear differential equations in either time or frequency domain. Four distinctive vessel types were studied for comparison purposes to have comparative results of nonlinear roll responses and restoring forces. The results show that using the

proposed nonlinear equation of roll motion with three different nonlinear damping terms for each vessel type, the peak amplitudes differ from one to another significantly. The peak factors at resonances are the most important factors leading to ship's capsizing. Taylan [44] suggested that the best way to verify the estimated amplitudes is to carry out experiments. The experimental results were compared with the theoretical results.

Vortex flow forces and potential flow forces are the two components of hydrodynamic loading. Further, the potential flow forces are of second order in amplitude of ambient velocity fluctuations. This was investigated and validated by Lighthill [45].

For waves with a period longer than the roll natural period of the structure vortices are generated near the structure corners and act in opposite direction to wave radiation damping. Kwang et al. [46] conducted a quantitative study of the flow pattern to explain the coupled interaction between the rectangular body motion and the waves as oppose to the qualitative studies presented by Kwang et al. [26].

Oshkai et al. [47] showed that for a cylinder submerged sufficiently deep the orbital nature of the wave motion results in multiple sites of vortex development along the surface of the cylinder followed by distinctive types of shedding from the cylinder. They concluded that decreasing the depth of submergence delays the orbital migration of shed concentrations of vorticity about the cylinder. Therefore submergence of the cylinder beneath the wave has a pronounced effect on the pattern of vorticity concentrations.

Santiago [48] showed that among heave, pitch and roll motions of a ship in sea which have some analogies with a spring-mass damper system, the roll motion is the one which presents less damping and therefore it is most probable one to enter resonance, thus drastically increasing the amplitude of motion. In this study roll motion was introduced and it served as a basis in understanding anti-rolling systems focusing on the study of bilge keels from constructive and operative point of view. Problems with rolling of ships increased from the

second half of the 19th century when steam machines replaced sailing propulsion and iron replaced wood. This led to design modifications in ships affecting transversal stability. Santiago [48] suggested that bilge keels with no moving parts are the simplest and cheapest element that may be incorporated on a ship to reduce the rolling. Bilge keels reduced rolling by increasing damping moment resulting from the viscous eddy flows around the bilge keel surface, the pressure resistance around it and the hydrodynamic lift in the forward sections of the bilge keels.

Nonlinear nature of viscous roll damping makes it difficult to model this phenomenon. Ray-Qing et al. [49] devised a new method for modelling the bilge keel roll damping effect based on the blockage mechanisms of an object in the potential flow. This method of blocking mechanisms describes the resistance of a solid object in a flow.

Korpus et al. [50] described a numerical technique for analysing the viscous unsteady flow around oscillating ship hulls. This technique was based on Reynolds-Averaged Navier-Stokes (RANS) capability and was intended to generate viscous roll moment data for incorporation of real flow effects into potential flow based ship motion programs. The roll moment component was breakdown in isolation into viscosity effect, vorticity and potential flow pressures.

El-Bassiouny [51] investigated effect of ship roll motions for determining the conditions under which a ship can experience dynamic capsizing. The technique employed is analytical but numerical in nature. The equation for relative roll angle in this study was expanded using different orders of its mathematical terms. He grouped the wave radiation and the viscous damping as linear term and damping due to frictional resistance and eddies behind the keels and hard bilge corners as cubic term. The averaging method and multiple time scale method were used. The viscous roll damping was considered to be linear in his computation.

Mulk et al. [52] looked in to the roll motion and its role in capsizing of ships. He studied the complete Euler's equation of six degrees of freedom. Since roll was considered to be the most critical ship motion of all the six modes of motion, emphasis was made on nonlinear roll motion. Interaction between roll and other modes of motion were considered in the studies. He showed that all six modes of motion affect one another. He made it clear that to study vessel's motion all the six degrees of freedom must be simultaneously studied. He also suggested that although nonlinear coupling of roll to heave and pitch quantitatively affect the roll, they do not have any qualitative effect on roll.

Roll damping coefficients calculated using Navier-Stokes solver are larger than the radiation damping coefficients evaluated by the linear potential theory due to viscous and vortex effect. Bangun et al. [53] applied the Navier-Stokes solver to laminar flows using the linear wave theory while the free surface condition was approached. Bangun et al. [53] were able to show that the values of the added mass and damping coefficients depend on the amplitude of the roll motion. The results from Navier-Stokes solver compare well with those obtained from the linear potential theory for both cases of floating body with and without bilge keels. The values of added mass were not much influenced by fluid viscosity.

Robert et al. [54] also explored the coupling between nonlinear roll motion and other motions such as sway, pitch and heave. He devised a new method of estimating the damping and excitation moments. The method employed was based on estimating the drift and diffusion coefficients from roll response data and using the estimates in conjunction with the theoretical expression for the response data.

Ikeda [55] modified his method to improve its accuracy and extend its applicability to different ship types. His method was based on components in which each component was predicted by both theoretical and empirical solutions. He used the new method to determine optimum size and location of bilge keels. The original method he proposed was based on simple cross section and location of bilge keels. The pressure on the hull surface was integrated over

the simply assumed hull shape. His assumption was found to cause large errors because the cross section and the location of bilge keels sometimes significantly differ from the simple assumption. He therefore improved his prediction to be able to take into account the cross section and exact location of bilge keels.

Viscous forces on the appendages are important and the nonlinear nature of roll response requires time domain modelling. Klaka et al. [56] studied the roll motion of a yacht at zero Froude number (zero speed). Due to the limitations of existing theoretical models of roll motion for application to bodies with large appendages, the appendages were treated as fully submerged flat plates. The calculation of the forces acting on the appendages was based on a strip wise Morison formulation. A time domain single degree of freedom roll motion was developed in order to identify the dominant excitation and damping sources. A series of full scale validation experiments was conducted in calm water and in ocean waves. Their results show that the keel, rudder and sail dominated the damping whilst the canoe body contributed very little. The hydrodynamic damping was nonlinear with respect to wave amplitudes.

Yuck et al. [57] assumed two components for roll damping namely wave making component which was determined from a far field momentum method and viscous component which was the result of subtracting the wave making component from the total damping. They determined roll damping of a series of unconventional midship sections and showed that a conventional barge midship section would experience more roll than a barge with a "top hat" shaped midship section referred to as a step section, due to decrease in vortex shedding.

Inoue and Islam [58] used far field and near field approach to determine slowly varying drift forces. Using the method they investigated the relationship between viscous roll damping and drift forces of multi-body floating systems in which the viscous damping was added empirically. Their work showed that accuracy of the predicted second order drift forces in regular and irregular waves depends on accuracy of the assumed viscous roll damping.

Seakeeping of high speed craft is dependent on estimation of viscous roll damping. de Jong et al. [59] used a free surface Green's function in a time domain boundary element method to assess seakeeping of a fast ship. In order to satisfy the two boundary conditions of zero normal flow on the body and the transom stern flow based on unsteady Bernoulli equation, they applied a combined source doublet formulation. They initially solved the source system in absence of the transom condition and then solved the doublet strength incorporating the previous source strength. They concluded that the small potential damping in seakeeping assessment of high speed ships signifies the importance of viscous damping in hydrodynamic characteristics of these vessels. The effect of viscous damping becomes more dominant around peak of the heave motion in which the vortex forces due to flow separation in the bilge region are significant. The oscillation frequency, Froude number and section shape were considered to be the parameters affecting magnitude of the vortex forces.

In recent years use of computational fluid dynamic (CFD) methods in calculating roll damping has become more possible due to developments in computing power however, this is still a hardware intensive method and the results require to be validated. The CFD calculation includes simulating motion of oscillatory bodies in real time.

Further attempts in predicting viscous damping of floating systems include a joint industry project named Roulis 2 which was set up to increase the accuracy of roll damping estimation methodologies especially for floating systems operating in deep water developments off West Coast of Africa using both numerical modelling and experimental measurements. Ledoux et al. [60] presented the main findings of this study. Their study demonstrated the significant effect of risers and moorings on roll damping of floating systems in deep waters. In this process a general purpose CFD code based on Pseudo-unsteady system was used to model the roll motion of a barge.

In industrial assessments usually the roll damping is calculated for a single wave or sea state and it is assumed that the calculated damping remains

constant for other sea states. Gachet et al. [61] investigated a method in which the roll damping was assessed for each sea state in a given scatter diagram. This was used to look in to the operability of a vessel. Their calculation showed that the roll damping is sea state dependent.

Following the work of Rott [62] and Brown et al. [63] Graham [64] developed an expression for the vortex force that makes allowance for an axial component of the flow. On this basis a theoretical method could be constructed to predict the viscous damping of body with zero forward speed. The analysis was based on replacing the operator $\frac{dU}{dx}$ for transverse sections of a slender body in steady forward speed U by $\frac{d}{dt}$ for a 2-D body equal to one of these transverse sections in time dependent flow and zero forward speed. This is a standard analogy which can be thought of as taking a series of snap shots following the slender body cross section as it moves rearwards along the slender hull at the free stream speed U. A study was carried out later by Al-Hukail [65] on using the vortex method to calculate roll damping on a slender ship with non-zero forward motion. In that case the operator was revised to $\frac{d}{dt} + \frac{dU}{dx}$. The sections along the hull were linked by the developing vortex shedding [66].

Further investigation by Wright et al. [67] showed that the roll damping in vicinity of the natural roll period is considerable and appropriate prediction of the roll damping around natural roll period is difficult.

A mathematical model was developed by Das et. al. [68] to investigate damping moment of nonlinear roll and yaw motions of a floating body in time domain under the action of sinusoidal waves. They approximated the time dependent coefficients to approximate the added mass and damping. Perturbation technique as well as Runge-Kutta method with adaptive step-size algorithm was used in their model to calculate the closed form solutions and higher order cases respectively. The results were then compared with model test results. The work showed that the roll damping is highly dependent on viscous effects while added mass variation affects yaw damping.

For the case of a rolling box shaped floating vessel vortex shedding is the dominant roll damping component. In order to estimate the vortex force on the shedding edge of a box shaped model Graham [3] implemented a simple discrete vortex analysis for flow about an infinite wedge in oscillatory flow in which the flow in an infinite half-plane, the ζ-plane, was transformed to flow about an isolated edge. In this method in order to satisfy the Kutta condition discrete vortices at each time step were introduced at the trailing edge of the infinite wedge. The discrete vortices were moved away from the shedding edge and rolled up to form vertical structures under the influence of the ambient flow (low Keulegan Carpenter oscillatory flow) and any other vortices present in the flow. His method was developed for sharp edges in a flow with no forward speed. The method enabled him to calculate a generalised vortex force on the infinite wedge in terms of length scale and velocity scale. By matching the flow about its edge to the local flow about the edge of a body of finite dimensions, a process which fixes the length and velocity scales, he was able to calculate a generalised vortex force and express it in form of Morison like equations. He then inferred the total force on a finite body with flow separation from its edges. He calculated the total force on the body due to separation from all its edges by repeating this process at each edge of the finite body. Downie [69] used Graham's method in a theoretical approach to calculate the roll response of a box shaped barge.

Subsequently Cozens [70] investigated vortex shedding of a rounded infinite wedge flow as well as an infinite wedge with a bilge keel both by using discrete vortex method and the cloud in cell method. He used Graham's dimensionless vortex force functions to express the vortex force calculated through his studies.

Theoretically the potential flow solution in Graham's method [3] turns out to be singular when the radius of the corner of the floating barge tends to zero. However Taylor et al. [71] used a high order panel method to calculate wave diffraction and radiation by a moving body with a small steady flow speed. They described the body surface by a sharp corner in a practical calculation.

Results were computed for different corner radii of series of truncated cylinders with the same radius and draught.

Downie et al. [4] developed Graham's method further by matching the local flow about the edge of the infinite wedge with the local flow about one corner of the barge on the basis that the vortex force should be same on both and provided a methodology for calculating the vortex force shed from bilge of a two dimensional floating barge. Based on this study Downie et al. [5] advanced the two dimensional vortex force calculation methodology to generate a methodology applicable for calculation of vortex force shed from a three dimensional floating body.

Noting that the total force imposed on an oscillating hull by a bilge keel is made up of two components of drag and inertia Downie et al. [81] investigated effect of maximizing drag component of bilge keel on the viscous roll damping. This study showed that the viscous roll damping increased by use of perforated plates which maximized the length of shedding edge per unit area.

Later on Graham et al. [72] used a Helmholtz split of velocity field to insert an inner viscous flow field within an outer potential flow. They then modelled the inner rotational flow filed using modified Navier Stokes equations and solved the equations using a spectral element code. In this process it was assumed that the inner rotational flow field is driven by the outer flow that is computed from a seakeeping program.

Hajiarab et al. [6] used Downie et al. [5] methodology to calculate a damped roll RAO of a box shaped barge and for the first time practically applied it to a three dimensional diffraction-radiation hydrodynamic model. They demonstrated that the produced results compare well with model test results in regular waves. In order to eliminate any uncertainty in the model test results used in [6] further model tests were conducted to validate application of this methodology in regular waves. In this study the roll damping was linearized for a given wave amplitude in each frequency [7]. The numerically calculated damped RAO was demonstrated to agree well with experimental data for a box

shaped floating barge. Furthermore they attempted to estimate the viscous roll damping of a box shaped floating body in irregular waves as well as in regular waves.

This dissertation provides detail insight in to the work presented in [6] and [7].

3 Background Theory

Accurate estimate of roll motion may not be a driving factor in design of seagoing ships however, it is one of the challenging issues to predict in design of floating offshore installations. It also plays a significant role in offshore operation activities such as transportation and installation of offshore jackets. This is due to the fact that unlike seagoing ships which are designed to be able to manoeuvre flexibly in sea, offshore floating installations generally have a passive weathervaning characteristic. In case of offshore operation and transportation again due to restrictions in manoeuvring during operation it is common to define set of limiting operational criteria such as roll, pitch and accelerations of the transportation barge which are then transformed to estimation of set of limiting environmental conditions in which the operation can be conducted safely.

Several numerical and experimental campaigns have been conducted to develop a method to estimate motions of a floating body as accurate as possible. However limitations of each method in estimating the floating vessel motions should be appreciated.

In this report the discrete vortex methodology which was originally developed by Graham [3] to predict viscous damping of a two dimensional body moving in waves is used as a basis. The method is expanded to make it compatible with current industry standard inviscid three dimensional seakeeping codes.

Since a three dimensional diffraction-radiation code is used in this work to calculate the velocities at the vortex shedding edge of an oscillating barge, a brief description of potential theory which is the basis of the code is presented in Section 3.1. Basis of the vortex shedding methodology developed by Graham [3] and the advancements made by Downie et al. [5] is presented in Sections 3.2 and 3.3 respectively.

3.1. Potential Theory

Assuming the fluid under study is incompressible, inviscid and irrotational the potential theory can be used to calculate wave loads on fixed structures and motions of a body floating in the fluid. The fluid in the potential theory is described by a velocity potential ϕ from which the fluid characteristics such as fluid velocity, fluid acceleration, fluid pressure and surface elevation can be found. Since fluid is assumed to be ideal in the potential theory, calculation of phenomena such as viscous damping, slamming pressure and forces on slender structures from this theory are not reliable. This is due to the fact that these phenomena are directly related to fluid behaviours such as viscosity, vortex shedding and compressibility. However these nonlinear phenomena can be considered in the theory by adding viscous terms.

Assuming the fluid is irrotational and incompressible the Laplace equation stands, where:

$$\nabla \times \vec{V} = \frac{\partial^2 \phi}{\partial x^2} + \frac{\partial^2 \phi}{\partial y^2} + \frac{\partial^2 \phi}{\partial z^2} = 0$$

Equation 3-1

Since the velocity potential is defined to describe the fluid velocity this is one of the conditions that should be satisfied for a floating oscillatory body, hence:

$$\bar{V} = \nabla\phi = \vec{\imath}\frac{\partial\phi}{\partial x} + \vec{\jmath}\frac{\partial\phi}{\partial y} + \vec{k}\frac{\partial\phi}{\partial z} = [\vec{u}, \vec{v}, \vec{w}]$$

Equation 3-2

where i, j, and k are unit vectors in x, y and z direction. By taking derivation of the equation in time the accelerations can be calculated as:

$$\bar{a} = \frac{\partial}{\partial t}(\nabla\phi)$$

Equation 3-3

Using the Bernoulli equation the associated pressure in the fluid field can be defined as:

$$p = -\rho\left(\frac{\partial\phi}{\partial t} + \frac{1}{2}\left|\vec{V}\right|^2 + gz\right) + P_a$$

Equation 3-4

in which ρ is the density of the fluid, g is the gravity and P_a is the atmospheric pressure. By linearizing Equation 3-4 and neglecting the atmospheric pressure the fluid pressure proportional to first order wave amplitude can be written as:

$$p = -\rho\frac{\partial\phi}{\partial t} - \rho gz$$

Equation 3-5

Knowing the fluid field pressure the forces on a floating body can be calculated. However the fluid field is defined by physical boundary conditions that should be considered in the calculations. These include free surface condition, body boundary condition and sea bottom boundary condition.

The free surface condition consists of two boundary conditions namely the dynamic boundary condition and the kinematic boundary condition. Since the pressure at the free surface should be equal to the atmospheric pressure, the dynamic boundary condition can be defined from Equation 3-5. Hence for surface of a wave with small amplitude of ζ we have:

$$-\rho\frac{\partial\phi}{\partial t}-\rho g\zeta=0\ \Rightarrow\ \frac{\partial\phi}{\partial t}+g\zeta=0$$

Equation 3-6

Since the fluid particle on the free surface is expected to remain on the free surface, by derivation of a function F the kinematic boundary condition can be derived as:

$$\frac{DF}{Dt}=\frac{\partial F}{\partial t}+\vec{V}\cdot\nabla F$$

Equation 3-7

By defining the surface elevation as $z=\zeta(x,y,t)$, and the function $F(x,y,z,t)=z-\zeta(x,y,t)=0$ and removing the higher order terms, it can be concluded that:

$$\frac{\partial\zeta}{\partial t}=\frac{\partial\phi}{\partial z}\quad at\quad z=0$$

Equation 3-8

Combining the kinematic boundary condition with the dynamic boundary condition results in:

$$\frac{\partial^2\phi}{\partial t^2}+g\frac{\partial\phi}{\partial z}=0\ \ at\ \ z=0$$

Equation 3-9

For an oscillatory velocity potential with frequency of ω the equation can be written as:

$$-\omega^2\phi+g\frac{\partial\phi}{\partial z}=0\ \ at\ \ z=0$$

Equation 3-10

The body boundary condition limits fluid motion through the body. Therefore the kinematic body boundary condition can be written as:

$$\frac{\partial \phi}{\partial n} = \vec{n} \cdot \overrightarrow{V_s}$$

Equation 3-11

where $\vec{n}$ is the normal vector of the body surface pointing into the fluid and $\overrightarrow{V_s}$ is the local velocity at the body surface.

The sea bottom boundary condition restricts the fluid motion through the seabed. In this case for a horizontal seabed in depth h the seabed boundary condition can be defined as:

$$\left.\frac{\partial \phi}{\partial n}\right|_{z=-h} = 0$$

Equation 3-12

The simplifications on the boundary conditions stated above are based on the assumption that the wave amplitude and floating body oscillation are small. This allows for the terms proportional to the higher order wave amplitudes to be neglected. Further, this assumption allows for calculation of the mean position of the body instead of the actual position in the fluid. The potential theory boundary conditions are shown in Figure 3-1.

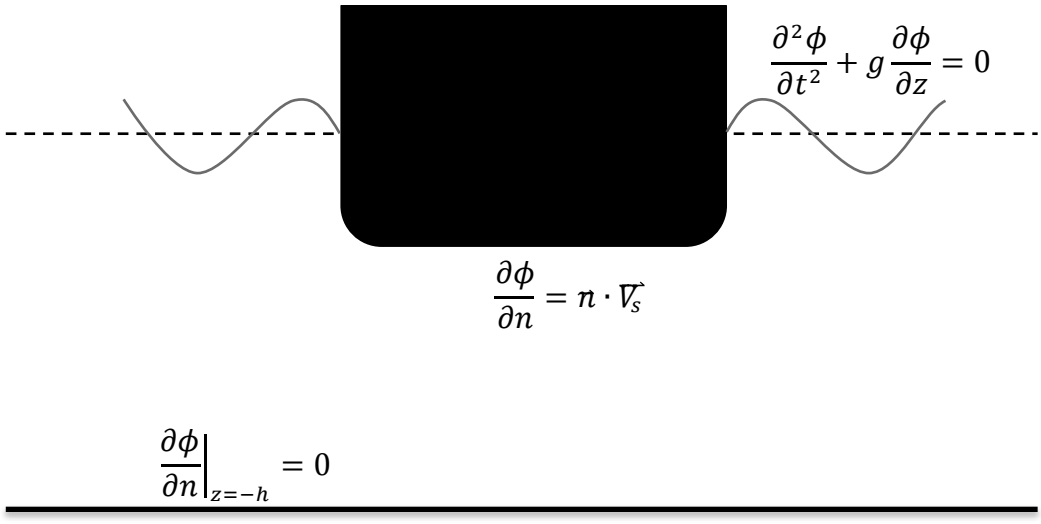

Figure 3-1: Potential theory boundary conditions [99]

If the sea can be simply defined with a regular wave the issue of a floating body in regular wave can be divided to two separate phenomena of diffraction and radiation.

For the diffraction case the excitation forces and moments can be characterised by Froude-Krylov load and diffraction load. The Froude-Krylov load is derived from the pressure of the wave field with no body present. However the diffraction load is the change in load due to the effect of structure on the fluid. By super positioning the total fluid potential can be written as:

$$\phi = \phi_I + \phi_D + \phi_R$$

Equation 3-13

where ϕ_I is the incident wave potential, ϕ_D is the diffracted wave potential and ϕ_R is the radiated wave potential.

In reality the sea waves do not follow characteristics of a regular wave. In order to characterize the irregular waves it is assumed that the irregular wave can be represented by super positioning of many regular waves with different amplitudes and frequencies. In this case an irregular wave propagating in x direction can be defined as:

$$\zeta = \sum_{j=1}^{N} A_j \sin\left(\omega_j t - k_j x + \varepsilon_j\right)$$

Equation 3-14

where A_j is the wave amplitude, ω_j is the wave frequency, k_j is the wave number and ε_j is the phase angle of the j-th wave component of the irregular wave. In this case assuming all the component regular waves are in the same direction the irregular wave can be assumed as a long crested wave.

Wave spectrum is used to represent energy of an irregular wave. The wave spectrum is a function of wave frequency and is described as following:

$$\frac{1}{2}A_j^2 = S(\omega_j)\Delta\omega$$

Equation 3-15

where $S(\omega_j)$ is the wave spectrum value at the j-th circular frequency. Further, the total area under the wave spectrum will be representative of the total energy of the irregular wave. Principals of transfer of waves in to response are presented in Figure 3-2.

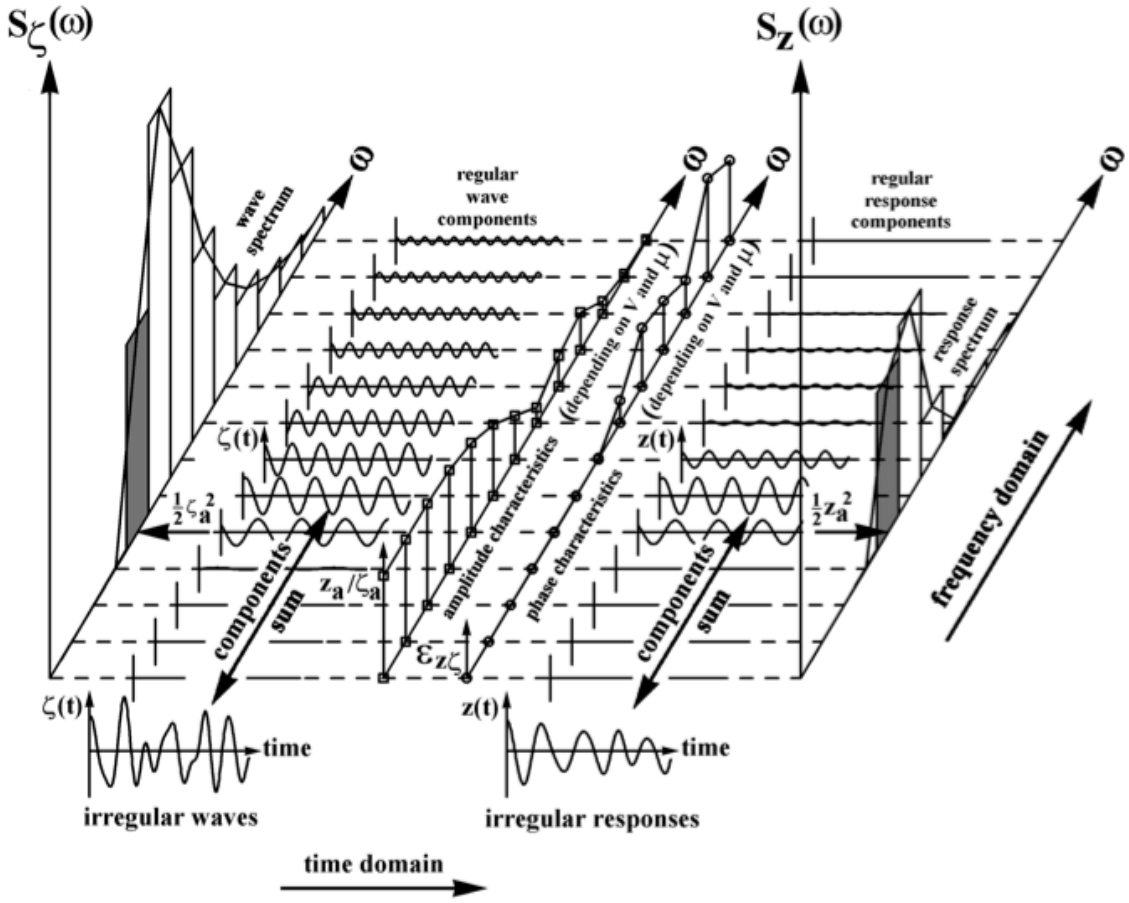

Figure 3-2: Principle of Transfer of Waves into Responses [95]

In order to consider directional characteristic of waves where θ is the wave propagation angle of the wave, the wave spectrum can be represented as:

$$S(\omega, \theta) = S(\omega)f(\theta)$$

Equation 3-16

In this case the surface of a short crested wave can be defined as:

$$\zeta = \sum_{j=1}^{N}\sum_{k=1}^{K}\sqrt{2S(\omega_j,\theta_k)\Delta\omega_j\Delta\theta_k}\,\sin(\omega_j t - k_j x\cos\theta_k - k_j\sin\theta_k + \varepsilon_{jk})$$

Equation 3-17

In order to calculate characteristics of a floating body in waves using the velocity potentials, the boundary conditions need to be solved. The most common method used in hydrodynamic packages to solve the velocity potential boundary conditions is the panel method. In this method the body surface boundary condition is defined by combination of source, sinks and dipoles to define the wetted surface of the floating body, hence the method is suitable for modelling unconventional hull shapes. The method is based on potential theory, hence oscillations are assumed to be small relative to the cross-sectional dimensions of the body. Using finite number of elements to define the body surface boundary the added mass, potential damping and restoring forces are calculated from the radiation waves and the exciting forces are calculated from diffraction waves.

Assuming that the strength of a source in potential theory can be defined by Q the velocity potential of a three-dimensional point source in still water with a radial distance of r from a point P can be written as:

$$\phi = -\frac{Q}{4\pi r}$$

Equation 3-18

In this case if ds is a surface element of a spherical surface with its centre at the source the velocity flux through the spherical surface can be written as:

$$\iint \frac{\partial\phi}{\partial t}ds = \frac{1}{4\pi}\frac{Q}{r^2}\,4\pi r^2$$

Equation 3-19

3.1.1 Two Dimensional Potential Theory

For a two dimensional body oscillating in an infinite fluid the two dimensional point source can be written as:

$$\phi = \frac{Q}{2\pi}\log r$$

Equation 3-20

By distributing the sources over the body surface the velocity potentials can be written as:

$$\phi(y,z) = \int_S q(s)\log\sqrt{\left(\left(y-\eta(s)\right)^2 + \left(z-\zeta(s)\right)^2\right)}\,ds$$

Equation 3-21

where $\eta(s)$ and $\zeta(s)$ are coordinates on the body surface, s is an integration variable along the body surface and y and z are coordinates in the fluid domain. S is the body surface and $q(s)$ is a source density. The source density $q(s)$ is found from satisfying the body boundary condition. The total velocity potential must satisfy all boundary conditions. In case of infinite fluid the only condition is the body boundary condition.

In order to solve the body boundary condition the body surface is approximated in to N straight elements as shown in Figure 3-3:

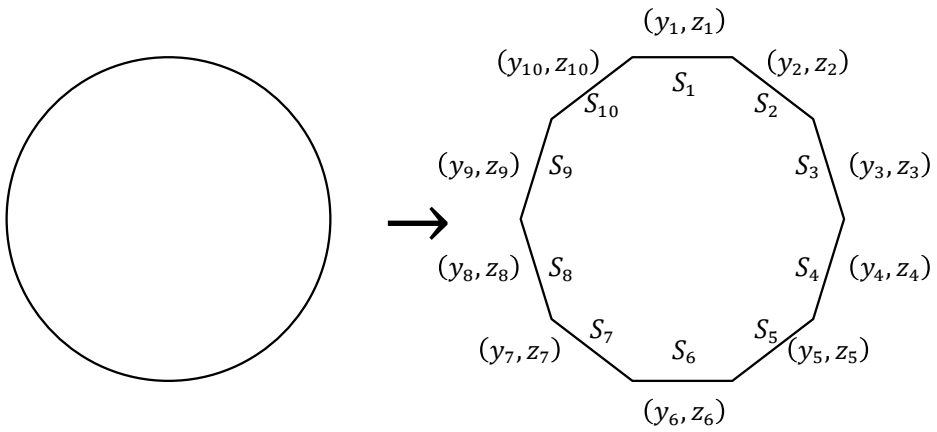

Figure 3-3: Two dimensional body surface approximation [99]

Then it is assumed that the source density over each element is constant. By this assumption the Equation 3-21 can be numerically solved as:

$$\phi = q_1 \int_S \log\sqrt{\left(\left(y-\eta(s)\right)^2 + \left(z-\zeta(s)\right)^2\right)}\,ds + \cdots$$

$$+q_{10} \int_S \log\sqrt{\left(\left(y-\eta(s)\right)^2 + \left(z-\zeta(s)\right)^2\right)}\,ds$$

Equation 3-22

The time dependent can then be separated and the equation can be solved for the body boundary condition on the midpoint of each element. The normalised source density for an oscillating body can be defined as:

$$q(s) = -\bar{q}(s)\eta_{3,a}\omega\cos\omega t$$

Equation 3-23

Furthermore, the body boundary condition can be defined from the body geometry. This results in the body boundary equation to become linear as:

$$A_{ij}\overline{q_J} = B_i$$

Equation 3-24

where i and j define number of elements. In this case from 1 to 10, see Figure 3-3, the surface integrals over each element in the surface are defined by matrix A. The normalised source densities are defined by $\bar{q}$ vector and the body geometry condition is characterised by B vector. In order to fulfil the surface boundary condition and avoid fluid penetration through the surface, the normal velocity from the source in (y_i, z_i) is set to opposite and equal to the normal velocity found from oscillation.

By defining the normalised velocity potential and solving the equation for $\bar{q}$ the normalised radiation velocity potential can be found as:

$$\phi = \bar{\phi}\dot{\eta}_3 = -\bar{\phi}\dot{\eta}_{3,a}\omega \cos \omega t$$

Equation 3-25

Using the normalised velocity potential the dynamic pressure from Bernoulli's equation can be calculated as:

$$p = -\rho \frac{\partial \phi}{\partial t} = -\rho \bar{\phi} \eta_{3,a} \omega^2 \sin \omega t$$

Equation 3-26

The added mass and damping terms can then be calculated from pressure distribution of the radiation case.

3.1.2 Three Dimensional Potential Theory

Following on from the two dimensional potential method the three dimensional potential method is used to calculate the linear wave induced motions and loads on large floating structures. Since the fluid field is not infinite further boundary conditions should be satisfied to resolve the velocity potential equation.

In this case for a ship with an oscillatory heave motion in waves and zero forward speed the velocity potential can be defined from the three dimensional Laplace equation, the linear free surface boundary condition for harmonic oscillation and the body boundary condition.

For deep waters the sea bottom condition will tend to infinity as:

$$|\nabla \phi| \to 0 \quad when \quad z \to -\infty$$

Equation 3-27

The radiation condition should be considered in the three dimensional velocity potential to account for the waves moving away from the floating body. For a point far away from the body with distance $r = \sqrt{y^2 + z^2}$ this is represented by:

$$\phi \sim \frac{Ae^{kz}}{\sqrt{r}} \sin(kr - \omega t + \varepsilon)$$

Equation 3-28

The hull of the floating body is represented in the three dimensional fluid field by quadrilateral panels. The source strength is considered constant over the panel. However in this case the source potential is different in comparison to the infinite fluid case since it should take the mean free surface boundary condition, the infinite water depth boundary condition and the radiation wave condition. Therefore the source density strength can be calculated from the body boundary condition to ensure no flow will pass through the body surface. The velocity potential for infinite water depth was calculated by Havelock [96] [97] as following:

$$G(x, y, z; \xi, \eta, \zeta)e^{-i\omega t} =$$

$$\left[\frac{1}{R} + \frac{1}{R'} - \frac{4\nu}{\pi}\int_0^\infty [\nu \cos k(z+\zeta) - k \sin k(z+\zeta)] \frac{K_0(kr)}{k^2 + \nu^2} dk\right.$$

$$\left. -2\pi\nu e^{\nu(z+\zeta)} Y_0(\nu r) + i2\pi\nu e^{\nu(z+\zeta)} J_0(\nu r)\right] e^{-i\omega t}$$

Equation 3-29

where i is the complex unit and (ξ, η, ζ) are the coordinates on the body surface. Further:

$$R = \sqrt{(x-\xi)^2 + (y-\eta)^2 + (z-\zeta)^2}$$

Equation 3-30

$$R' = \sqrt{(x-\xi)^2 + (y-\eta)^2 + (z+\zeta)^2}$$

Equation 3-31

$$r = \sqrt{(x-\xi)^2 + (y-\eta)^2}$$

Equation 3-32

$$\nu = \frac{\omega^2}{g}$$

Equation 3-33

In Equation 3-29 zero order Bessel function of the first kind is shown by J_0, zero order Bessel function of the second kind is shown by Y_0 and K_0 is the modified Bessel function of zero order.

The Bessel functions were explained further by Abramowitz et al. [98]. They used asymptotic expansions for the Bessel function for large r values to satisfy the radiation condition with the Green function:

$$Re\left\{\left(-Y_0(\nu r) + iJ_0(\nu r)\right)e^{-i\omega t}\right\} \approx$$

$$Re\left\{\left[-\sqrt{\frac{2}{\pi\nu r}}\sin\left(\nu r - \frac{\pi}{4}\right) + i\sqrt{\frac{2}{\pi\nu r}}\cos\left(\nu r - \frac{\pi}{4}\right)\right]e^{-i\omega t}\right\} =$$

$$-\sqrt{\frac{2}{\pi\nu r}}\sin\left(\nu r - \omega t - \frac{\pi}{4}\right)$$

Equation 3-34

The three dimensional velocity potential which was explained here can be generalised to calculate oscillatory motion of a floating body in any degree of freedom. However in comparison to two dimensional methods the three dimensional velocity potential requires more boundary conditions to be satisfied. Further the source densities in the three dimensional method are more complex. The source expressions in this case are more complicated and there is possibility of occurrence of irregular frequencies in the calculation which is a numerical problem. Finally the velocities close to the body and at sharp corners cannot be correctly represented due to singularities and lack of possibility of modelling boundary layer separation in the method.

Further accuracy of the calculated responses from the panel method depends on density of the panels representing the body surface. Dense panel grid results in long solution time while light panel grid density results in uncertain

responses. Hence an ideal panel density is the one that produces good enough results in a reasonable amount of time.

Dynamic motion characteristics of a floating body can be calculated by solving the dynamic equilibrium equation of the body for regular waves with different frequencies. For a floating body in waves the dynamic equilibrium equation for six degrees of freedom can be established from Newton's 2nd law as:

$$\sum_{k=1}^{6}\left[\left(M_{jk}+A_{jk}\right)\ddot{\eta}_k+B_{jk}\dot{\eta}_k+C_{jk}\eta_k\right]=F_j\,e^{-i\omega t}\qquad ,j=1\ldots6$$

Equation 3-35

where η_k is motion in mode k, $\dot{\eta}_k$ velocity in mode k, $\ddot{\eta}_k$ is acceleration in mode k, M_{jk} is the generalized mass (inertia) matrix component in mode j due to motion in mode k, A_{jk} is the added mass(inertia) matrix component in mode j due to motion in mode k, C_{jk} is the restoring matrix component in mode j due to motion in mode k, F_j is the complex amplitude of exciting force in mode j with the force/moment components given by the real part of $F_j e^{-i\omega t}$ and ω is the wave excitation frequency.

In order to calculate the transfer functions of the vessel the equation system should be solved for different frequencies. By normalising the calculated responses for the incident wave amplitude the response amplitude operators (RAO) of the motion are calculated. This requires the mass, added mass, damping and restoring matrixes and excitation forces to be defined.

The excitation forces are due to the waves that result in an oscillatory force on the body. Using diffraction theory the excitation forces are calculated directly from pressure distribution.

The mass matrix consists of the generalized mass and inertia terms. These terms are multiplied by acceleration to generate the inertia force or moment. Added mass is defined as an addition to the body's mass or inertia. This is due

to the accelerated fluid surrounding the oscillating body. The added mass can be represented with a finite addition of the mass in the motion equation.

Damping defines dissipation of the energy of an oscillatory body in the fluid. The total damping of a floating body consists of potential damping and viscous damping. The potential damping is calculated from solving the radiation problem. However since in the potential theory the fluid is assumed to be ideal the viscous damping cannot be calculated from the potential method. Hence the viscous damping should be considered in the calculation separately. In the roll motion viscous damping can have a significant effect on the response especially around its natural frequency. Hence a viscous damping term is added to the potential damping term in form of:

$$F_{VD}^{non-linear} = B_{44}\dot{\eta}_4|\dot{\eta}_4|$$

Equation 3-36

In order to include the viscous damping term in the equation of motion, it needs to be linearized hence the linear viscous damping term is defined as following:

$$F_{VD}^{linear} = B_{44}^{*}\dot{\eta}_4$$

Equation 3-37

The brief potential theory methodology explained here is the basis used in the diffraction-radiation software to calculate hydrodynamic characterises of a floating body. The aim is to define a linearized viscous damping to approximate the viscous effects in roll motion of a floating box shaped barge.

3.2. Vortex Shedding Phenomena

Oscillation of a body in a still fluid can be assumed to be kinematically same as oscillatory flow of fluid around a fixed body including Froude-Krylov forces. These Froude-Krylov forces represent the pressure gradient of the imposed

flow on the body and are in phase with the body accelerations. Therefore in order to understand the flow on shedding edge of an oscillatory barge the oscillatory flow interacting with a sharp edged bluff cylinder may be investigated.

Displacement of fluid particles in undisturbed flow is small in comparison with the scale of the body at low Keulegan-Carpenter numbers. This results in vortices moving away from the shedding edge under the influence of other vortices. Hence it can be assumed that the vortex shedding from one edge may be independent from other vortex shedding edges. On this basis it can be concluded that the local flow could be equal to an infinite wedge subjected to an oscillatory flow.

Singh [84] conducted experiments on sharp edged bluff cylinders and concluded that the frequency of vortex shedding from a single isolated edge is one vortex per shed per cycle in low Keulegan-Carpenter numbers. The vortex shed in a half cycle is then swept back in the next half cycle to create a pair with a new growing vortex. As soon as both vortices gain the same strength the first vortex then moves rapidly away from the body.

Keulegan and Carpenter [85] used the flow field of a standing water wave to study oscillatory flow around both flat plates and circular cylinders. They showed that the drag coefficient C_D and the inertia coefficient C_m for a measured force in flow direction in Morison's equation were functions of the Keulegan-Carpenter number $K_c = U_0 T/d$ as stated in Equation 3-38 below:

$$F = \frac{1}{2}\rho U|U|dC_d + \frac{1}{4}\pi\rho\dot{U}d^2C_m$$

Equation 3-38

where U is the free stream velocity with amplitude U_0, T is the period of oscillation, ρ the fluid density and d the body diameter.

Graham [3] conducted a discrete point vortex analysis assuming that the regular vortex shedding from an isolated edge should occur in Keulegan-

Carpenter numbers less than 10. The point vortices were calculated as they shed sequentially from an infinite wedge and traced as they moved with the fluid particles of an oscillatory flow. He attempted to provide a prediction of the vortex force component F_v which should be added to the flow inertia component as shown in Equation 3-39:

$$F = \frac{1}{4}\pi\rho C_{m0} d^2 \dot{U} + F_v$$

Equation 3-39

In this case Graham demonstrated that as $K_c \to 0$ and by defining the in-line vortex force coefficient as:

$$C_{Fv} = \frac{F_v}{\frac{1}{2}\rho U_0^2 d}$$

Equation 3-40

where $U = U_0 Sin\left(\frac{2\pi t}{T}\right)$ for oscillatory flow we would have:

$$C_{Fv} = K_c^{\frac{3-2\delta}{2\delta-1}} \Psi(\frac{t}{T})$$

Equation 3-41

where Ψ is a dimensionless function and δ depends on the internal angle of the edge of the body at the separation point. Therefore the Morison's equation presented in Equation 3-38 can be written as:

$$F = \frac{1}{4}\pi\rho\dot{U} d^2 C_{m0} + \frac{1}{2}\rho U_0^2 d K_c^{\frac{3-2\delta}{2\delta-1}} \Psi(\frac{t}{T})$$

Equation 3-42

By taking a Fourier integral of Equation 3-42 for a rectangular wedge over one cycle of the flow Graham showed that the coefficients in Equation 3-38 are:

$$C_D = AK_c^{\frac{3-2\delta}{2\delta-1}} \qquad \text{where} \qquad A = \frac{3\pi}{4}\int_0^1 \Psi(\tau) Sin(2\pi\tau) d\tau$$

Equation 3-43

and

$$C_m = C_{m0} + BK_c^{\frac{2}{2\delta-1}} \qquad \text{where} \qquad B = \frac{2}{\pi^2}\int_0^1 \Psi(\tau) Cos(2\pi\tau) d\tau$$

Equation 3-44

In this case for an inviscid analysis to be valid the Reynolds number $U_0 d/v$ should remain sufficiently large while the Keulegan-Carpenter number $U_0 T/d$ should be small.

Graham [3] concluded that for a cylinder in an oscillatory flow the vortex force and drag coefficients are proportional to $K_c^{(\frac{3-2\delta}{2\delta-1})}$ where K_c is the Keuligan-Carpenter number.

3.3. Rolling Barge in Potential Flow

Downie et al. [4] presented Equation 3-43 as:

$$C_D = \frac{3\pi}{4T}\int_0^T \frac{F_v\left(\frac{t}{T}\right)}{\frac{1}{2}\rho U_0^2 L} Sin\left(\frac{2\pi}{T}t\right) dt$$

Equation 3-45

where the parameters are same as the one defined for Equation 3-38 and L is a length scale that is characteristic of the body.

They used a Schwartz-Christoffel conformal transformation to map a semi-rectangle in to a half plane in order to represent a rectangular barge in a complex plane.

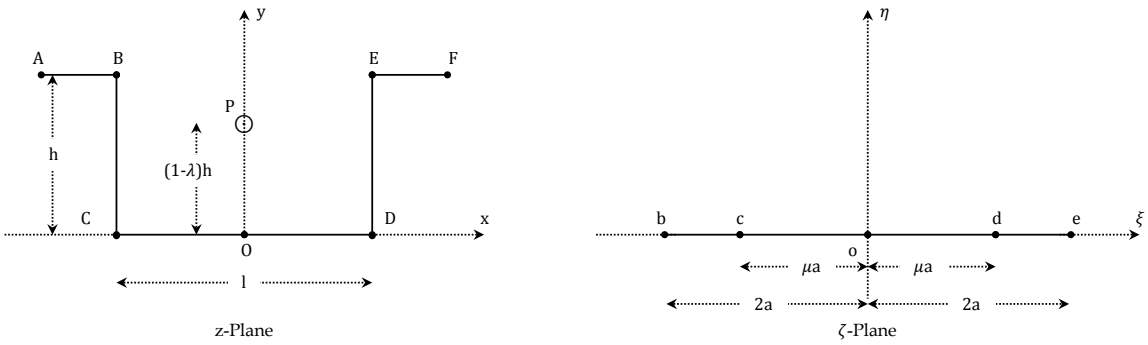

Figure 3-4: Box shaped barge transformation

Noting the notation in Figure 3-4 the complex conformal transformation used was defined as:

$$z = \int_0^{\zeta} \left(\frac{\zeta^2 - \zeta_d^2}{\zeta^2 - \zeta_e^2} \right)^{\frac{1}{2}} d\zeta$$

Equation 3-46

For a body rotating anticlockwise about the point O in z-plane with angular velocity of $\dot{\alpha}$ Downie et al. [4] calculated the instantaneous velocity directed towards the fluid at any point of the body as following:

$$V_n = \begin{bmatrix} iy\dot{\alpha} \\ x\dot{\alpha} \\ -iy\dot{\alpha} \end{bmatrix} = \begin{bmatrix} I\{z\} \\ R\{z\} \\ -I\{z\} \end{bmatrix} \dot{\alpha} \qquad \begin{matrix} x < 0 & y < 0 \\ & y = 0 \\ x > 0 & y < 0 \end{matrix}$$

Equation 3-47

The corresponding velocity in ζ-plane is then given as:

$$V_n' = V_n \frac{dz}{d\zeta}$$

Equation 3-48

A source distribution along the ξ axis with strength per unit length of $m(\zeta)$ was assumed in ζ-plane to represent the instantaneous boundary conditions as:

$$m(\zeta) = 2V_n'$$

Equation 3-49

Therefore the velocity q at any point ζ_p on the ξ axis of the transformed panel was demonstrated to be:

$$q = \frac{1}{2\pi}\int_{\zeta_b}^{\zeta_e} \frac{m(\zeta)}{\zeta_p - \zeta} d\zeta$$

Equation 3-50

From Figure 3-4 it is noted that the shedding edge in the real plane is at z_D. Hence the velocity q_d at the corresponding point ζ_d in the transformed plane was demonstrated as:

$$\begin{aligned}
q_d &= q_{bc} + q_{cd} + q_{de} \\
&= \frac{\dot{\alpha}}{2\pi}\left[\int_{\zeta_b}^{\zeta_c}\left\{\frac{f_1(\zeta)(\zeta_c-\zeta)^{\frac{1}{2}}}{(-\zeta_c-\zeta)^{\frac{1}{2}}(-\zeta_b-\zeta)^{\frac{1}{2}}(\zeta-\zeta_b)^{\frac{1}{2}}} - \frac{f_1(\zeta)|_b(\zeta_c-\zeta_b)^{\frac{1}{2}}}{(-\zeta_c-\zeta_b)^{\frac{1}{2}}(-2\zeta_b)^{\frac{1}{2}}(\zeta-\zeta_b)^{\frac{1}{2}}}\right\}d\zeta\right. \\
&\left. + \frac{2f_1(\zeta)|_b(\zeta_c-\zeta_b)}{(-\zeta_c-\zeta_b)^{\frac{1}{2}}(-2\zeta_b)^{\frac{1}{2}}}\right] \\
&+ \frac{\dot{\alpha}}{2\pi}\left[\int_{\zeta_c}^{\zeta_d}\left\{\frac{f_2(\zeta)(\zeta_d+\zeta)^{\frac{1}{2}}}{(\zeta_d-\zeta)^{\frac{1}{2}}(\zeta_e^2-\zeta^2)^{\frac{1}{2}}} - \frac{f_2(\zeta)|_d(2\zeta_d)^{\frac{1}{2}}}{(\zeta_d-\zeta)^{\frac{1}{2}}(\zeta_e^2-\zeta_d^2)^{\frac{1}{2}}}\right\}d\zeta\right. \\
&\left. + \frac{2f_2(\zeta)|_d(2\zeta_d)^{\frac{1}{2}}(\zeta_d-\zeta_c)^{\frac{1}{2}}}{(\zeta_e^2-\zeta_d^2)^{\frac{1}{2}}}\right] \\
&+ \frac{\dot{\alpha}}{2\pi}\left[\int_{\zeta_d}^{\zeta_e}\left\{\frac{f_3(\zeta)(\zeta_d+\zeta)^{\frac{1}{2}}}{(\zeta-\zeta_d)^{\frac{1}{2}}(\zeta_e^2-\zeta^2)^{\frac{1}{2}}} - \frac{f_3(\zeta)|_e(\zeta_d+\zeta_e)^{\frac{1}{2}}}{(\zeta_e-\zeta_d)^{\frac{1}{2}}(2\zeta_e)^{\frac{1}{2}}(\zeta_e-\zeta)^{\frac{1}{2}}}\right\}d\zeta\right. \\
&\left. + \frac{2f_3(\zeta)|_e(\zeta_d+\zeta_e)^{\frac{1}{2}}}{(2\zeta_e)^{\frac{1}{2}}}\right]
\end{aligned}$$

Equation 3-51

where:

$$f_1(\zeta) = -2\int_{\zeta_d}^{-\zeta}\left(\frac{\zeta^2-\zeta_d^2}{\zeta_e^2-\zeta^2}\right)^{\frac{1}{2}} d\zeta$$

Equation 3-52

$$f_2(\zeta) = 2\int_0^{\zeta}\left(\frac{\zeta_d^2 - \zeta^2}{\zeta_e^2 - \zeta^2}\right)^{\frac{1}{2}} d\zeta$$

Equation 3-53

$$f_3(\zeta) = -2\int_{\zeta_d}^{\zeta}\left(\frac{\zeta^2 - \zeta_d^2}{\zeta_e^2 - \zeta^2}\right)^{\frac{1}{2}} d\zeta$$

Equation 3-54

Downie et al. [4] then derived the local velocity of the fluid relative to the point ζ_d in the transformed plane for a body rotating anticlockwise about any point P in the real plane as:

$$u = q_d + h(1-\lambda)\dot{\alpha}$$

Equation 3-55

Hence for a barge rolling with an oscillatory motion about point P, for which the oscillatory motion can be expressed as $\dot{\alpha} = \omega\hat{\alpha}Sin(\omega t)$, the relative fluid velocity was:

$$u_0 = [q_d' a + h' a(1-\lambda)]\omega\hat{\alpha} = \left[\frac{q_d'}{l'} + \frac{h'}{l'}(1-\lambda)\right] l\omega\hat{\alpha}$$

Equation 3-56

where $q_d = q_d' a\dot{\alpha}$, $l = l'a$, $h = h'a$ and $\omega = \frac{2\pi}{T}$.

Since the forces on the isolated edge associated with the vortex shedding are known in terms of drag coefficient as presented in Equation 3-45, in order to calculate the drag coefficient Downie et al. [5] had to match the two flows in the immediate vicinity of the shedding edge. In order to do this a conformal transformation was used as below to map an infinite wedge into a half plane, see Figure 3-5:

$$z' = e^{-i\frac{\pi}{2}} L^{-\frac{1}{2}} \zeta^{\frac{3}{2}}$$

Equation 3-57

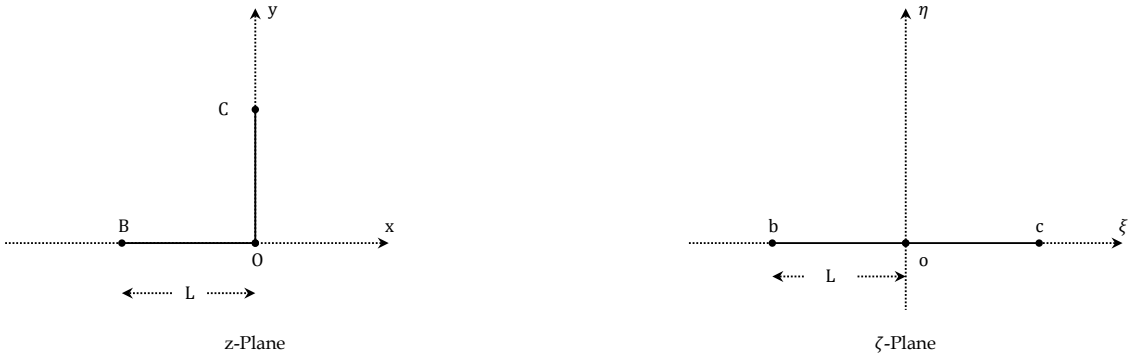

Figure 3-5: The 90° infinite wedge transformation

Noting that the distance of any point z from the shedding edge of the barge located at z_D in the real plane is:

$$z - z_D = \int_{\zeta_d}^{\zeta} \left\{ \frac{(\zeta + \zeta_d)(\zeta - \zeta_d)}{(\zeta + \zeta_e)(\zeta - \zeta_e)} \right\}^{\frac{1}{2}} d\zeta$$

Equation 3-58

close to the shedding edge where $\zeta \to \zeta_d$ the distance from the shedding edge is:

$$z' = e^{-i\frac{\pi}{2}} \left(\frac{2\zeta_d}{\zeta_e^2 - \zeta_d^2} \right)^{\frac{1}{2}} \zeta'^{\frac{3}{2}}$$

Equation 3-59

where $z - z_D$ and $\zeta - \zeta_d$ were presented as z' and ζ' respectively. Hence in order for Equation 3-57 to become equal to Equation 3-59 it was concluded that:

$$L = \frac{9}{4} \left(\frac{4 - \mu^2}{2\mu} \right) a$$

Equation 3-60

where $\zeta_d = \mu a$ and $\zeta_e = 2a$, or:

$$\frac{L}{l} = \frac{9}{4l'} \left(\frac{4 - \mu^2}{2\mu} \right)$$

Equation 3-61

It was demonstrated from Equation 3-61 that:

$$Q_E = u_0 \frac{d\zeta}{dz}\Big|_{z,\zeta \to z_D,\zeta_d}$$

Equation 3-62

concluding that if the ratio of the length scale $\frac{L}{l}$ is equal to $\frac{9}{4l'}\left(\frac{4-\mu^2}{2\mu}\right)$ and if the velocity U_0 is same in both cases the velocity field in the near vicinity of the infinite wedge is identical to the local velocity field round the shedding edge of the rolling barge.

Noting the geometry presented in Figure 3-6 which demonstrates the relationship between the damping torque χ and the vortex force in single edge F_v Downie et al. [4] concluded that:

$$\chi(t/T) = 2[RF_v(t/T)Cos\beta] = \frac{l}{\sqrt{2}}\left[1 + \frac{2h'}{l'}(1-\lambda)\right]F_v(t/T)$$

Equation 3-63

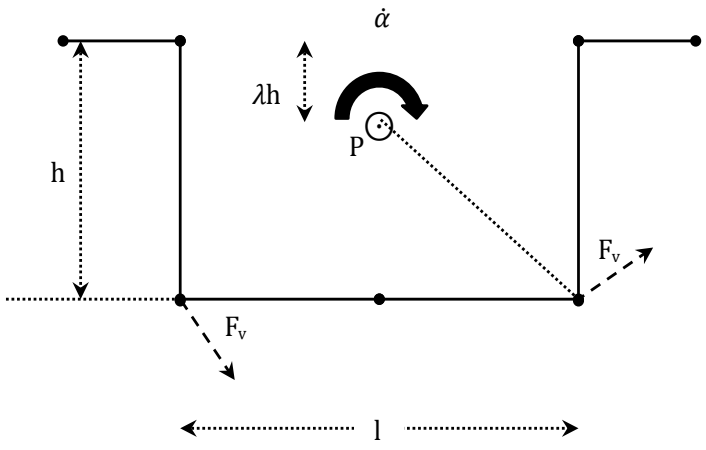

Figure 3-6: Damping torque

The earlier analysis indicates that the F_v acts near the edge and perpendicular to the edge's bisector. By rewriting Equation 3-63 as a Fourier series:

$$\chi(t/T) = \rho\omega^2 l^4 \hat{\alpha}^2 \sum \hat{\chi}_n \, Sin(n\omega t)$$

Equation 3-64

and assuming the barge motion will follow equation of $I\ddot{\alpha} + \varepsilon\dot{\alpha} + \omega^2 I\alpha = 0$ the equivalent linearized damping force was demonstrated to be:

$$\varepsilon = \rho\omega l^4 \hat{\alpha}\hat{\chi}_1 = \rho\omega l^4 \hat{\alpha} \, \frac{2}{T}\int_0^T \frac{\chi(t/T)}{\rho\omega^2 l^4 \hat{\alpha}^2} Sin(\omega t)dt$$

Equation 3-65

Finally Downie et al. [4] presented the following expression for the damping coefficient:

$$\hat{\chi}_1 = c\left[\frac{q'_d}{l'} + \frac{h'}{l'}(1-\lambda)\right]\left|\left[\frac{q'_d}{l'} + \frac{h'}{l'}(1-\lambda)\right]\right|\left[1 + \frac{2h'}{l'}(1-\lambda)\right]$$

Equation 3-66

where c is constant dependent on geometry of the barge and is given by:

$$c = 0.529\left(\frac{4-\mu^2}{\mu l'}\right)$$

Equation 3-67

Noting Figure 3-4, for shedding edges of D and E in z-plane Downie et al. [5] presented Equation 3-46 as:

$$z_D = \zeta_e \int_0^{\mu}\left(\frac{r^2-\mu^2}{r^2-1}\right)dr + ih = \zeta_e[E(\mu^2) - (1-\mu^2)K(\mu^2)] + ih$$

Equation 3-68

$$z_E = z_D - i\zeta_e \int_{\mu}^{1}\left(\frac{r^2-\mu^2}{1-r^2}\right)dr = z_D - i\zeta_e[E(1-\mu^2) - \mu^2 K(1-\mu^2)]$$

Equation 3-69

therefore:

$$l = 2\zeta_e[E(\mu^2) - (1-\mu^2)K(\mu^2)] = 2\zeta_e I_2$$

Equation 3-70

$$h = \zeta_e[E(1-\mu^2) - \mu^2 K(1-\mu^2)] = \zeta_e I_1$$

Equation 3-71

where $\mu = \zeta_d/\zeta_e$, $r = \zeta/\zeta_e$ and K and E are complete elliptical integrals of first and second kind respectively.

The body matching parameter a_{fv} was defined in terms of elliptical integrals as:

$$a_{fv} = -\frac{i}{2\pi}\int_b^e \frac{\left(\zeta^2 - {\zeta_d}^2\right)^{\frac{1}{2}}}{(\zeta-\zeta_d)\left(\zeta^2 - {\zeta_e}^2\right)^{\frac{1}{2}}} dr = \frac{1}{\pi}(iI_3 - I_4)$$

Equation 3-72

where $I_3 = \mu K(\mu^2)$ and $I_4 = \mu K(1-\mu^2)$.

In a same manner the edge matching parameter was presented as:

$$L = \frac{9}{4}\frac{\mu^2 - 1}{2\mu}\frac{l}{2I_2}$$

Equation 3-73

In line with Equation 3-40 the vortex force at one edge of a floating body was stated to be:

$$f_v = \frac{1}{2}\rho U_0^2 L\Psi(t)a_{fv} = \frac{1}{2}\rho U_0^2 l\frac{9}{4}\left(\frac{1-\mu^2}{2\mu}\right)\frac{1}{\pi}\left(\frac{I_3 - iI_4}{2I_2}\right)\Psi(t)$$

Equation 3-74

Downie et al. [5] assumed that if the potentials ϕ_v and ϕ_h are calculated at a point either side of a shedding edge the U_0 at the shedding edge must be equal to $|\phi_v - \phi_h|/|\Delta\zeta|$ where $\Delta\zeta$ is the distance between the corresponding points in ζ-plane. In this case the vortex shedding roll moment F_{v4} was formulated as:

$$F_{v4} = \frac{1}{2}\rho c_4 l^{\frac{4}{3}} \left|\frac{\phi_v - \phi_h}{\Delta\zeta}\right|^2 \Psi(t)$$

Equation 3-75

in which c_4 is a coefficient representing the lever arm for the vortex roll moment, ϕ_v is the velocity potential at the vertical side of the shedding edge, ϕ_h is the velocity potential at horizontal side of the shedding edge, $\Delta\zeta$ is the distance between points in the ζ-plane on either side of the edge and $\Psi(t)$ is the dimensionless vortex force coefficient which is pre-calculated using the discrete vortex method [3].

In a similar manner the sway vortex force F_{v2} and the heave vortex force F_{v3} was stated to be:

$$F_{v2} = \frac{1}{2}\rho c_2 l^{\frac{1}{3}} \left|\frac{\phi_v - \phi_h}{\Delta\zeta}\right|^2 \Psi(t)$$

Equation 3-76

$$F_{v3} = \frac{1}{2}\rho c_3 l^{\frac{1}{3}} \left|\frac{\phi_v - \phi_h}{\Delta\zeta}\right|^2 \Psi(t)$$

Equation 3-77

4 Viscous Damping Mathematical Development

The methodology explained in Section 3.3 is used in this work as a basis to develop a practical procedure for calculating the vortex force due to sway, heave and roll motions of a box shaped barge in regular waves. The procedure is then advanced further to include calculation of the viscous roll damping in irregular waves.

As outlined previously Downie et al. [5] demonstrated that the oscillatory motion of a boxed shape vessel could be reasonably predicted by use of discrete vortex method including the viscous effects. In their method the relative fluid velocity at the shedding edge was calculated directly. This required several assumptions to be made in order to estimate the relative fluid velocity from the mathematical model of the rolling barge. Therefore significant amount of effort was made to estimate the relative velocity which was then used in a final step to calculate the final viscous damping.

The new development was based on use of conventional diffraction radiation software to calculate the velocity at the shedding edge. Therefore the mathematical developments are needed to be such to allow integration of the method with the utilised diffraction radiation software.

The latest mathematical formulation based on the background methodology explained in Section 3.3 is presented here. Implementation of the method as an add-on black box software is explained in Chapter 5.

4.1. Mathematical Linearization for Regular Waves

A rectangular body with oscillating flow around its boundaries is shown in Figure 4-1.

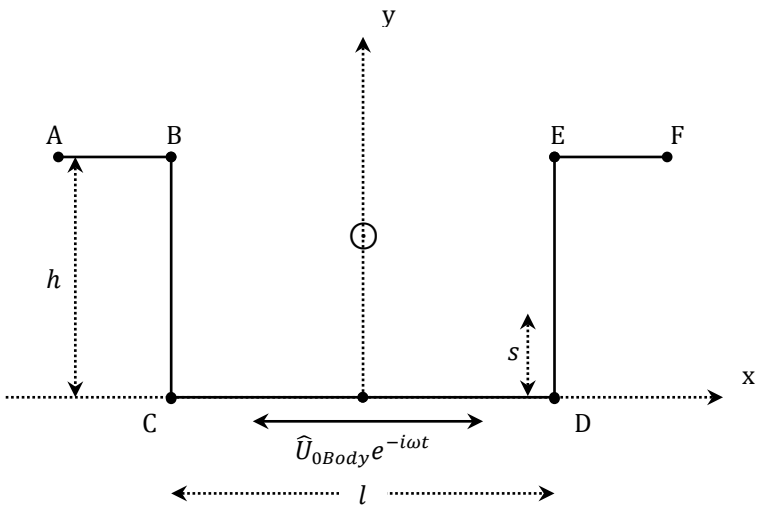

Figure 4-1: Oscillating body

Noting the transformation methodology outlined in Chapter 3 a conformal transformation can be used to map an infinite wedge into a half plane as shown in Figure 3-5.

We consider the case of a general rectangular hull with beam l, draught h and apply the Schwartz-Christoffel transformation between the physical z-pannel and the transformed ζ-plane as outlined in Chapter 3.

From [3] or by considering the relative size of the q^2 term in the pressure which $q^2 \to 0$ relatively as $K_c \to 0$ and as $W = \Phi + i\Psi$ where Ψ is constant on the body we have:

$$p = -\rho \frac{\partial \Phi}{\partial t} = -\rho \frac{\partial W}{\partial t}\Big|_{on\ body}$$

Equation 4-1

Consider a vortex shed from the edge D, strength Γ and position z_0 (or ζ_0). Since W is linear in Γ the effects of many vortices can be added together. The vortex at ζ_0 (position in ζ-plane) has an image $-\Gamma$ at ζ_0^* where ζ_0^* is complex conjugate of ζ_0. Note that the vortex strength Γ is preserved in a conformal transformation. Therefore the complex potential representing the flow field due to the vortex is:

$$W_v = \frac{i\Gamma}{2\pi}\{\ln(\zeta - \zeta_0) - \ln(\zeta - \zeta_0^*)\}$$

Equation 4-2

The free stream only contributes to the inertia C_M. It can now be assumed that the force comes from the pressure field over the whole of the body not just close to the edge which will be shown to be true. Therefore since we are assuming small amplitude motion and noting the notation shown in Figure 3-5, for most of the p contribution to the forces we have $|\zeta - \zeta_d| \gg |\zeta_0 - \zeta_d|$. Therefore by expanding the logs we have:

$$W_v \to \frac{-i\Gamma(\zeta - \zeta_0^*)}{2\pi(\zeta - \zeta_d)}$$

Equation 4-3

hence:

$$p = -\frac{i\rho}{2\pi}\frac{\partial}{\partial t}\{\Gamma(\zeta_0 - \zeta_0^*)\}\frac{1}{\zeta - \zeta_d}$$

Equation 4-4

The singularity is a dipole along the real axis $\zeta = \xi$. The potential distribution has a discontinuity at $\xi = \zeta_d$ which represents the jump $\Delta\Phi = \Gamma$ that occurs at the path crossing the vortex sheet joining Γ to the edge. This jump is correct for

the potential and is consistent with the pressure to be continuous across the edge when the q^2 term is considered. Assuming constant total pressure of:

$$\frac{p_1}{\rho} + \frac{\partial \Phi_1}{\partial t} + \frac{1}{2} q_1^2 = \frac{p_2}{\rho} + \frac{\partial \Phi_2}{\partial t}$$

Equation 4-5

since $q_2 = 0$ (stagnation) on the underside of the sheet and

$$\frac{\partial \Gamma}{\partial t} = \frac{1}{2} q_1^2$$

Equation 4-6

therefore if $\Phi_1 - \Phi_2 = \Gamma$, then:

$$p_1 = p_2$$

Equation 4-7

The dipole discontinuity in Φ at D is infinite but it does overall correctly approximate the result for the vortex plus image at a finite distance from the edge. In particular both distributions show that $p \to 0$ at large distances from the edge at a rate proportional to $[\xi^{-1}(\zeta - plane)]$ i.e. $s^{-\frac{1}{3}}$. The force on the edge DE is therefore:

$$F_{DE} = i \int_D^E p dz = -\frac{\rho}{2\pi} \frac{\partial}{\partial t} [\Gamma(\zeta_0 - \zeta_0^*)] \int_{\zeta_d}^{\zeta_e} \frac{1}{(\zeta - \zeta_d)} \frac{dz}{d\zeta} d\zeta$$

Equation 4-8

Using the Schwartz-Christoffel formula for $\frac{dz}{d\zeta}$ we have:

$$F_{DE} = +\frac{i\rho}{2\pi} \frac{\partial}{\partial t} [\Gamma(\zeta_0 - \zeta_0^*)] \int_1^{\lambda} \left(\frac{(\sigma + 1)}{(\sigma - 1)(\lambda^2 - \sigma^2)} \right)^{\frac{1}{2}} d\sigma$$

Equation 4-9

where $= \frac{1}{\mu} = \frac{\zeta_e}{\zeta_d}$, $\sigma = \frac{\xi}{\zeta_d}\left(= \frac{\Re(\zeta)}{\zeta_d}\right)$ and $\zeta_0 - \zeta_0^*$ is imaginary. Note in this last expression that there is a degree of ambiguity as to whether $+i$ or $-i$ should be taken. It is assumed that $+i$ gives the correct solution, similarly:

$$F_{CD} = +\frac{\rho}{2\pi}\frac{\partial}{\partial t}[\Gamma(\zeta_0 - \zeta_0^*)]\int_{-1}^{1}\left(\frac{(\sigma+1)}{(1-\sigma)(\lambda^2-\sigma^2)}\right)^{\frac{1}{2}} d\sigma$$

Equation 4-10

$$F_{BC} = +\frac{i\rho}{2\pi}\frac{\partial}{\partial t}[\Gamma(\zeta_0 - \zeta_0^*)]\int_{-\lambda}^{-1}\left(\frac{-\sigma-1}{(1-\sigma)(\lambda^2-\sigma^2)}\right)^{\frac{1}{2}} d\sigma$$

Equation 4-11

$$F_{DE} = +\frac{i\rho}{2\pi}\frac{\partial}{\partial t}[\Gamma(\zeta_0 - \zeta_0^*)]\int_{1}^{\lambda}\left(\frac{(\sigma+1)}{(\sigma-1)(\lambda^2-\sigma^2)}\right)^{\frac{1}{2}} d\sigma$$

Equation 4-12

Combining these we have:

$$F_x = F_{DE} + F_{BC} = \frac{i\rho}{2\pi}\frac{\partial}{\partial t}[\Gamma(\zeta_0 - \zeta_0^*)]\int_{1}^{\lambda}\left(\frac{1}{(\sigma^2-1)(\lambda^2-\sigma^2)}\right)^{\frac{1}{2}} 2\sigma d\sigma$$

Equation 4-13

It should be noted that the force is suction on DE and pressure on BC. By substituting $\sigma^2 = 1 + (\lambda^2 - 1)(\sin\theta)^2$ we have:

$$F_x = \frac{i\rho}{\pi}\frac{\partial}{\partial t}[\Gamma(\zeta_0 - \zeta_0^*)]$$

Equation 4-14

This is half the result given in [3] for a closed body which is same for all $\frac{h}{l}$. Then the vertical force is:

$$F_y = F_{CD} = \frac{\rho}{\pi}\frac{\partial}{\partial t}[\Gamma(\zeta_0 - \zeta_0^*)]\mu K(\mu^2)$$

Equation 4-15

where K is an elliptic integral. For $AR = 1$ (i.e. $h = \frac{l}{2}$ and $\mu = \frac{1}{\sqrt{2}}$), $K(\mu^2) = 1.845$, so:

$$F_y = 0.417\rho \frac{\partial}{\partial t}[\Gamma(\zeta_0 - \zeta_0^*)]$$

Equation 4-16

Moments about O where O is in the middle of CD may be similarly evaluated as:

$$M_{vo} = -i\rho \int pz^* dz = M_{BC} + M_{DE} + M_{CD}$$

Equation 4-17

where M_{BC} , M_{CD} and M_{DE} represent moments due to force acting on these faces and:

$$M_{BC} + M_{DE}$$
$$= -\frac{i\rho\zeta_d}{2\pi}\frac{\partial}{\partial t}[\Gamma(\zeta_0 - \zeta_0^*)]\int_1^{\lambda} \frac{2\sigma}{\{(\sigma^2-1)(\lambda^2-\sigma^2)\}^{\frac{1}{2}}}\left\{\int_1^{\sigma}\left(\frac{\sigma'^2-1}{\lambda^2-\sigma'^2}\right)^{\frac{1}{2}} d\sigma'\right\} d\sigma$$

Equation 4-18

$$M_{CD} = \frac{i\rho\zeta_d}{2\pi}\frac{\partial}{\partial t}[\Gamma(\zeta_0 - \zeta_0^*)]\int_0^{1} \frac{2\sigma}{\{(1-\sigma^2)(\lambda^2-\sigma^2)\}^{\frac{1}{2}}}\left\{\int_0^{\sigma}\left(\frac{1-\sigma'^2}{\lambda^2-\sigma'^2}\right)^{\frac{1}{2}} d\sigma'\right\} d\sigma$$

Equation 4-19

Therefore the moment about the axis at the free surface is given by:

$$M_v = M_{vo} + F_x h = \frac{i\rho h}{2}\frac{\partial}{\partial t}\{\Gamma(\zeta_0 - \zeta_0^*)\}\left[1 + \frac{\mu(I_{CD} - I_{BCDE})}{\pi\big(E(1-\mu^2) - \mu^2 K(1-\mu^2)\big)}\right]$$

Equation 4-20

where E and K are elliptical integrals and:

$$I_{CD} = \int_0^1 \frac{2\sigma}{\{(1-\sigma^2)(\lambda^2-\sigma^2)\}^{\frac{1}{2}}} \left\{ \int_0^\sigma \left(\frac{1-\sigma'^2}{\lambda^2-\sigma'^2} \right)^{\frac{1}{2}} d\sigma' \right\} d\sigma$$

Equation 4-21

$$I_{BCDE} = \int_1^\lambda \frac{2\sigma}{\{(\sigma^2-1)(\lambda^2-\sigma^2)\}^{\frac{1}{2}}} \left\{ \int_1^\sigma \left(\frac{\sigma'^2-1}{\lambda^2-\sigma'^2} \right)^{\frac{1}{2}} d\sigma' \right\} d\sigma$$

Equation 4-22

The roll moment about the origin O (middle of base) is given by:

$$M_{vo} = \frac{\rho\zeta_d}{2\pi} \frac{\partial}{\partial t} \{\Gamma(\zeta_0 - \zeta_0^*)\}[I_{CD} - I_{BCDE}]$$

Equation 4-23

Note the change of sign as F_x and F_y exert opposite moments at O. Using the fact that $F_x = \frac{\rho}{2} \frac{\partial}{\partial t} \{\Gamma(\zeta_0 - \zeta_0^*)\}$, the conventional moment about the centre of the barge at the mean free surface is:

$$M_v = \frac{i\rho h}{2\pi} \frac{\partial}{\partial t} \{\Gamma(\zeta_0 - \zeta_0^*)\} \left[\pi + \frac{\mu(I_{CD} - I_{BCDE})}{\big(E(1-\mu^2) - \mu^2 K(1-\mu^2)\big)} \right]$$

Equation 4-24

This is the moment over the whole barge hull due to shedding from edge D, hence:

$$M_v(both\ edges) = \frac{i\rho h}{\pi} \frac{\partial}{\partial t} \{\Gamma(\zeta_0 - \zeta_0^*)\} \left[\pi + \frac{\mu(I_{CD} - I_{BCDE})}{\big(E(1-\mu^2) - \mu^2 K(1-\mu^2)\big)} \right]$$

Equation 4-25

The moment is generated by $q_e s^{\frac{1}{3}}$ at the shedding edge. Generally for a rectangular edge body with edge angle of 90° if F_v is assumed to be the force due to vortex shedding on one edge of the body, from the scaling analysis we have:

$$\frac{F_{v_{Body}}(1\ edge)}{F_{v\ Inf.\ edge}} = \frac{\left(q_e s^{\frac{1}{3}}\right)^3_{Body}}{\left(q_e s^{\frac{1}{3}}\right)^3_{Inf.\ edge}} \cdot \frac{U_{0\ Inf.\ edge}}{U_{0\ Body}}$$

Equation 4-26

where s is the distance along the surface from edge in physical plane and q_e is the surface velocity generated by potential flow (i.e. diffraction-radiation code) at a distance of s from the edge.

Noting Equation 4-26 it can be written that:

$$C_{Fv\ Body} = \frac{F_{v\ Body}}{\frac{1}{2}\rho U^2_{0Body} d}$$

Equation 4-27

where d is a length scale of body. Then using the analysis for a flow past an infinite edge it can be concluded that:

$$C_{Fv\ Body} = \frac{27A}{8d}\left(\frac{q_e s^{\frac{1}{3}}}{U_0}\right)^3_{Body}$$

Equation 4-28

Hence to calculate the force on the body edge it is just necessary to evaluate the following equation:

$$C_{Fv\ Body} = \frac{27A}{8}\left[\left(\frac{q_e}{U_0}\right)\left(\frac{s}{d}\right)^{\frac{1}{3}}\right]^3_{Body}$$

Equation 4-29

where A is a pre-calculated factor by Graham [3].

It should be noted that in this case as $s \to 0$ the q_e becomes singular but $q_e s^{\frac{1}{3}}$ tends to a finite value.

Continuing from Equation 4-26 and from the Schwartz-Christoffel transformation expanding $\frac{\mathrm{dz}}{\mathrm{d}\zeta}$ near $\zeta = \zeta_d$, $z = z_D \pm (i)$s where s is the distance from the edge we have:

$$U_{0\ Inf.\ edge} = \frac{3}{2}\left(q_e s^{\frac{1}{3}}\right)^3_{Inf.\ edge}$$

Equation 4-30

and

$$U_{0\ Body}(rect.hull) = \left(\frac{3\zeta_d}{(\zeta_e^2-\zeta_d^2)}\right)^{\frac{1}{3}}\left(q_e s^{\frac{1}{3}}\right)_{Body}$$

Equation 4-31

Also

$$F_{v\ Inf.\ edge} = \frac{1}{2}\rho U^2_{0\ Inf.\ edge}\cdot A$$

Equation 4-32

where A is the coefficient given in [3]. Then:

$$F_{v_{Body}}(1\ edge) = 1.170\rho A\left(\frac{1}{\mu^2}-1\right)^{\frac{1}{3}}\left(q_e s^{\frac{1}{3}}\right)^2_{Body}\cdot\zeta_d$$

Equation 4-33

However $F_{v\ Inf.\ edge}$ which is given in [3] is obtained by integrating using the Residue Theorem around a closed contour. This is not possible for a body floating at the free surface. In the case of floating hull F_v and M_v come from integration of the pressure $\left(\rho\frac{\partial W}{\partial t}\right)$ along the finite open line $BCODE$ or $-\zeta_e \le \xi\left(\equiv \Re(\zeta)\right) \le +\zeta_e$. Hence the results given above for F_v and M_v on a rectangular hull replace the result in [3] $Z_v\ (i.e.\ F_v) = (-i)\rho\frac{\partial}{\partial t}\{\Gamma(\zeta_0 - \zeta_0^*)\}$, hence:

$$F_{v_{hull}}(1\ edge) = F_{v\ Inf.\ edge}\left[\frac{1}{2}, \frac{\mu}{\pi}K(\mu^2)\right]$$

Equation 4-34

These are the two components (F_x, F_y) of F_v and the $\sqrt{2}$ coming from the fact that $F_{v\ Inf.\ edge}$ is perpendicular to the bisector of the 90° edge. Similarly:

$$M_{v_{hull}}(1\ edge) = \frac{1}{2}\left[1 + \frac{\mu(I_{CD} - I_{BCDE})}{\pi\big(E(1-\mu^2) - \mu^2 K(1-\mu^2)\big)}\right] F_{v\ Inf.\ edge} \cdot h$$

Equation 4-35

Therefore for a floating hull with two sharp 90° edges we have:

$$F_x[sway] = 1.170\rho A\left(\frac{\frac{1}{\mu} - \mu}{\big(E(1-\mu^2) - \mu^2 K(1-\mu^2)\big)}\right)^{\frac{1}{3}}\left(q_e s^{\frac{1}{3}}\right)^2 \cdot h^{\frac{1}{3}}$$

Equation 4-36

$$F_x[heave] = 2.340\rho A\frac{\mu K(\mu^2)}{\pi}\left(\frac{\frac{1}{\mu} - \mu}{\big(E(1-\mu^2) - \mu^2 K(1-\mu^2)\big)}\right)^{\frac{1}{3}}\left(q_e s^{\frac{1}{3}}\right)^2 \cdot h^{\frac{1}{3}}$$

Equation 4-37

$$M_v[roll] = 1.170\rho A\left[1 + \frac{\mu(I_{BD} - I_{ABDE})}{\pi\big(E(1-\mu^2) - \mu^2 K(1-\mu^2)\big)}\right]$$
$$\left(\frac{\frac{1}{\mu} - \mu}{\big(E(1-\mu^2) - \mu^2 K(1-\mu^2)\big)}\right)^{\frac{1}{3}}\left(q_e s^{\frac{1}{3}}\right)^2 h^{\frac{4}{3}}$$

Equation 4-38

For a box shaped barge defined in Figure 4-2 F_{vj} is defined as the force per unit length due to vortex shedding where j is index of the motion under study i.e. $j = 2$ indicates sway, $j = 3$ indicates heave and $j = 4$ indicates roll of the barge, hence $F_x[sway] = F_{v2}$, $F_x[heave] = F_{v3}$ and $M_v[roll] = F_{v4}$.

Noting that the beam and draught of the barge are defined by l and h respectively the barge cross sectional aspect ratio can be defined as $R = \frac{l}{2h}$.

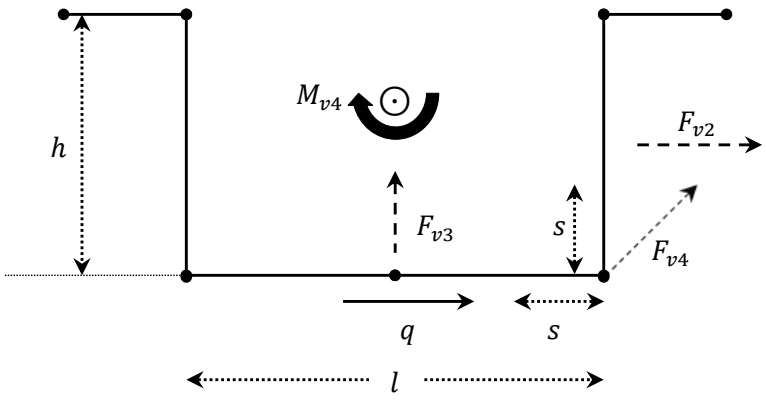

Figure 4-2: Barge geometry

The tangential fluid velocity at body surface relative to axes fixed in body is denoted by q where $q = \sum q_j = \sum i\omega\eta_j$ in which ω is the oscillatory motion frequency and η_j is the j-th degree of freedom of the barge.

The distance from the vortex shedding edge in which the relative velocity is calculated is shown by s.

The vortex force coefficient $A + iB$ from discrete vortex method pre-calculated for an infinite right angle edge is taken to be $1.566 - 0.157i$. The Schwartz-Christoffel ratio μ as defined in Section 3.3 can be calculated by iterative method for a given AR.

Noting Equation 3-70 from which I_2 is defined as $[E(\mu^2) - (1 - \mu^2)K(\mu^2)]$ in which K and E are complete elliptical integrals of first and second kind respectively, the sway and heave vortex shedding forces as well as roll vortex shedding moment can be defined as:

$$F_{v2} = a_2 + ib_2 = \frac{3^{\frac{5}{3}}}{2^{\frac{4}{3}}}\frac{(A+iB)}{\pi^2}\rho l\left(\frac{1-\mu^2}{\mu I_2}\right)^{\frac{1}{3}}\left\{\frac{\pi}{2}\right\}\left|\frac{qs^{\frac{1}{3}}}{l^{\frac{1}{3}}}\right|\left(\frac{q_2 s^{\frac{1}{3}}}{l^{\frac{1}{3}}}\right)\frac{H}{2}x$$

Equation 4-39

$$F_{v3} = a_3 + ib_3 = \frac{3^{\frac{5}{3}}}{2^{\frac{4}{3}}}\frac{(A+iB)}{\pi^2}\rho l\left(\frac{1-\mu^2}{\mu I_2}\right)^{\frac{1}{3}}\{\mu K(\mu^2)\}\left|\frac{qs^{\frac{1}{3}}}{l^{\frac{1}{3}}}\right|\left(\frac{q_3 s^{\frac{1}{3}}}{l^{\frac{1}{3}}}\right)\frac{H}{2}x$$

Equation 4-40

$$F_{v4} = a_4 + ib_4 = \frac{3^{\frac{5}{3}}}{2^{\frac{4}{3}}}\frac{(A+iB)}{\pi^2}\rho l\left(\frac{1-\mu^2}{\mu I_2}\right)^{\frac{1}{3}}\left\{\frac{\mu l I_c}{4I_2}\right\}\left|\frac{qs^{\frac{1}{3}}}{l^{\frac{1}{3}}}\right|\left(\frac{q_4 s^{\frac{1}{3}}}{l^{\frac{1}{3}}}\right)\frac{H}{2}x$$

Equation 4-41

where a_j is the vortex induced added mass and b_j is the vortex induced damping coefficient.

Applying the formulation to a three dimensional hydrodynamic model of a box shaped barge in an industry standard inviscid seakeeping code, q is the total fluid velocity relative to the body at the shedding edge calculated for the combined six degree of freedom motion and q_j is the total velocity relative to the body at the shedding edge calculated in the forced motion mode for the degree of freedom under study. In this case s is the distance from vortex shedding edge to centre of the facet in which the velocity is calculated, x is width of the facet along the length and H is the height of the regular wave for which the viscous damping is linearized.

Since the Schwartz-Christoffel ratio μ can be calculated by iteration for a given aspect ratio and noting the aspect ratio of the cross section of the barge which is defined as $AR = \frac{l}{2h}$ from a Schwartz-Christoffel transformation it can be shown that $AR = \frac{I_2}{I_1} = \frac{E(\mu^2)-(1-\mu^2)K(\mu^2)}{E(1-\mu^2)-\mu^2 K(1-\mu^2)}$ [5].

Finally if $\kappa = \frac{1}{\mu}$ then:

$$I_c = \int_1^{\kappa} \left\{ \int_{\sigma}^{\kappa} \left(\frac{\sigma'^2 - 1}{\kappa^2 - \sigma'^2} \right)^{\frac{1}{2}} d\sigma' \right\} \frac{2\sigma \, d\sigma}{[(\kappa^2 - \sigma^2)(\sigma^2 - 1)]^{\frac{1}{2}}}$$

$$+ \int_0^1 \left\{ \int_1^{\sigma} \left(\frac{1 - \sigma'^2}{\sigma'^2 - \kappa^2} \right)^{\frac{1}{2}} d\sigma' \right\} \frac{2\sigma \, d\sigma}{[(\kappa^2 - \sigma^2)(1 - \sigma^2)]^{\frac{1}{2}}}$$

Equation 4-42

The velocity at the tip of the shedding edge becomes singular in the sharp edged potential flow model. Therefore the velocity of the fluid at the edge for combined motion (i.e. q) and the forced mode motion (i.e. q_j) are calculated using weighted averaging of the velocity at the two facets on each side of the vortex shedding edge. Weights are based on the distance between the centres of the facets to the shedding edge (i.e. s). This will eliminate the problem of having a singularity in the calculation of relative fluid velocity at the tip of the shedding edge.

By integrating the calculated vortex force on assumed vortex shedding strips along the length of the barge the total vortex shedding force can be calculated. It should be noted that since the relative velocity between the body and the fluid is not same in portside and starboard side of the vessel, the calculated vortex forces in either sides are different.

4.2. Mathematical Linearization for Irregular Waves

After developing the numerical model for the regular waves, an attempt was made to apply the method to calculation of the vortex shedding damping in irregular waves.

Initial investigation was based on the equivalent linearization method introduced by Kaplan [86]. For the equation of the roll motion of a floating

vessel Kaplan [86] assumed that the nonlinearity is to be in form of velocity square damping as following:

$$\ddot{\eta}_4 + 2\alpha\dot{\eta}_4 + \beta\dot{\eta}_4|\dot{\eta}_4| + \omega_0^2\eta = \omega_0^2 f(t)$$

Equation 4-43

where $f(t)$ is an arbitrary random function equivalent to the effective wave slope. Kaplan then provided the mathematical formulation for estimation of the equivalent linear roll damping coefficient in a given irregular wave spectrum.

Following successful implementation of the methodology stated in Section 5.2.1 and noting Kaplan's methodology [86] preliminary investigation of roll damping linearization in irregular waves was done which consisted of discretising the given wave spectrum to several regular waves and calculating the roll RAO amplitude for the estimated representative regular waves.

This approach was based on the assumption that if an irregular wave can be deconstructed to several regular waves as shown in Figure 4-3 then the viscous damping can be calculated for each representative regular wave individually. In this case the damped RAO linearized for variation of regular wave heights within the irregular wave frequency range can be calculated.

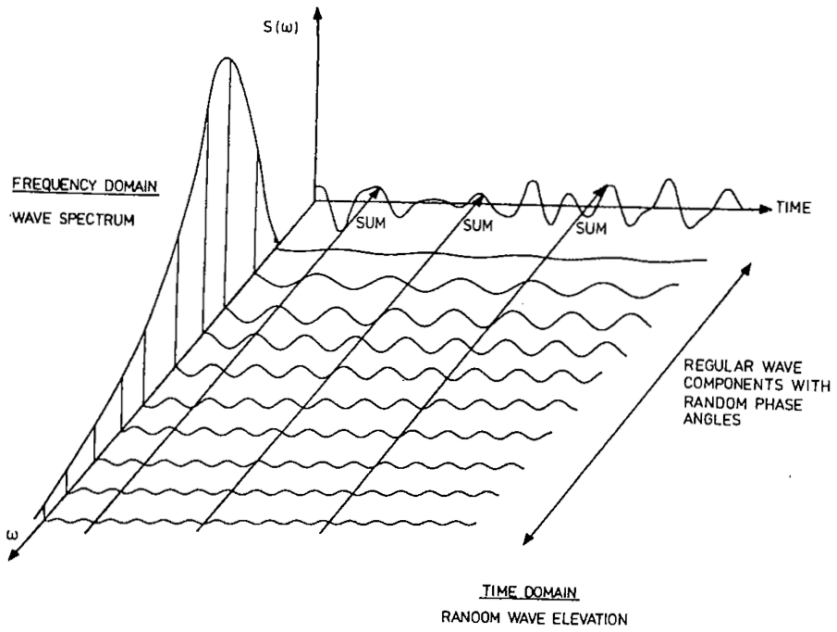

Figure 4-3: Connectione between frequency domain and time domain representation of waves [13]

However since the calculated roll damping is dependent on the assumed regular wave height amplitude and the amplitude of the regular wave height depends on the assumed width of the frequency bin on the wave spectrum the method did not seem to be sound. This was due to the fact that change in number of discretisation frequency bins on the irregular wave spectrum resulted in change in amplitude of the calculated wave heights for each bin. Consequently the calculated viscous damping for each bin varied resulting in an inconsistent damped RAO.

Based on this experience it was concluded that any viscous roll damping linearization for an irregular wave spectrum should be such that variations in wave spectrum frequency discretisation do not affect the final calculated RAO amplitude for each assumed frequency bin.

In this regards for calculating the viscous roll damping for a given wave spectrum the mathematical development presented in Section 4.1 was modified. The modification included calculation of the additional viscous damping demonstrated in Equation 4-41 using the root mean square of the velocities. These are the relative fluid velocities q and q_4 calculated for all of the frequency bins assumed along the frequency range of the irregular wave. In this case the damping assumed in each hydrodynamic iteration is constant for all the assumed frequency bins.

As explained above the methodology for linearization of the motion RAOs for a given wave spectrum utilises the exact same mathematical formulation provided in Section 4.1 but the sequence of the procedure is different to the regular wave linearization. This is explained in detail in Section 5.3.

5 Viscous Damping Calculation Code Development

The code development outlined in this chapter is based on the mathematical development explained in Chapter 4. The procedure utilises a three dimensional diffraction-radiation hydrodynamic code to calculate relative velocity between an oscillating body and surrounding fluid at its vortex shedding edge. Furthermore, the procedure is coded as an add-on black box with potential to be used with any conventional three dimensional diffraction-radiation hydrodynamic software.

5.1. Investigation on the available hydrodynamic software

Initial investigation was conducted to assess possibility of using three different linear diffraction-radiation hydrodynamic codes in calculating the referenced relative velocity at bilge of a floating box shaped barge. The hydrodynamic codes studied initially where ANSYS AQWA, MARTEC FD-Waveload and PRECAL.

Noting the flexibility and unlimited access to functionalities of FD-Waveload provided by MARTEC, this code was chosen for further development of the viscous roll damping black box. However it should be noted that the developed black box has the potential to be used with any diffraction-radiation

hydrodynamic code as long as the input module of the black box is modified to enable it to take in the velocity calculations from the hydrodynamic code and there is access from hydrodynamic code to allow automatic input of the calculated additional damping into the iterative hydrodynamic calculation.

In order to calculate the potential on the model in a linear diffraction-radiation hydrodynamic code the fluid is assumed to be ideal and irrotational which allows potential theory to be used. The other assumption is that the incident wave acting on the body is of small amplitude when compared to its length (i.e. small slope). The theory may be used to calculate the active wave excitation on fixed bodies and the reactive wave forces on floating bodies.

Since the theory is first order the linear theory may be used to formulate the velocity potential within the fluid domain. The fluid flow field to be characterised by a velocity potential can be defined as:

$$Q(X,Y,Z,t) = \phi(X,Y,Z)e^{-i\omega t}$$

Equation 5-1

This complex potential function ϕ may be separated into contributions from the six modes of body motion, the incident wave field and the diffracted or scattered wave field. The problem can be considered to be a combination of two separate problems. Since the linear super position holds then this is acceptable.

The two problems may be viewed as:

- The problem of a floating body undergoing harmonic oscillations in still water. The body motions will cause the fluid to react on the body and this is the cause of the reactive body forces. It should be noted that these reactive forces will then be a function of motions and are commonly written in terms of added mass and wave damping coefficients.
- The problem of a fixed body being subjected to a regular incident wave train. The wave forces acting on the fixed body are considered to be the wave excitation forces. Again it is worth noting that these are

usually broken down into two components being the Froude-Krylov and wave diffraction force components.

The potential may therefore be written as:

$$\phi(X,Y,Z)e^{-i\omega t} = \left[(\phi_I + \phi_d) + \sum_{j=1}^{6} \phi_j \eta_j\right] e^{-i\omega t}$$

Equation 5-2

where:

ϕ_I is the incident wave potential

ϕ_d is the diffracted wave potential

ϕ_j is the potential due to j-th motion

η_j is the j-th motion (per unit wave amplitude)

ω is the frequency of incident wave

The potential for the undisturbed incident wave field at a point (X, Y, Z) in the fluid domain is known and may be written as:

$$\phi_I = \frac{-i \cdot g \cdot \cosh[k(d+Z)] e^{ik(X\cos\theta + Y\sin\theta)} e^{-i\omega t}}{\omega \cosh(kd)}$$

Equation 5-3

where:

d is the depth of water

k is the wave number (i.e. 2π/wavelength)

θ is the wave direction (0 degrees along $+X$ axis)

This incident wave function represents a cosine wave travelling in the positive X direction. The relationship between the wave number k and the angular frequency ω is given by:

$$\omega^2 = g \cdot k \cdot \tanh(kd)$$

Equation 5-4

The potential functions are complex but the resultant physical quantities such as fluid pressure and body motions will be obtained by considering the real part only. However the imaginary part contains the phase information.

The equation should be solved for the unknown potentials and this is done by using Green's Theorem together with the required boundary conditions on the surfaces which enclose the fluid domain. The potentials are solved at a discrete number of points on the wetted body surface.

A simplistic box shaped barge model was developed in the hydrodynamic software referenced above to assess possibility of calculating the fluid velocity relative to the body motion in the vortex shedding edge. Outline of the model is presented in Figure 5-1 below.

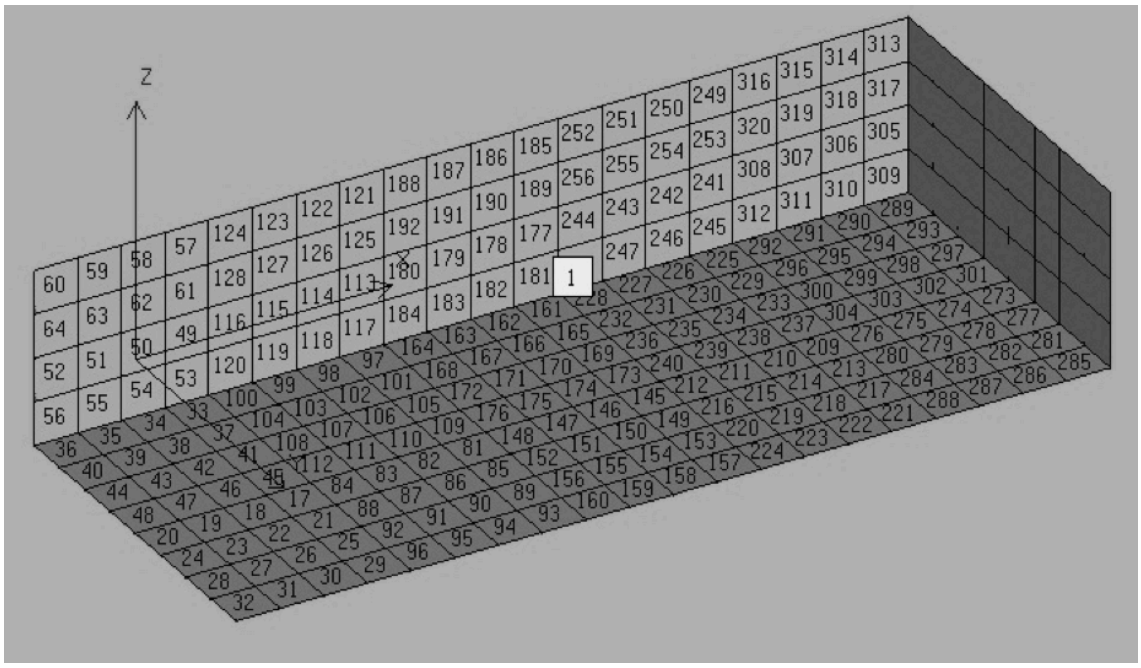

Figure 5-1: Simplistic box shaped barge model

The AQWA-Line output files were post-processed using AQWA-Flow software to calculate the fluid velocity and the body velocity defined points at centre of facets along the length of the barge and adjacent to the vortex

shedding edge. The same parameters where calculated from MARTEC FD-Waveload and PRECAL software using Macros developed in this study.

During this process strip of facets where defined along the length of the model separately in portside and starboard side. Each strip consists of two facets at the side and two facets at the bottom of the model. For example referring to Figure 5-2, one of the strips along the length of the model consist of facet numbers 180 and 184 at side and facet numbers 164 and 168 at the bottom on starboard side.

In each frequency the fluid velocity from potential calculations is defined in centre of each facet as well as the body velocity. By deducting these velocities the relative velocity between the oscillating body and the fluid is calculated at centre of each facet. These velocities are then combined using weighted averaging to calculate the representative velocity at the tip of the shedding edge.

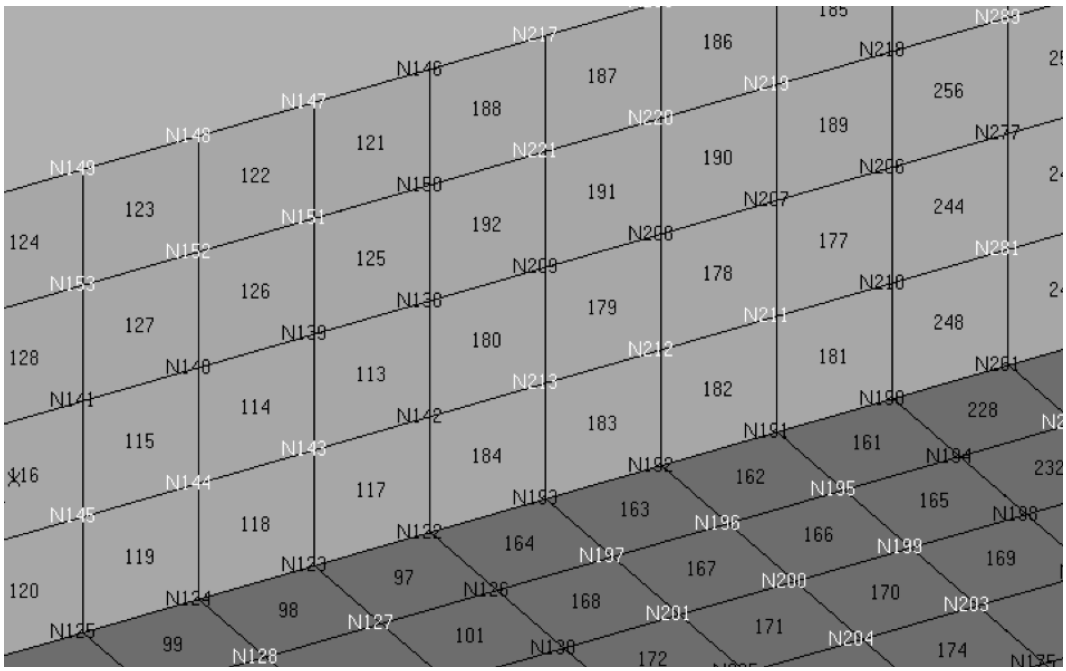

Figure 5-2: Details of the vortex shedding edge

Since in each iteration the calculated viscous damping is required to be input back in to the equation of motion, it is crucial to be able to conduct this process automatically.

Among the initially chosen hydrodynamic software only MARTEC provided access to FD-Waveload source code and allowed implementation of the automatic damping inputting function. Hence FD-Waveload was chosen in this study for further development of the black box.

After identifying the most appropriate code, a preliminary roll damping calculation exercise was conducted to estimate viscous roll damping for set of existing model test data in regular waves [82]. Details of this exercise is discussed in Section 6.1.

5.2. Code Development for Regular Waves

Use of diffraction-radiation hydrodynamic codes in calculating motion of a floating body in regular waves is a common practice. There are several commercially available codes that use the linear potential theory to calculate motion characteristics of a vessel. The motion characteristics are normally presented in form of Response Amplitude Operators (RAO) and are normalised for incident regular waves within a range of frequencies and unit amplitude.

Since the roll RAO is the most sensitive to the assumed damping value among other responses, this section of the dissertation concentrates on application of Equation 4-41 in estimate of roll damping coefficient. The calculated damping coefficient can then be used in a conventional linear diffraction-radiation hydrodynamic code as an additional linear roll damping. The same procedure is applicable to estimate of sway and heave damping coefficients using the formulation given in Equation 4-39 and Equation 4-40.

Noting Equation 4-41, the key parameter in calculating roll damping is the relative velocity of the fluid at the shedding edge in combined six degree of freedom motion (i.e. q) and in forced roll mode (i.e. q_4).

5.2.1 Step-by-Step Viscous Roll Damping Calculation in Regular Waves

Calculation of the final roll RAO with viscous damping consists of following steps for each frequency within the assumed frequency range individually:

Step 1:

A potential flow calculation is conducted and equations of motion are solved to calculate the fluid velocity relative to the vessel at the centre of facets along the shedding edge in a six degree of freedom coupled motion for a given frequency. This consists of calculating the velocity in the fluid field at centre of the facets adjacent to the shedding edge as well as calculating velocity of the floating body at centre of the same facets in each frequency. By deducting the fluid velocity from the body velocity the relative velocity between fluid and the body at centre of the facets adjacent to the shedding edge is calculated.

Step 2:

The fluid velocity relative to the vessel at the centre of the facets along the shedding edge in forced roll mode is calculated separately. This follows the same procedure as in Step 1 above but the software control parameters are modified to conduct the potential calculations in a one degree of freedom mode. In this case the degree of freedom is the degree under study i.e. roll, heave or sway.

Step 3:

Since the relative fluid velocity at tip of the shedding edge becomes singular from diffraction-radiation calculations the relative fluid velocity at the tip of the shedding edge is assumed to be equal to the weighted average of the relative fluid velocity at four facets in each strip i.e. two vertical facets and two horizontal facets adjacent to the tip. In this process the weight is defined based on the distance from centre of the facet to the vortex shedding tip. The process is conducted separately for velocities calculated in Step 1 and Step 2 above and individually for each frequency.

Step 4:

Based on the vortex shedding edge velocities calculated from Step 3, the b_4 (i.e. vortex shedding damping) value is calculated using Equation 4-41 for each strip of facets separately on the port and starboard sides. The b_4 values calculated are then integrated along the full length of the model and in port side as well as the starboard side of the model to calculate the total vortex shedding damping.

Step 5:

The calculated total vortex shedding damping is then compared with the damping value used in the potential calculations in Steps 1 and 2. If the difference between the damping values is more than the pre-defined convergence tolerance, the new viscous damping value is put back in to the hydrodynamic model for motion calculation in Steps 1 and 2 above.

Step 6:

Steps 1 to 5 are iterated for the regular wave frequency under study until the difference in the calculated additional roll damping from successive iterations is within a pre-defined limit. If this is the case then convergence is assumed and the RAO from the last iteration is assumed to be the final damped RAO.

The procedure is repeated separately for each frequency. Flowchart of the viscous roll damping procedure is presented in Figure 5-3.

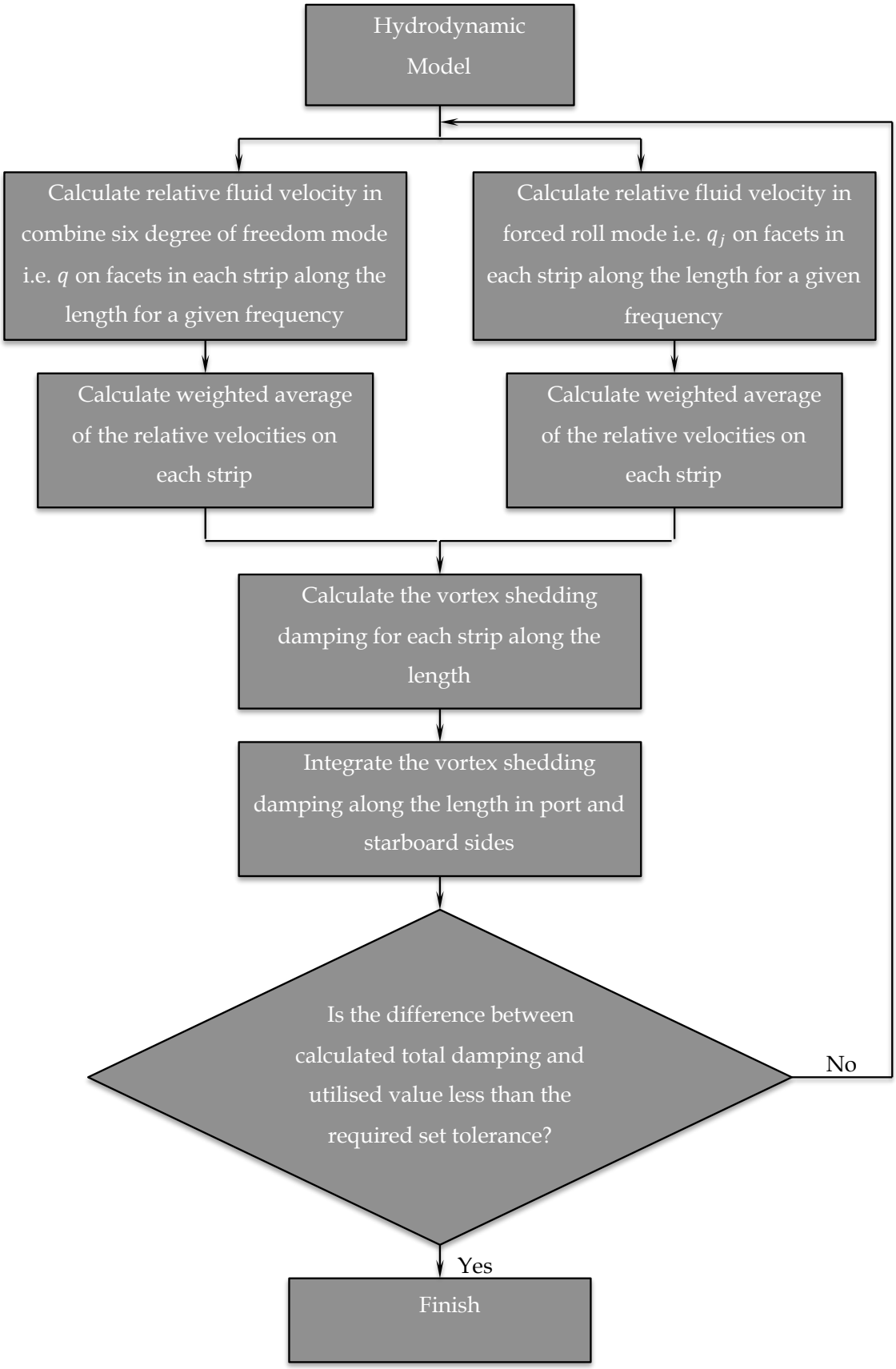

Figure 5-3: Flowchart for viscous roll damping calculation procedure for a given regular wave frequency

5.3. Code Development for Irregular Waves

Noting the viscous damping formulation presented in Section 4.1 and using the code developed for the approach explained in Section 5.2.1 a new step-by-step methodology was developed to estimate viscous roll damping of a floating body for a given irregular wave spectrum.

The methodology in Section 5.2.1 consists of running the code for a set of regular wave frequencies. This results in computing the barge responses and hence the averaged velocity values of a shedding edge at a set frequency. These velocity values are obtained for every element at the edge along both bilges of the barge and are summed over the incident and diffracted waves for both six degree of freedom mode and forced motion mode separately. The values are then stored for each frequency and a nonlinear component of damping is computed for each frequency. Finally this process is repeated iteratively by inserting the calculated damping value from each iteration into the dynamic equation corresponding to each frequency until the response converges. This process results in calculating a viscous damping for a given frequency.

In order to apply the same methodology to irregular wave the hydrodynamic code is run for range of frequencies representing frequency range of the Irregular wave spectrum simultaneously. This requires discretization of the irregular wave spectrum and identification of the representative frequency for each frequency bin. This is normally chosen to be the midpoint of the frequency bin.

The barge responses are then computed resulting in calculation of the relative velocity values for each edge and in each frequency. These velocity values are obtained for every element of edge along both bilges of the barge and are summed over the incident and diffracted waves. Same as before this is done separately in the six degree of freedom mode as well as the forced mode.

Since in this process the relative velocities are calculated simultaneously for all the frequencies in each iteration a mean square over all frequencies can then

be calculated from these sinusoidal values as below and is stored for each strip along the shedding edge:

$$q_{rms}(i) = \sqrt{\sum_j \frac{1}{2} q(i,j) \cdot conj\big(q(i,j)\big)}$$

Equation 5-5

where i denotes the assumed strip at the shedding edge and j denotes the number of frequencies representing the full frequency range of the irregular wave spectrum.

Then the nonlinear component of damping is calculated from $K \cdot q_{rms}(i)$, which is independent of the frequency.

Regarding the value of K Borgman [83] has the same relationship (See Equation 69 of [83]) to get an equivalence between $v|v|$ and $K \cdot v \cdot v_{RMS}$ where v is the velocity and $v = v_0 \cos\theta$. If this is substituted into the relationship and both sides are multiplied by $\cos\theta$, by integrating over the flow cycle of 0 to 2π the result will be $= \frac{8\sqrt{2}}{3\pi} \cong 1.2$. This weighting of the integral corresponds to weighting by the velocity that in turn corresponds to what is done in Morison's equation to evaluate the drag coefficient.

An alternative would be to multiply by the sign of the velocity and just equate to mean of the two sides equivalent to equating means over each half cycle. In that case the result will be $= \frac{\pi}{\sqrt{8}}$.

Borgman's assumption to get to the value of $K \cong \sqrt{\frac{8}{\pi}}$ in [83] is not clear. It may be in order to get to this bigger value he is assuming that the waves have higher extremes and he is incorporating some nonlinear wave theory.

In this dissertation K is assumed to have a value somewhere in the range 1.2 to $\sqrt{2}$.

The process is iterated by inserting the calculated viscous damping value into the dynamic equation for each frequency until response is converged. It should be noted that unlike the regular wave viscous damping calculation procedure the same viscous damping value is used for all frequencies and it only changes for each iteration step.

In contrast to the regular wave case in which the absolute values of edge velocities in each frequency are used in the calculation, in the irregular wave case the root mean square of the edge velocities which is a universal value for all frequencies at each edge element is used in calculating the damping.

5.3.1 Step-by-Step Viscous Roll Damping Calculation in Irregular Waves

The process starts with a known irregular wave spectrum for which the viscous damping needs to be linearized. The wave spectrum is then divided in to several frequency bins along its frequency range. Each frequency bin consists of two frequencies denoting beginning and end of the assumed bin. The frequency at the centre of the bin is considered to be the representative frequency of the bin and used in the viscous damping calculation. The amplitude of a regular wave which is representative of the assumed frequency bin (i.e. $A_{rep.}$) can then be calculated from Equation 5-6 as below:

$$A_{rep.} = \sqrt{2 \sum S(\omega) \cdot \Delta\omega}$$

Equation 5-6

The $A_{rep.}$ of each frequency bin is then used individually to calculate the relative fluid velocity at the shedding edge at each associated frequency however, the velocities are then averaged to calculate a single damping value that is applicable to the wave spectrum frequency range.

Noting the procedure explained in Section 5.3 calculation of final roll RAO including viscous damping linearized for a given irregular wave spectrum is defined in a step-by-step process below:

Step 1:

A potential flow calculation is conducted and equations of motion are solved to calculate the fluid velocity relative to the vessel at the centre of facets along the shedding edge in a six degree of freedom coupled motion. This is done for range of frequencies representing the frequency band of the given irregular wave spectrum. This consists of calculating the velocity in the fluid field at centre of the facets adjacent to the shedding edge. Velocities of the floating body at centre of the same facets in each frequency are calculated using same damping value in each iteration for all the frequencies in the range but for the $A_{rep.}$ values associated to each frequency bin. By deducting the fluid velocities from the body velocities the relative velocities between fluid and the body at centre of the facets adjacent to the shedding edge are calculated for all frequencies using a damping value constant for the iteration.

Step 2:

The fluid velocities relative to the vessel at the centre of the facets along the shedding edge in forced roll mode are calculated separately. This follows the same procedure as in Step 1 above but the software control parameters are modified to conduct the potential calculations in a one degree of freedom mode. In this case the degree of freedom is the degree under study i.e. roll, heave or sway.

Step 3:

Since the relative fluid velocity at tip of the shedding edge becomes singular from diffraction-radiation calculations the relative fluid velocity at the tip of the shedding edge is assumed to be equal to the weighted average of the relative fluid velocity at four facets in each strip (i.e. two vertical facets and two horizontal facets adjacent to the tip). In this process the weight is defined based on the distance from centre of the facet to the vortex shedding tip. The process is conducted separately for velocities calculated in Step 1 and Step 2 above and individually for each frequency.

Step 4:

A root mean square average is taken over the weighted averaged velocities calculated in all frequencies within the iteration. This is done separately for the six degree of freedom mode as well as the forced motion mode. The process results in a root mean square average velocity representing the average relative velocity at the tip of the shedding edge over all frequencies.

Step 5:

Using the root mean square averaged velocities calculated for the free floating mode and forced mode from Step 4 the b_4 (i.e. vortex shedding damping) value is calculated using Equation 4-41 for each strip of facets separately on the port and starboard sides. The b_4 values calculated are then integrated along the full length of the model and in port side as well as the starboard side of the model to calculate the total vortex shedding damping.

Step 6:

The calculated total vortex shedding damping is then compared with the damping value used in the potential calculations in Steps 1 and 2. If the difference between the damping values is more than the pre-defined convergence tolerance the new viscous damping value is put back in to the hydrodynamic model for motion calculation in Steps 1 and 2 above.

Step7:

Steps 1 to 6 are iterated using a constant damping value for all frequencies in each iteration until the difference in the calculated additional roll damping from successive iterations is within a pre-defined limit. If this is the case then convergence is assumed and the RAO from the last iteration is assumed to be the final damped RAO.

Flowchart of the viscous roll damping procedure in irregular waves is presented in Figure 5-4.

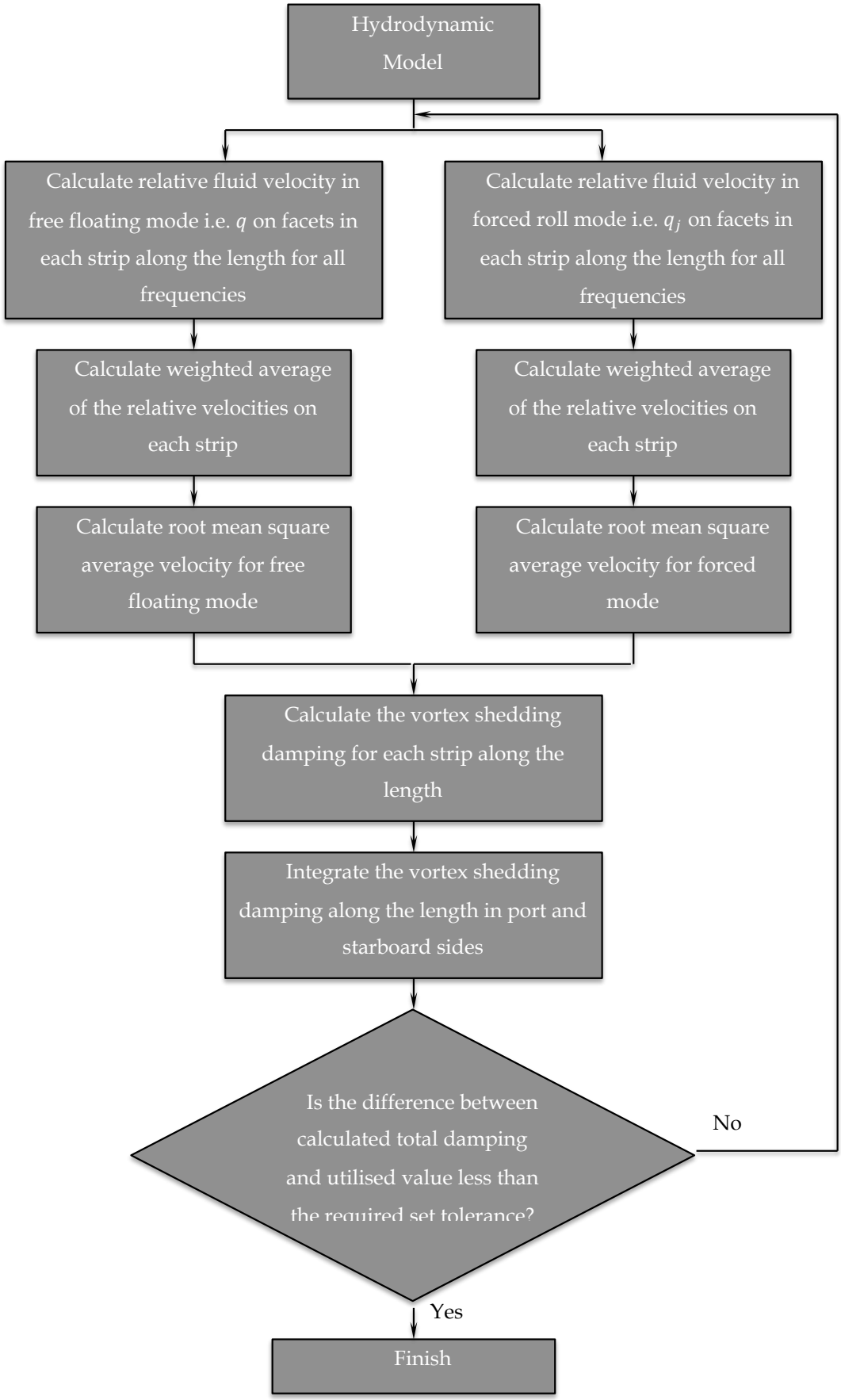

Figure 5-4: Flowchart for viscous roll damping calculation procedure in a given irregular wave frequency

6 Implementation of the Numerical Model

Noting the viscous damping calculation development outlined in Chapter 4 and using the code development outlined in Chapter 5 an initial attempt was made to apply the method in calculation of viscous roll damping coefficient. The calculated roll damping value representing the viscous effects was then used in linear diffraction-radiation hydrodynamic software to calculate the damped RAO in regular weaves. This was to conduct preliminary assessment of validity of the procedure in comparison to set of available model test data [82] before embarking on a dedicated model test campaign. The initial numerical results were confirmed to agree well with the available model test data. Details of this initial assessment are presented in Section 6.1.

Following a good agreement achieved between the theoretical calculation and the existing model test data an independent model test campaign was conducted to eliminate any ambiguity from outcome of the preliminary comparisons. This assessment consisted of building a physical model of a new box shaped barge as well as the associated hydrodynamic model. The model test campaign was conducted in the Newcastle University model test facilities. Further details on this assessment are provided in Section 6.2.

6.1. Preliminary Validation Study

Initially a comparison was conducted between theoretical results and model test data for a sharp keel-edge profile provided by Brown et al. [82]. This consisted of preparation of a three dimensional diffraction-radiation potential hydrodynamic model based on the main characteristics presented by Brown et al. [82]. The main characteristics of the model are presented in Table 6-1. The model was used to calculate the required relative velocities at the shedding edges for a given frequency in each iteration as outlined in Section 4.1.

Table 6-1: Main characteristics of the Brown et al. [82] model

Main characteristic	-
Length (m)	2.4
Beam (m)	0.8
Draught (m)	0.105
Mass (kg)	200.8
Longitudinal Centre of Gravity from AP (m)	1.2
Vertical Centre of Gravity from keel (m)	0.111
Roll Radius of Gyration (m)	0.244
Pitch Radius of Gyration (m)	0.688
Yaw Radius of Gyration (m)	0.598

Using the calculated relative velocities in Equation 4-41 the viscous roll damping was calculated. The viscous roll damping was then input back in to the software as additional roll damping iteratively until the damping was converged within defined tolerances. Consequently the final damped Response Amplitude Operator (RAO) was calculated. The set damping tolerance in this case was equal to a variation of ±1° between the calculated RAO amplitudes in every two consecutive iteration.

The hydrodynamic model associated to parameters defined in Table 6-1 is presented in Figure 6-1 showing the boundary element panel discretisation.

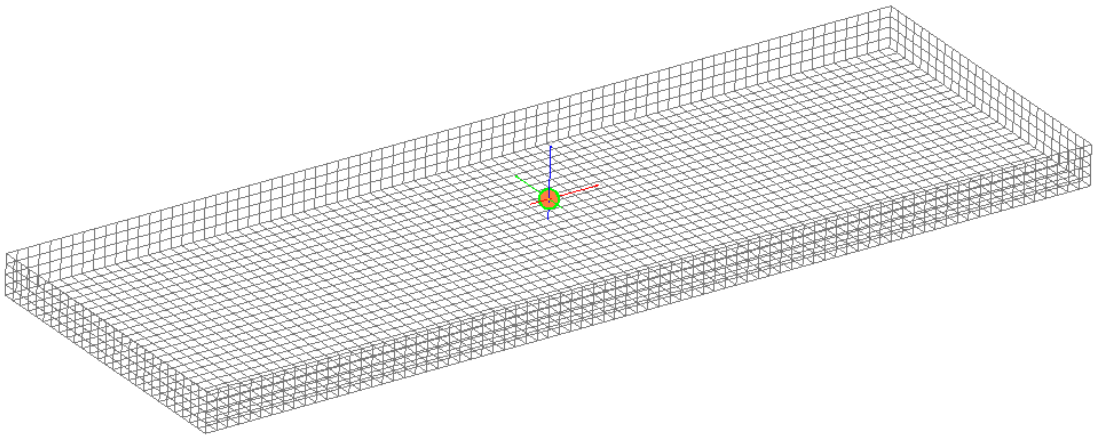

Figure 6-1: Hydrodynamic model of the Brown et al. [82] barge

Outcome of the comparison form this assessment is presented in Section 7.1.

6.2. Independent Model Test

Noting the good agreement achieved between the model test data and the calculated damped RAO amplitudes presented in Figure 7-3, attempt was made to conduct a dedicated model test campaign to confirm the validity of the procedure further and eliminate any ambiguity in the RAO comparison.

The model test was conducted in the Newcastle University Marine Hydrodynamics Laboratory. The laboratory consists of a towing tank that is equipped with wave maker. The wave maker can be used to generate regular waves up to 0.12m height and wave periods in range of 0.5 to 2 seconds. It can also be used to generate long crested random seas using variety of wave spectra.

Dimensions of the towing tank are presented in Table 6-2.

Table 6-2: Dimensions of the towig tank

Length (m)	37
Width (m)	3.7
Water depth (m)	1.25

In this exercise an optical motion sensor (Qualisys IR Tracking System) was used to measure motion of the floating barge in waves. The system consisted of two infrared optical cameras emitting a beam of infrared light to a set of three retro-reflective markers located on the barge. Sensors on the cameras capture the reflected infrared lights from the markers. These digital data are then used to calculate motion of the floating body. The post processed data is presented in form of six degree of freedom motion time series.

Furthermore a wave height probe was used in vicinity of the floating barge to measure height of the incident wave in each test.

The waves generated in the tank by a group of paddle wave makers located at one end of the tank. Layout of the tank together with the wave making paddles at the end is shown in Figure 6-2.

Figure 6-2: Tank layout and wave maker paddles

A wedge type beach at the other end of the tank absorbs the generated waves. The beach consists of energy absorbing sheets that eliminate reflection of the

waves from opposite side of the tank. Figure 6-3 demonstrates the energy absorbing sheets arrangement in the tank.

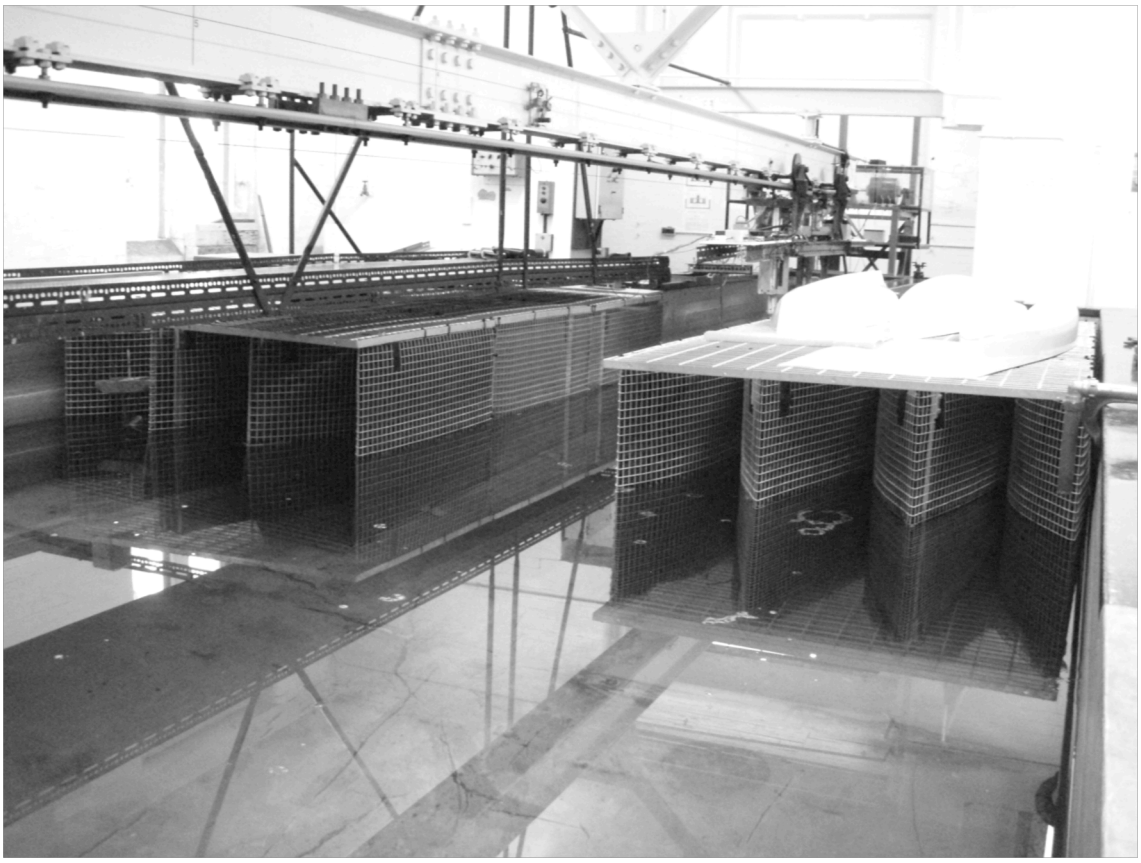

Figure 6-3: Energy absorbing sheets in the towing tank

A boxed shape model was built and used for the model test activities. Extent of the model is presented in Figure 6-4. The barge was built from 4 mm thick polyvinyl chloride (PVC) sheets. The main characteristics of the box shaped model with rectangular bilge keels are outlined in Table 6-3.

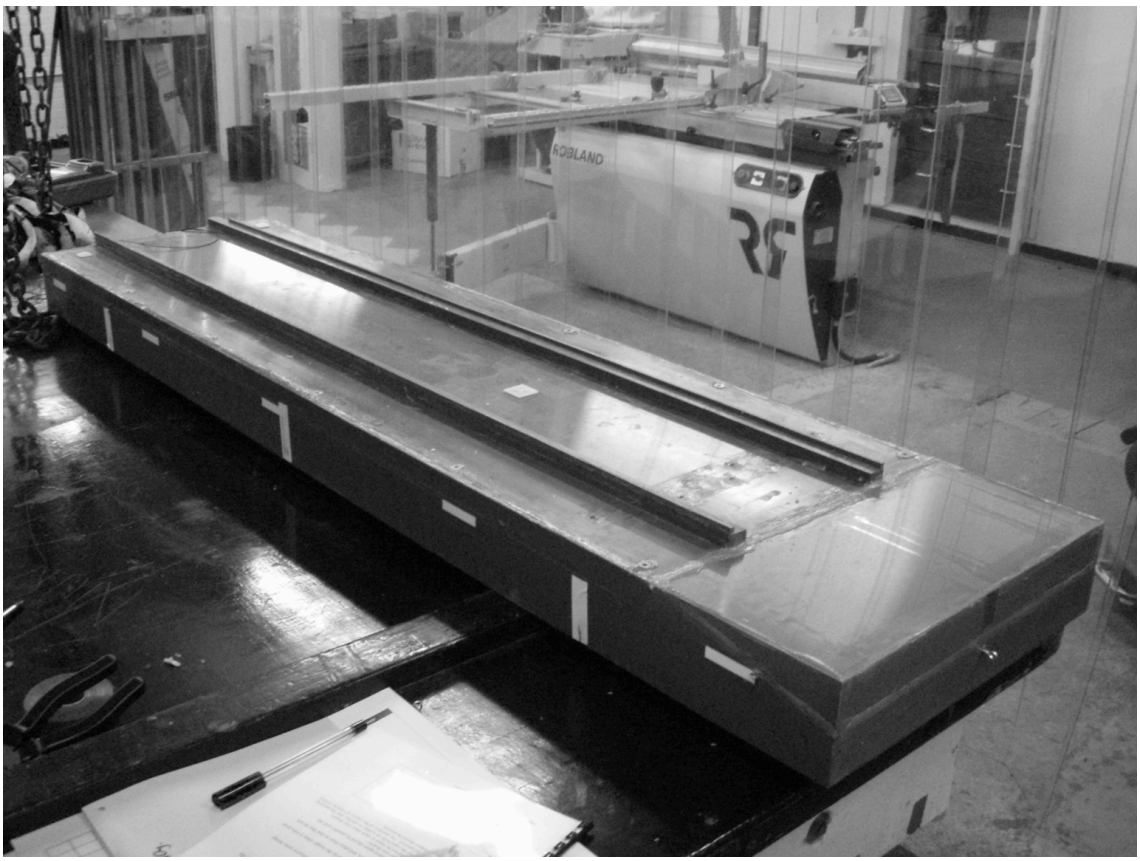

Figure 6-4: Extent of the box shaped model

Table 6-3: Main characteristics of the model

Main characteristic	-
Length (m)	1.538
Beam (m)	0.403
Draught (m)	0.064
Mass (kg)	39.67
Longitudinal Centre of Gravity from AP (m)	0.004
Vertical Centre of Gravity from keel (m)	0.032
Roll Radius of Gyration (m)	0.1405
Pitch Radius of Gyration (m)	0.4306
Yaw Radius of Gyration (m)	0.4306

Hydrostatic characteristics of the model including weight, centre of gravity, radius of gyration and calculation of metacentric height were done in the laboratory in advance of positioning the model in to the tank. Figure 6-5 shows part of the measurements conducted on the model before placing it in to the tank.

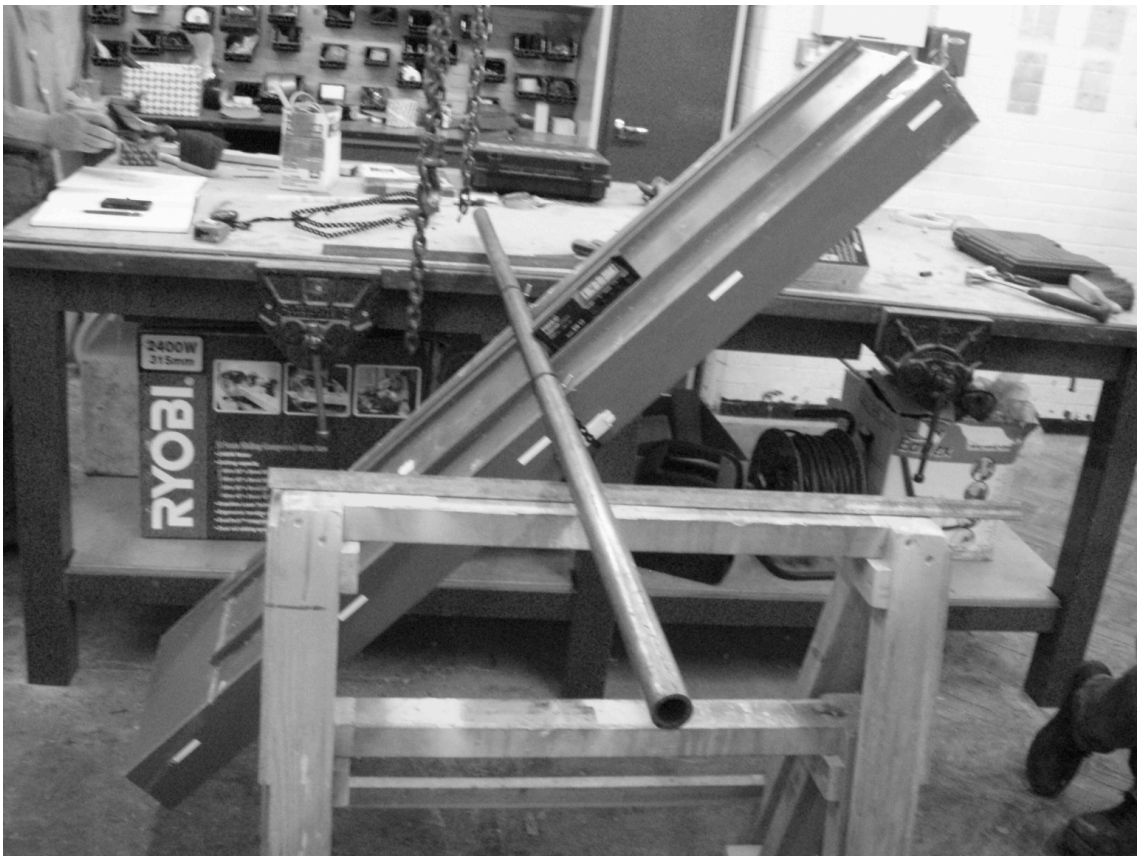

Figure 6-5: Measurmnet of hydrostatic charactristics of the model

Figure 6-6 shows the model during model test in regular waves. The model was secured in its place using four strings including a soft spring in each string. The strings were connected to pins in both ends of the model. This ensured the heading of the model remains beam to the incident waves.

A wave amplitude probe was situated in vicinity of the model to measure the incident wave amplitude generated by the wave maker. The probe is visible in Figure 6-6. The measured incident wave height was then used in linearization of the measured roll amplitudes in each frequency to accurately calculate the roll RAO in each tested frequency.

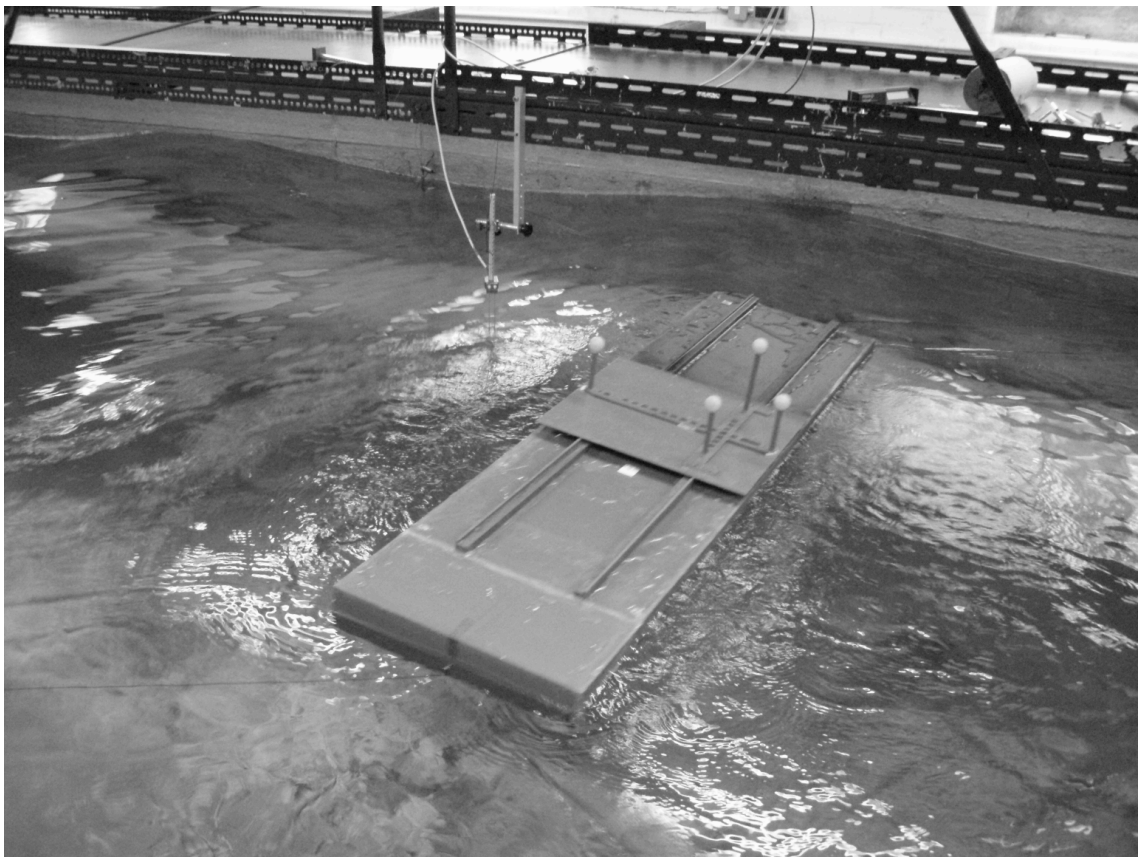

Figure 6-6: The model during model test

Two separate model tests were conducted to measure the response of the model in regular waves and irregular waves. Results of the model test exercises are presented in Sections 7.2 and 7.3.

7 Results and Discussions

The numerical calculations together with associated preliminary model test data and the data generated from independent model test campaign are presented in this chapter. The results consist of roll RAOs from potential calculations and the roll RAOs calculated for the estimated viscous damping. No additional damping is assumed to represent the viscous damping in potential calculations however, the estimated viscous damping is considered in calculation of the damped RAOs as additional linear damping.

Details of preliminary application of the viscous roll damping procedure and final confirmation of validity of the procedure are discussed in this chapter. Calculations are done for regular waves as well as irregular waves. The resulted roll RAOs for regular wave calculations are presented in Sections 7.1 and 7.2. The calculated RAOs are compared with model test data for the preliminary validation and the independent model test data respectively. The results and comparisons for irregular waves are presented in Section 7.3.

7.1. Preliminary Assessment Results

Results of the preliminary assessment from numerical calculation were compared with the model test roll RAOs presented by Brown et al. [82].

Figure 7-1 shows the potential roll RAO calculated from a hydrodynamic model of the Brown et al. barge as defined in Table 6-1 without any additional viscous roll damping.

The vertical axis in Figure 7-1 demonstrates the roll RAO amplitude that is normalised for the incident wave height. Hence the unit for the vertical axis demonstrates the roll angle per millimetre wave height of the incident wave (i.e. deg./mm). The longitudinal axis in Figure 7-1 represents frequency of the incident wave in radians per second (i.e. rad/s).

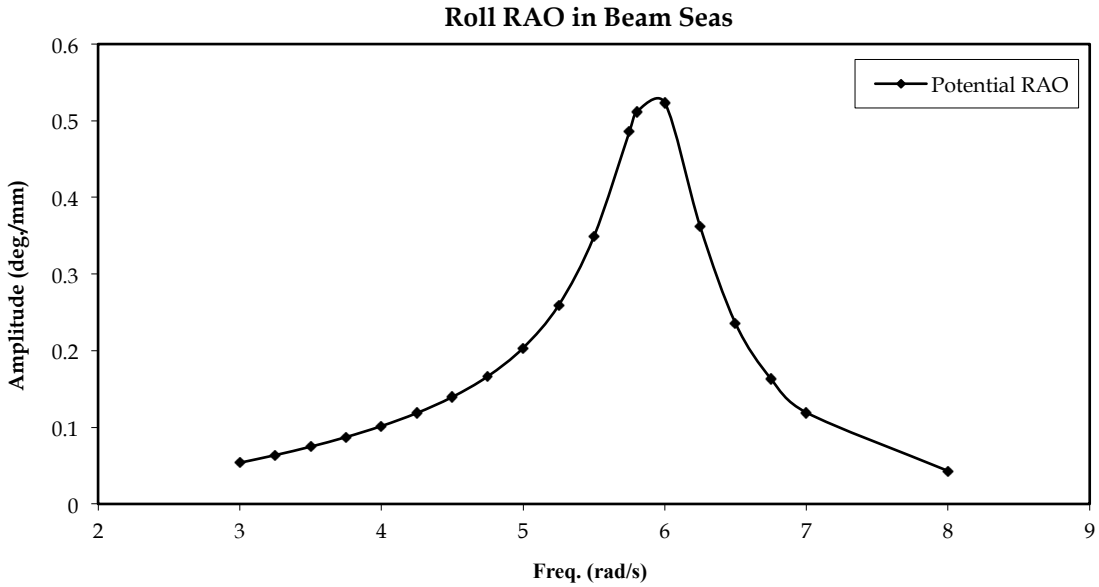

Figure 7-1: Potential roll RAO in beam seas for Brown et al. [82] model

Tabulated values associated to Figure 7-1 are presented in Table 7-1 below:

Table 7-1: Tabulated values of the potential RAO for Brown et al. [82] model

Freq. (rad/s)	3	3.25	3.5	3.75	4	4.25	4.5	4.75	5
Amp. (deg./mm)	0.0538	0.06368	0.07472	0.08721	0.1016	0.1186	0.1395	0.1664	0.2035
Freq. (rad/s)	5.25	5.5	5.75	5.80	6	6.25	6.5	6.75	7.00
Amp. (deg./mm)	0.2589	0.3487	0.4852	0.511101	0.5235	0.362	0.2355	0.1632	0.11929

The damped RAO in each frequency including effect of the additional viscous damping calculated using the procedure outlined in Section 4.1 is presented in Figure 7-2.

Since viscous damping is a function of incident wave height the damped RAO was calculated for a 24mm regular wave height. In this calculation the calculated damped RAO amplitude in each frequency is converged to a tolerance of 0.1 degree per meter of incident wave height.

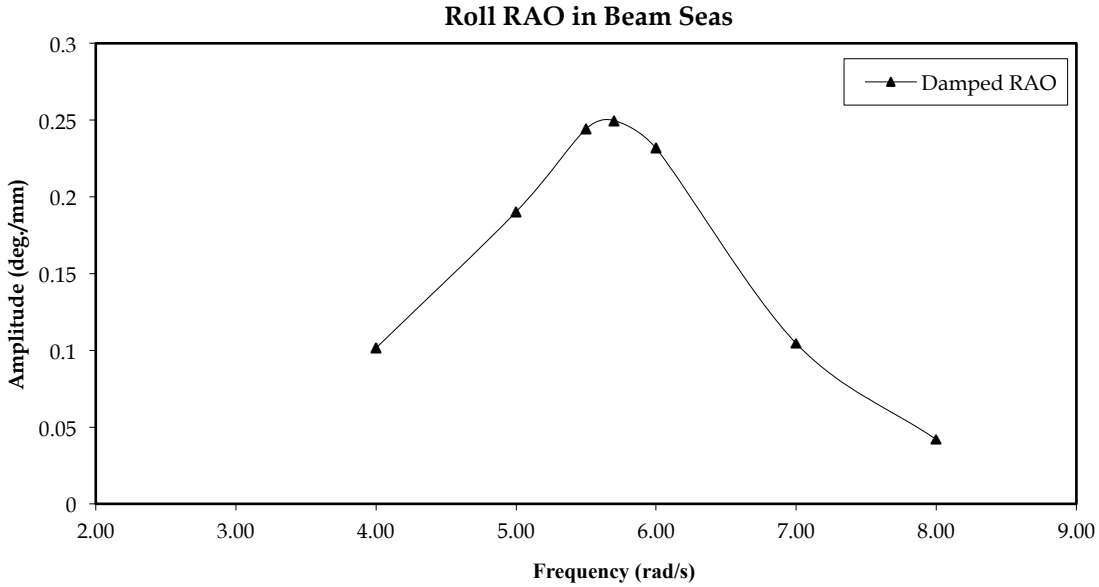

Figure 7-2: Damped roll RAO in beam seas for Brown et al. [82] model

Tabulated values associated to Figure 7-2 are presented in Table 7-2 below:

Table 7-2: Tabulated values of the damped RAO for Brown et al. [82] model

Freq. (rad/s)	4	5	5.5	5.7	6	7	8
Amp. (deg./mm)	0.10136	0.1902	0.24423	0.2497	0.2315	0.1045	0.0419

The RAOs shown in Figure 7-1 and Figure 7-2 represent the roll RAOs in beam seas for a 1:36 scale model with a sharp keel-edge profile. The associated model test roll RAO in beam seas from the Brown et al. [82] paper is presented in Appendix Figure A- 1. These RAOs are represented in Figure 7-3 for ease of

comparison. Effect of additional viscous damping can be clearly seen in comparison between the potential RAO and the damped RAO.

Furthermore the calculated damped RAO seems to be agreeing well with the model test data recovered from Brown et al. [82].

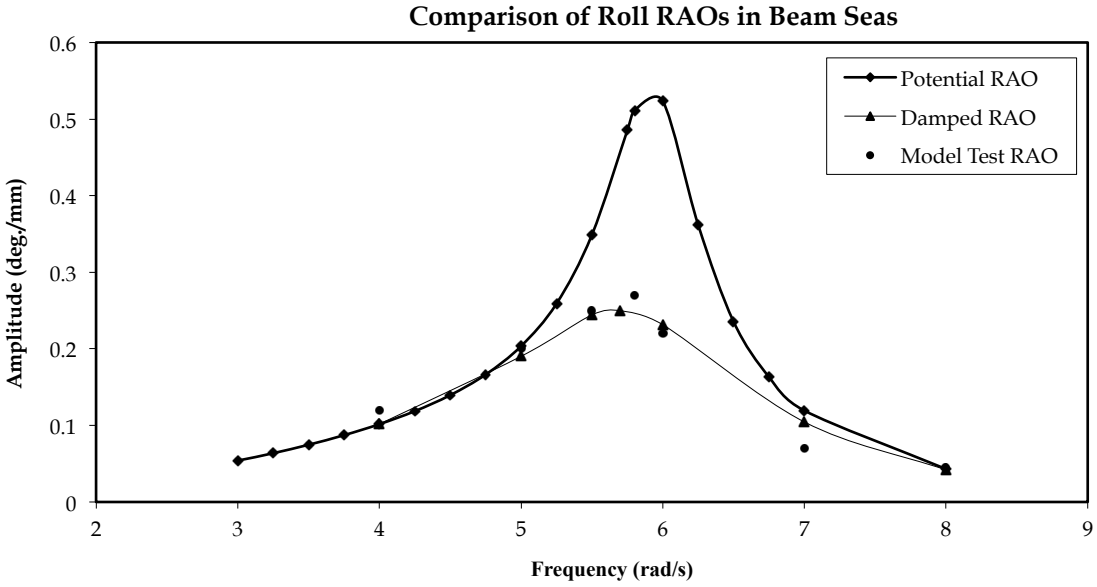

Figure 7-3: Comparison of roll RAO in Beam Seas for Brown et al. [82] model

7.2. Roll Response in Regular Waves

A new hydrodynamic model of the barge given in Table 6-3 was built in FD-Waveload hydrodynamic software to calculate the potential roll RAO of the independent model test assessment.

During post processing the model test data the measured regular incident wave amplitudes and the measured motion responses were used to calculate the model test RAO for each frequency.

The calculated potential roll RAO of the model is presented in Figure 7-4. No additional damping is considered in calculation of the potential RAO.

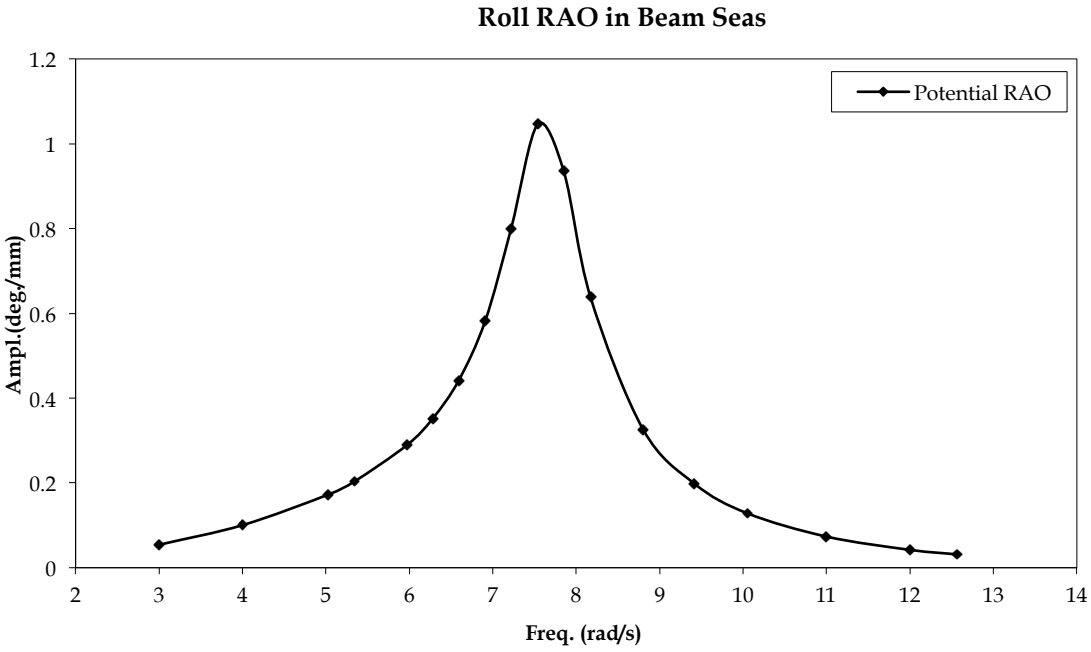

Figure 7-4: : Potential roll RAO in beam seas for the Hajiarab et al. [7] model

Tabulated values associated with the roll RAO presented in Figure 7-4 are provided in Table 7-3.

Table 7-3: Tabulated values of the potential RAO for Hajiarab et al. [7] model

Freq. (rad/s)	3	4	5.02	5.34	5.97	6.28	6.59
Amp. (deg./mm)	0.05	0.10	0.17	0.20	0.29	0.35	0.44
Freq. (rad/s)	6.91	7.22	7.54	7.85	8.17	8.8	9.42
Amp. (deg./mm)	0.58	0.80	1.05	0.94	0.64	0.33	0.20
Freq. (rad/s)	10.05	11	12	12.56	13	14	15
Amp. (deg./mm)	0.13	0.07	0.04	0.03	0.02	0.01	0.01

The same hydrodynamic model is used together with the viscous roll damping procedure outlined in Section 5.2 to calculate the damped roll RAO of the model characterised in Table 6-3. The calculated damped roll RAO is presented in Figure 7-5.

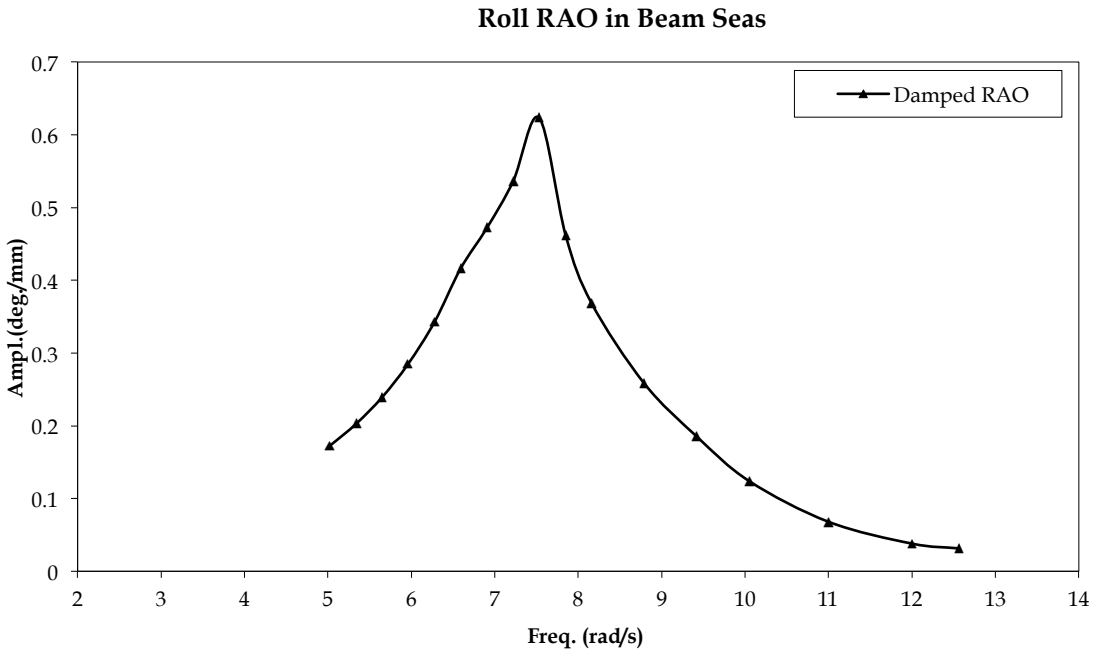

Figure 7-5: Damped roll RAO in beam seas for Hajiarab et al. [7] model

The tabulated data associated to Figure 7-5 are presented in Table 7-4 below:

Table 7-4: Tabulated values of the damped RAO for Hajiarab et al. [7] model

Freq. (rad/s)	5.02	5.34	5.65	5.96	6.28	6.59
Amp. (deg./mm)	0.17	0.20	0.24	0.28	0.34	0.41
Freq. (rad/s)	6.91	7.22	7.53	7.85	8.16	8.79
Amp. (deg./mm)	0.47	0.53	0.62	0.46	0.37	0.26
Freq. (rad/s)	9.42	10.05	11	12	12.56	
Amp. (deg./mm)	0.19	0.12	0.07	0.04	0.03	

The RAO amplitudes in each frequency in the damped RAO presented in Figure 7-5 are individually linearized for the wave heights measured during the model test for each frequency.

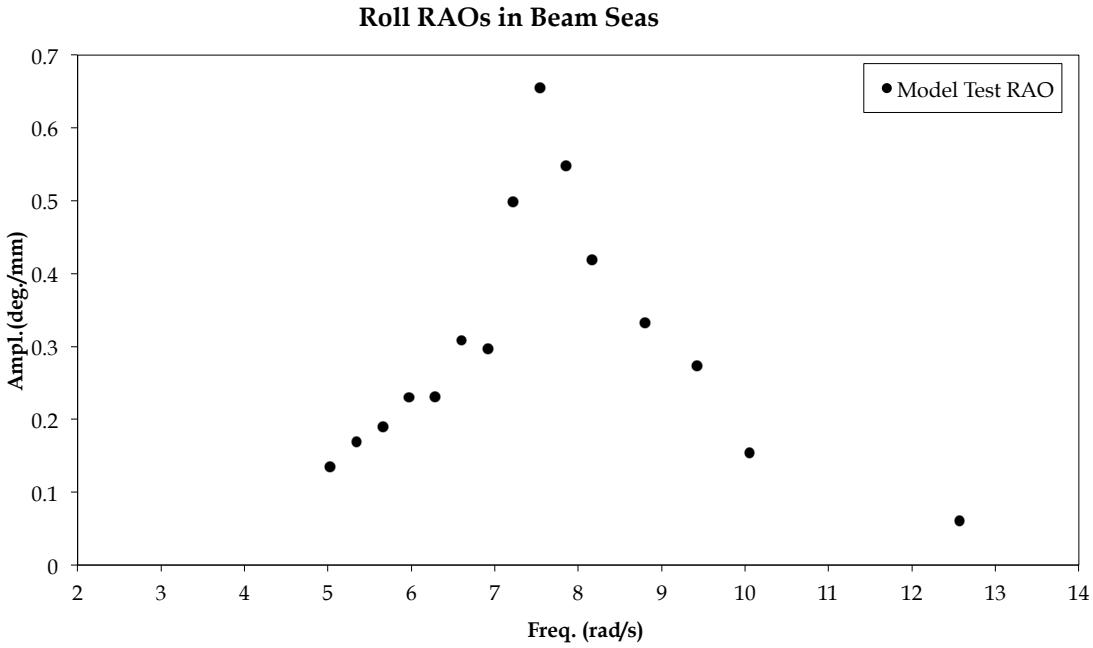

Figure 7-6: Model test roll RAO in beam seas for Hajiarab et al. [7] model

The wave height amplitudes for which the damping is linearized are presented in Table 7-5 together with the tabulated model test RAO data associated to Figure 7-6.

Table 7-5: Measured model test RAO and incident wave amplitudes for Hajiarab et al. [7] model

Freq. (rad/s)	5.03	5.34	5.65	5.97	6.28
Amp. (deg./mm)	0.14	0.17	0.19	0.23	0.23
Wave Amp. (mm)	10.73	11.59	10.86	9.07	10.09
Freq. (rad/s)	6.60	6.91	7.23	7.54	7.85
Amp. (deg./mm)	0.31	0.30	0.50	0.65	0.55
Wave Amp. (mm)	9.45	12.97	11.14	7.27	12.23
Freq. (rad/s)	8.17	8.80	9.42	10.05	12.57
Amp. (deg./mm)	0.42	0.33	0.27	0.15	0.06
Wave Amp. (mm)	14.43	13.98	8.66	9.27	4.90

The roll RAO amplitudes are calculated by post processing the measured roll amplitude time series in each incident wave frequency. The roll motion of the barge is measured in time steps of 0.01 second. Same time step is used for measurement of the incident wave amplitudes.

The measured model test RAO and the calculated Damped RAO together with the Potential RAO are compared in Figure 7-7.

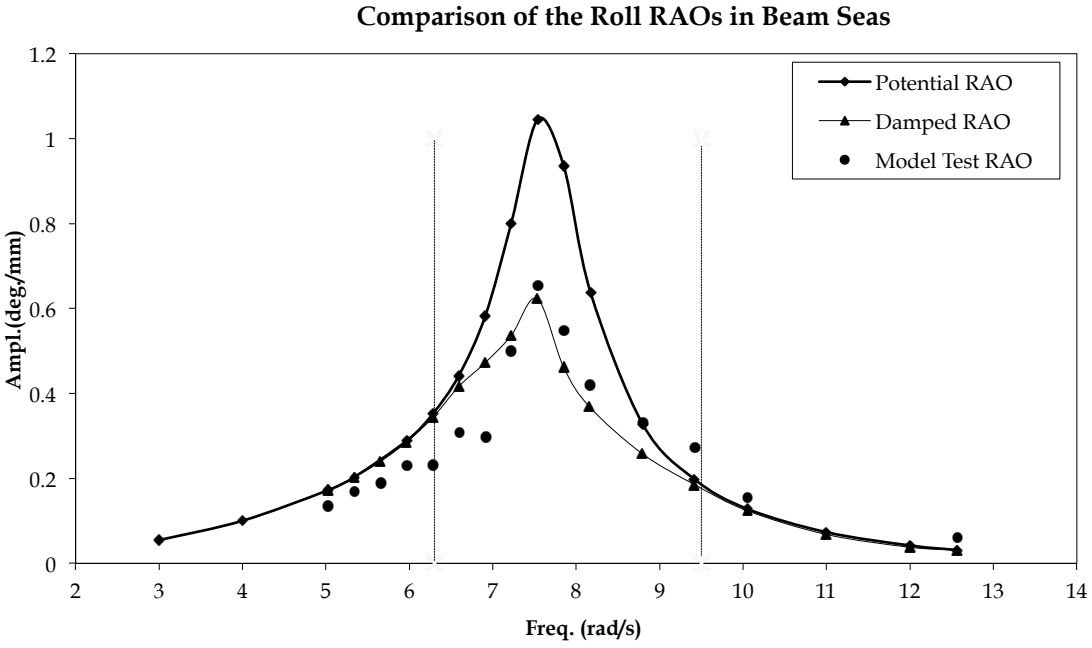

Figure 7-7: Comparison of Roll RAOs in Beam Seas for Hajiarab et al. [7] model

Since the calculated viscous damping is dependent on the assumed incident wave height further calculation was done to assess effect of wave height on the final damped RAO. A range of damped RAOs linearized for regular wave amplitudes of 5mm, 8mm, 10mm, 12mm and 14mm were calculated to assess effect of damping linearization with respect to wave amplitude. Outcome of these calculations are presented in Figure 7-8.

Effect of variation in the assumed linearization wave height on the final damped RAO is clear in Figure 7-8. Increase in the assumed linearization wave height results in decrease in the damped roll RAO amplitude, demonstrating generation of higher viscous damping accordingly.

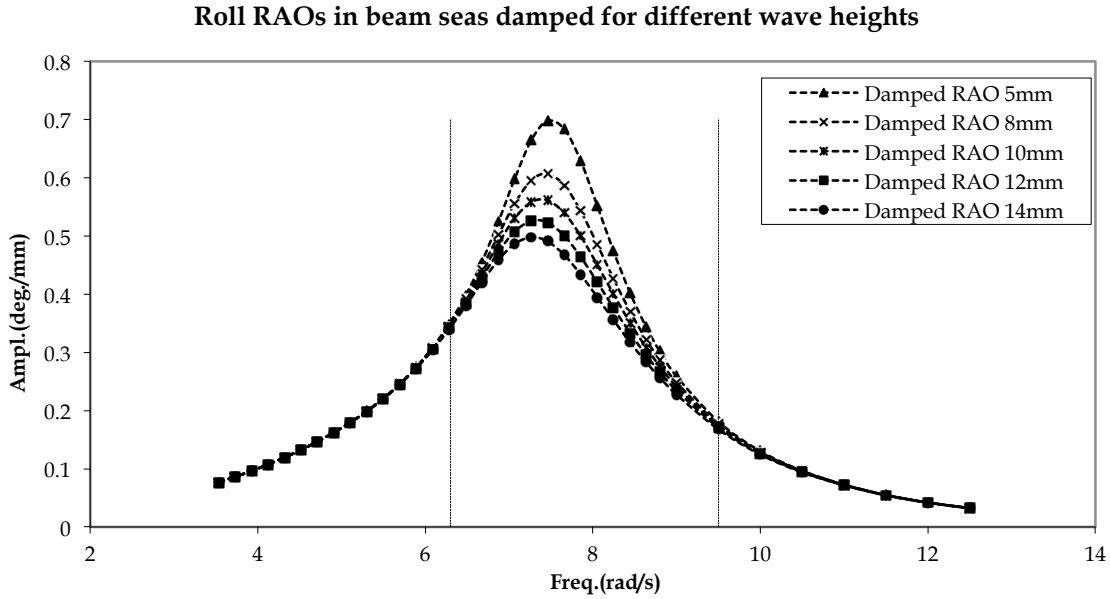

Figure 7-8: Comparison of roll RAOs damped for different incident wave amplitudes

It should be noted that the calculation converges after few iterations for frequencies away from the peak frequency. As the calculation approaches to the peak frequency, number of iterations to converge the calculation increases significantly. This determines the time needed to conduct the calculation in each frequency.

7.3. Roll Response in Irregular Waves

In order to utilise the viscous damping procedure outlined in Section 5.3 to estimate the damped RAO in irregular waves represented by an irregular wave spectrum, a wave spectrum was assumed as the incident wave. This wave spectrum was a Pierson-Moskowitz spectrum with $H_s = 0.03$ meter and peak frequency of $\omega = 7.54$ rad/s.

Frequency bins were considered along the frequency axis of the spectrum. The frequency bins are shown in Figure 7-9. For each frequency bin the associated regular wave amplitude is calculated using Equation 5-6.

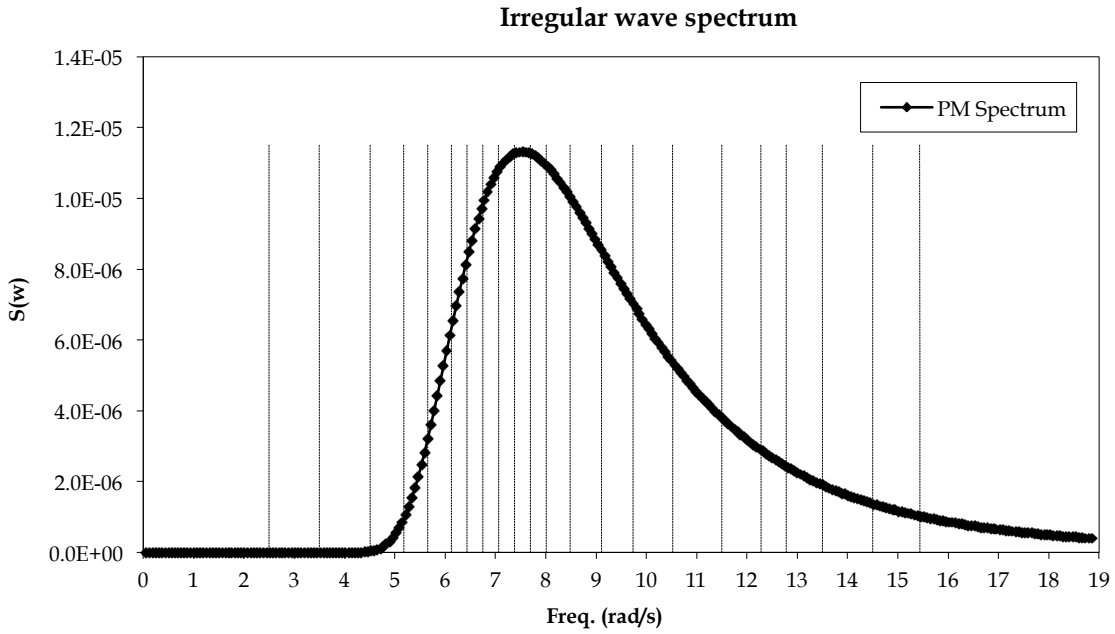

Figure 7-9: The incident Pierson-Moskowitz irregular wave spectrum and frequency bins

Using the methodology in Section 5.3 the calculated damped roll RAO linearized for the given Pierson-Moskowitz spectrum is shown in Figure 7-10.

The calculated damped roll RAO demonstrated in Figure 7-10 confirmed convergence of the method outlined in Section 5.3.

In order to assess sensitivity of the method to variation in frequency bin sizes further two bin sizes were assumed for the same given Pierson-Moskowitz spectrum namely Bin#2 and Bin#3. The size of the frequency bins in Bin#2 and Bin#3 are half and twice of the frequency bin sizes assumed in the initial assessment (i.e. Bin#1) presented in Figure 7-10 respectively.

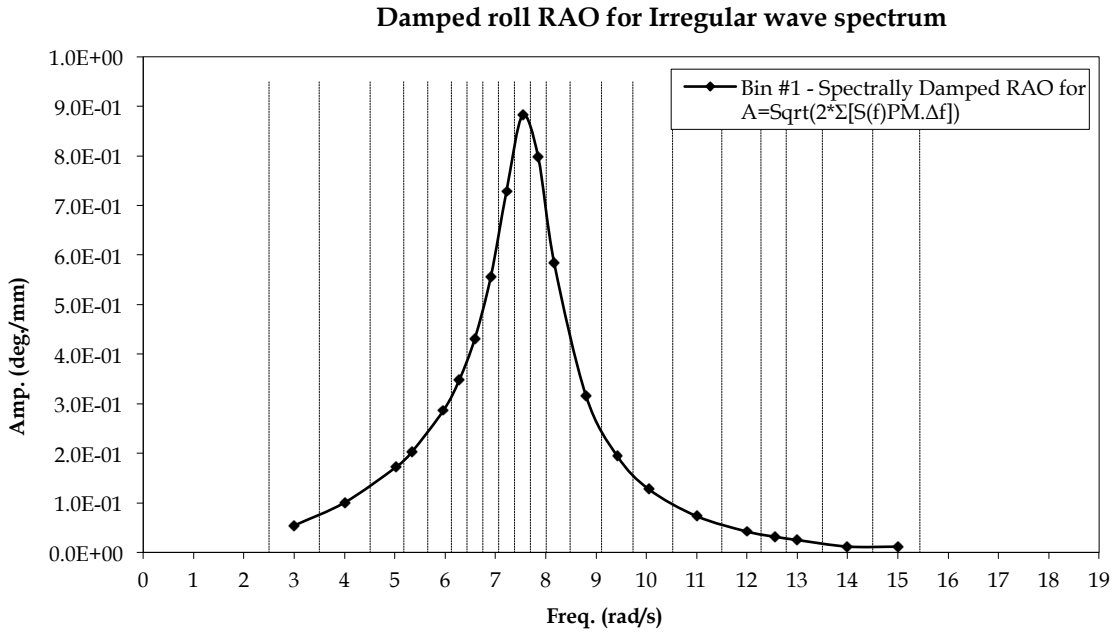

Figure 7-10: Calculated damped roll RAO associated to the Pierson-Moskowitz spectrum

A comparison between calculated damped RAOs for the three bin sizes is presented in Figure 7-11.

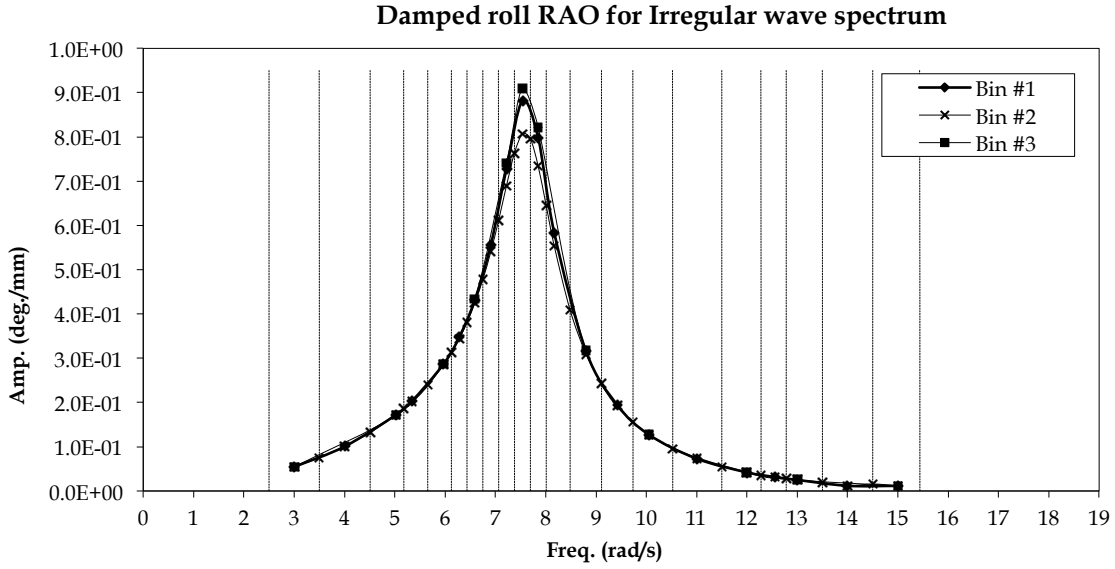

Figure 7-11: Sensitivity of the method to variation in frequency bin sizes

The tabulated data associated to the damped RAO for frequency bin sizes of Bin#1 are provided in Table 7-6.

Table 7-6: Tabulated data associted to damped RAO calculation for Bin#1

Freq. (rad/s)	Frequency Bin		Bin Wave Amplitude (m)	Damped RAO (deg/mm)
	Lower Limit	Upper Limit		
3.00	2.50	3.50	3.07E-08	5.43E-02
4.00	3.50	4.51	9.97E-05	1.00E-01
5.02	4.51	5.18	6.57E-04	1.72E-01
5.34	5.18	5.66	1.43E-03	2.03E-01
5.97	5.66	6.13	2.07E-03	2.87E-01
6.28	6.13	6.44	2.15E-03	3.48E-01
6.59	6.44	6.75	2.39E-03	4.31E-01
6.91	6.75	7.07	2.55E-03	5.57E-01
7.22	7.07	7.38	2.64E-03	7.29E-01
7.54	7.38	7.70	2.66E-03	8.82E-01
7.85	7.70	8.01	2.64E-03	7.98E-01
8.17	8.01	8.49	3.25E-03	5.83E-01
8.80	8.49	9.11	3.40E-03	3.16E-01
9.42	9.11	9.74	3.11E-03	1.95E-01
10.05	9.74	10.53	3.15E-03	1.27E-01
11.00	10.53	11.50	2.90E-03	7.31E-02
12.00	11.50	12.28	2.23E-03	4.21E-02
12.56	12.28	12.78	1.63E-03	3.15E-02
13.00	12.78	13.50	1.79E-03	2.50E-02
14.00	13.50	14.50	1.79E-03	1.17E-02
15.00	14.50	15.44	1.48E-03	1.16E-02

A comparison of the calculated potential roll RAO with the calculated damped RAOs for the three different assumed frequency bin sizes is presented in Figure 7-12.

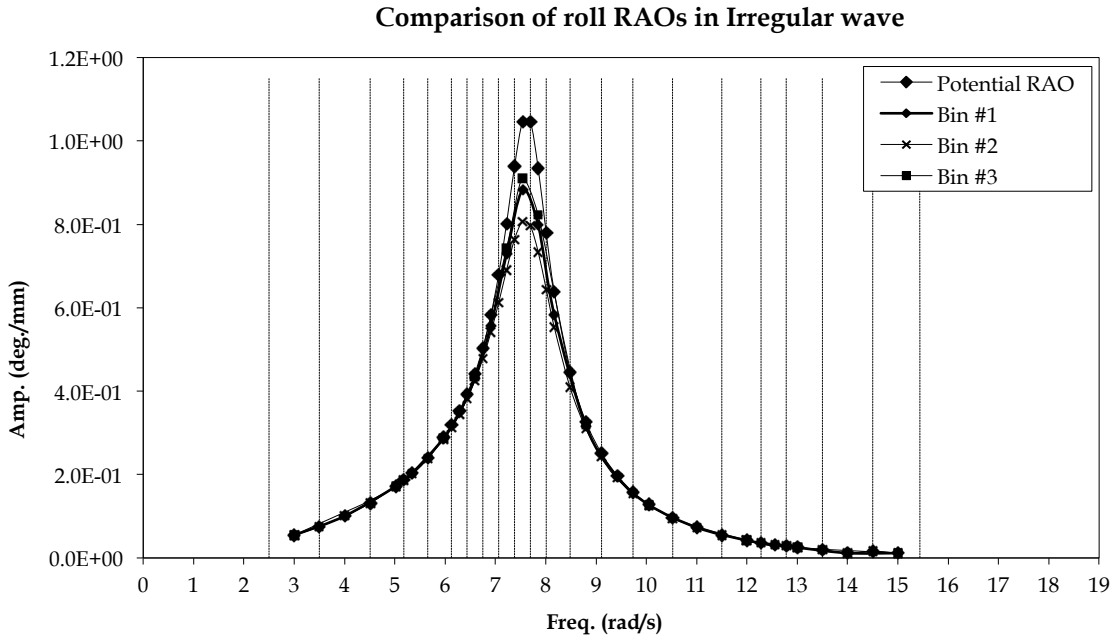

Figure 7-12: Comparison of roll RAOs for an irregular wave

8 Conclusions and Recommendations

Results of implementing the developed methodology to calculating the viscous roll damping in regular waves was presented in Chapter 7. This chapter also included the results of numerical assessments on application of the viscous damping methodology to an irregular wave spectrum. Conclusions on the presented results and recommendations for future work are presented in this chapter.

8.1. Main Conclusions

As demonstrated in Figure 7-3 initial comparisons showed that there is a good agreement between the model test RAO and the damped RAO in regular waves. This indicated that the theoretical method provides a good estimate of the viscous damping of the vessel due to vortex shedding from its edges.

Further comparison with dedicated model test data and new model characteristics presented in Figure 7-7 provided further assurance that the developed methodology provides reliable estimation of the damped roll RAO in regular waves. The good agreement between the model test RAO and the damped RAO presented in Figure 7-7 provides further evidence of the applicability of the Discrete Vortex Method for calculating the viscous roll damping of an oscillating box shaped vessel due to vortex shedding from its edges in regular waves.

Noting the potential RAO, damped RAO and the model test RAO presented in Figure 7-7 it can be seen that the effect of the viscous damping is considerable within certain frequency range. In this study the frequency range was shown to be between 6.3 rad/s and 9.5 rad/s.

Figure 7-8 demonstrates further the effect of roll damping linearization for a range of constant wave amplitudes. It can be observed that the effect of viscous damping increases with increase in the regular wave amplitude for which the damping is linearized especially in the peak region of the RAO. This is an expected relationship between the amplitude of the linearization wave and the roll RAO amplitude.

It can also be observed from Figure 7-8 that the amplitude of the roll RAO varies with wave amplitude in a certain frequency band only. The frequency band in this case lies between 6.3 rad/s and 9.5 rad/s same as what was observed in Figure 7-7. Therefore it can be concluded that the effect of linearization of roll damping for a sea state seems to be focused on a frequency band around the peak of the RAO. Outside of this frequency band the effect of viscous damping becomes insignificant.

Although sway and heave motions are not as sensitive as the roll motion to the assumed viscous damping, the same methodology can be used to calculate viscous damping for both sway and heave as well. In order to do this the same methodology as the one outlined for the roll viscous damping calculation can be used but the viscous damping values outlined in Equation 4-39 and Equation 4-40 shall be used.

As tangential relative fluid velocities are used in the method the same final velocities can be used to calculate skin friction damping. In this study skin friction damping is considered to be negligible and is ignored in calculation of the damped roll RAOs presented in this report.

Noting the above, attempt was made to apply the method to calculating a damped roll RAO that is linearized for a given irregular wave spectrum. Outcome of this attempt is shown in Figure 7-10. The roll RAO presented in

Figure 7-10 confirmed that the revised method in considering effect of all frequencies in the irregular wave spectrum frequency band in calculating the damped roll RAO does converge. This was done for a set of assumed frequency bins within the frequency range of the irregular wave.

The next step was to assess sensitivity of the method to variation in size of frequency bins. This was done for two different bin sizes, one twice the size of the original bin sizes and the other half of the size of the original bin sizes. Outcome of this assessment is presented in Figure 7-11.

A considerable difference between calculated damped RAOs associated to Bin#1 and Bin#2 can be noted in Figure 7-11. Size of the frequency bins in the case of Bin#2 is half the bin sizes in the case of Bin#1. However by increasing the frequency bin sizes to twice the original bin sizes (i.e. Bin#3) the variation in the final damped roll RAO is minimal.

Comparing the calculate damped roll RAOs with the associated potential RAO in Figure 7-12 shows that although the amplitude of the potential RAO is reduced to the calculated damped RAOs due to the assumed additional viscous damping within certain range in vicinity of the peak of the RAO, the reduction in RAO amplitude is not as much as what is seen for linearization for a regular wave.

Further dedicate model tests and mathematical investigations in irregular waves are required to precisely calibrate the method for calculating the viscous damping in irregular waves.

8.2. Recommendations for Future Work

The study conducted demonstrates applicability of the discrete vortex method to the viscous roll damping problem. Since the developed method can be coded as a black box it can be used as an add-on together with any conventional hydrodynamic package to calculate viscous damping of a floating

system. This eliminates use of empirical formula or the need for conducting dedicated model tests. The methodology is also much simple in comparison to computational fluid dynamic (CFD) application.

The methodology presented in this report should however be considered as a basis for further development of the method.

8.2.1 Application of the Method to Rounded Bilge Vessels

Application of the discrete vortex method to box shaped floating vessel using a hydrodynamic diffraction-radiation code was demonstrated in this report to be successful. However, most of the vessels especially the offshore floating systems such as FPSOs consist of a rounded bilge.

It is known that an oscillatory rounded bilge sheds weaker vortexes in comparison to a rectangular edge hence resulting in less roll damping relatively. In practice this is compensated by addition of bilge keels to the vessel.

The development presented in this work can be used as a basis to develop the method for application to floating vessels with a round bilge and furthermore to a floating vessel with round bilge with bilge keels. This should include conducting dedicated model tests to validate the development.

Similar to this study the development can include estimation of the viscous damping for regular waves as well as irregular waves.

8.2.2 Calibration of the Method for Irregular Waves

Although the method was demonstrated to be converging for calculating the viscous damping in irregular waves, dedicated model test measurements should be conducted to calibrate the method for this application. This could consist of measuring the incident irregular wave spectrum and the associated roll response. The measured irregular wave spectrum can be used to calculate a damped roll RAO that is linearized for the measured wave spectrum. The damped RAO and the irregular wave spectrum can then be used to calculate a

response spectrum associated to the calculated damped RAO. Comparison of the response spectrum from measurements with the one calculated from the damped RAO can provide further understanding of calibration of the method in irregular waves.

8.2.3 Use of Dipole Element to Represent Vortex Force

Noting the vortex shedding basis explained in [3] if a vortex shedding in a transformed plane can be defined by Γ_m then the vortex force associated to the shedding could be formulated accordingly. In this case the potential due to the shedding at a point far away from the edge can be written in transformed plane. This will be the potential due to a dipole.

The source-sink dipole can be represented by a sheet element of length l_v in physical z-plane lying along bisector of the shedding edge.

Assuming the total strength of this sheet element is defined by μ_z then the dipole density can be defined as $\frac{\mu_z}{l_v}$. This can be thought of as equivalent to a vortex of strength $\Gamma_0 = \frac{\mu_z}{l_v}$ at each end of the sheet element. In this case if the transformation local to the rectangular vortex shedding edge is defined as $z = c\zeta^{\frac{3}{2}}$, then the sheet element corresponding to vortex Γ_0 at the point $\zeta_0 = \left(\frac{l_v}{c}\right)^{\frac{2}{3}}$ in ζ plane can be formulated accordingly.

Assuming the dipole sheet element can be implemented in a hydrodynamic package the vortex shedding forces at a shedding edge in a hydrodynamic model can be calculated directly using these predefined elements.

9 References and Bibliography

[1] Salvesen, N., Tuck, E.O., and Faltinsen, O, 1970, "Ship motions and sea loads," Transactions of The Society of Naval Architects and Marine Engineers, 78, pp. 250-287.

[2] Downie, M.J., 1987, "The discrete vortex method and the calculation of ship motions," International Seminar on Engineering Applications of the Surface and Cloud Vorticity Methods, 2, pp. 1-18.

[3] Graham, J.M.R., 1980, "The forces on sharp-edged cylinders in oscillatory flow at low Keulegan-Carpenter number," Journal of Fluid Mechanics, 97(1), pp. 331-346.

[4] Downie, M.J., Graham J.M.R., Bearman, P.W., 1987, "The effect of vortex shedding on the roll damping of rectangular barge," Fluid Loading Report No. F.L.42, Department of Aeronautics, Imperial College London.

[5] Downie, M.J., Jillians, W., Graham J.M.R., 1996, "Theoretical prediction of the viscous damping and response of three-dimensional floating structures," EPSRC Grant Reference GR/J23631 (Newcastle), Newcastle University, UK.

[6] Hajiarab, M., Graham, J.M.R., Downie, M.J., 2010, "Prediction of roll damping in the frequency domain using the discrete vortex method," Proceedings of the ASME 2010 29th International Conference on Ocean,

Offshore and Arctic Engineering, Shanghai, China, OMAE2010-21000, 3, pp.625-627, ISBN 978-0-7918-4909-5.

[7] Hajiarab M., Downie M., Graham J.M.R, 2010, "A study on viscous roll damping of a box-shaped vessel in the frequency domain using the discrete vortex method," Transactions of the Royal Institution of Naval Architects Part A: International Journal of Maritime Engineering, 153, pp. 149-152.

[8] Orozco, J.M., Raposo, C.V., 2002, "A practical procedure for the evaluation of the roll motions of FPSO's including the non-potential damping," OTC14234, Offshore Technology Conference, Houston, Texas, ISBN 978-1-55563-249-6.

[9] Froude, W., 1861, "On the rolling of ships," Transactions of the Institution of Naval Architects, 2, pp. 180-227.

[10] Vugts, J.H., 1968, "The hydrodynamic coefficients for swaying, heaving and rolling cylinders in a free surface," International Shipbuilding Progress, 15(167), pp. 251- 276.

[11] Vugts, J.H., 1967, "Pitch and heave with fixed and controlled bow fins," International Shipbuilding Progress, 15(3), pp. 191-215.

[12] Himeno, Y., 1981, "Prediction of ship roll damping – State of the art," Research Project Report no. 239, College of Engineering, The University of Michigan.

[13] Faltinsen, O., 1990, "Sea loads on ships and offshore structures," Cambridge University Press, UK, ISBN 0 521 45870 6.

[14] Souza, J.R., Fernandes, A.C., Masetti, I.Q., daSilva, S., Kroft, S.A.B., 1998, "Nonlinear roll of an FPSO with larger than usual bilge keels," Proceedings of the ASME 1998 17th International Conference on Ocean, Offshore and Arctic Engineering, Lisbon, Portugal, OMAE98-0412.

[15] Oliveira, A.C., 2003, "Investigacoes sobre a teoria bilinear na analise do

blnco transversal de FPSOs (Investigation about the bilinear theory for the analysis of FPSO Rolling)," Ocean Engineering, Federal University of Rio de Janeiro (In Portuguese).

[16] Fernandes, A.C., Kroft, S.A.B., 2000, "Bi-linear modelling of wider, longer and continues bilge keels for FPSOs roll motion control," Proceedings of the ASME 2000 19th International Conference on Ocean, Offshore and Arctic Engineering, New Orleans, USA, OMAE2000-OFT-4072.

[17] Standing, R.G., 1991, "Prediction of viscous roll damping and response of transportation barges in waves," Proceedings of the 1st International Offshore and Polar Engineering Conference, Edinburgh, UK, ISBN 0-9626104-61, 3, pp. 409-420.

[18] Choi, Y.R., Kim, J.H., Song, M.J., Kim, Y.S., 2004, "An experimental and numerical study of roll motions for a barge type LNG FPSO," Proceedings of the 14th International Offshore and Polar Engineering Conference, Toulon, France, 1, pp. 672-675.

[19] Van Dijk, R.R.T., Quiniou_Ramus, V., Le-Marechal, G., 2003, "Comparison of full scale measurements with calculated motion characteristics of a west of Africa FPSO," ASME 2003 22nd International Conference on Offshore Mechanics and Arctic Engineering, Cancun, Mexico, OMAE2003-37182, pp. 335-339.

[20] Park, I.K., Shin, H.S., Ham K.S., Cho J.W., 1999, "An experimental study on roll damping for tanker-based FPSO," Proceeding of the 9th International Offshore and Polar Engineering Conference, Brest, France, ISBN 1-880653-39-7.

[21] van 't Veer, R., Fathi, F., 2011, "On the roll damping of an FPSO with riser balcony and bilge keels," Transactions RINA, International Journal Maritime Engineering, Part A2, 153.

[22] Aloisio, G., Di Felice, F., 2006, "PIV analysis around the bilge keel of a ship model in free roll decay," XIV Convegno Nazionale A.I.VE.LA, Roma,

Italy.

[23] van Kessel, J.L.F., van der Velde, W.J., 2008, "The effect of dual drift hull on the motion behaviour of a pipelay/heavylift vessel," Proceedings of the ASME 27th International Conference on Offshore Mechanics and Arctic Engineering, Estoril, Portugal, OMAE2008-57357.

[24] Jung, K.H., Chang K.A., Chen H.C., Huang, E.T., 2003, "Flow analysis of rolling rectangular barge in beam sea condition," Proceeding of the 13th International Offshore and Polar Engineering Conference, Honolulu, Hawaii, ISBN 1-880653-60-5.

[25] Huang, Z.J., Esenkov, O.E., O'Donnell, B.J., Yung T.W., Sandstrom, R.E., 2007, "Improved prediction of full scale roll motions for vessels with large liquid tanks," Proceeding of the 17th International Offshore and Polar Engineering Conference, Lisbon, Portugal, ISBN 978-1-880653-68-5.

[26] Kwang, H.J., Kuang-An, C, Hyo, J.J., 2006, "Viscous Effect on the Roll Motion of a Rectangular Structure," Journal of Engineering Mechanics, 132(2), pp. 190-200, ISSN 0733-9399.

[27] Wu, X., Tao, L., Li, Y., 2005, "Nonlinear Roll Damping of Ship Motions in Waves," Journal of Offshore Mechanics and Arctic Engineering, 127(3), pp. 205-211, ISSN 1528-896X.

[28] Rae, H.Y., Dong, H.L., Hang, S.C., 2003, "A study on Roll Damping of 2-D Cylinders," International Journal of Offshore and Polar Engineering, 13(3), pp. 205-208, ISSN 1053-5381.

[29] Douglas, B.C., 1982, "The Effect of Forward Speed on Ship Roll Damping," M.Sc. dissertation, Memorial University of Newfoundland.

[30] Ikeda, Y., Katayama, T., 2000, "Roll Damping Prediction Method for a High-Speed Planning Craft," Proceedings of the 7th International Conference on Stability of Ship and Ocean Vehicles, B, pp. 532-541.

[31] Incecik, A., 1982, "Design aspects of the hydrodynamic and structural

loading on floating offshore platforms under wave excitation," Ph.D. thesis, Department of Naval Architecture and ocean Engineering, Glasgow University.

[32] Kerwin, J.E., 1955, "Notes on rolling in longitudinal waves," International Shipbuilding Progress, 2, pp. 597–614.

[33] Haddara M.R., 1971, "On the stability of ship motion in regular oblique waves," International Shipbuilding Progress, 18(207), pp. 416–434.

[34] Dalzell, J.F., 1978, "Note on the form of ship roll damping," Journal of Ship Research, 22(3), pp. 178–185.

[35] Haddara, M.R., 1984, "A note on the effect of damping moment form on rolling response," International Shipbuilding Progress, 31(363), pp. 285–290.

[36] Nayfeh, A.H.,Khdeir, A.A., 1986, "Nonlinear rolling of ships in regular beam seas," International Shipbuilding Progress, 33, pp. 40-49.

[37] Peyton Jones, J.C., Cankaya, I., 1986, "The effect of constant heeling moment on the main and super-harmonic roll response of ship in regular beam seas," International Shipbuilding Progress, 33, pp. 84-93.

[38] Journée, J.M.J., 2001, "Theoretical Manual of SEAWAY," Delft University of Technology, Ship hydromechanics Laboratory.

[39] Journée, J.M.J. , 1992, "Quick strip theory calculations in ship design", PRADS'92, Conference on Practical Design of Ships and Mobile Structures, Vol. I, Newcastle upon Tyne, UK.

[40] Schmitke, R.T., 1978, "Ship sway, roll and yaw motions in oblique seas," SNAME Transactions, 86, pp. 26-46.

[41] Lee, J.H., Incecik, A., 2007, "The simplified method for the prediction of radiation damping coefficients," Proceedings of the Sixteenth International Offshore and Polar Engineering Conference, Lisbon, Portugal, pp. 2178-

2183, ISBN-13 978-1-880653-68-5.

[42] Arne, B, Faltisen O.M., 1988, "Application of a Vortex Tracking Method to Roll Damping," Advances in Underwater Technology and Offshore Engineering, Technology Common to Aero and Marine Engineering, 15, pp. 177-193, ISBN 1-85333-054-X.

[43] Chakrabarti, S., 2001, "Empirical Calculation of Roll Damping for Ships and Barges," Ocean Engineering, 28(7), pp. 915-932.

[44] Taylan, M., 2000, "The Effect of Nonlinear Damping and Restoring in Ship Rolling," Ocean Engineering, 27(9), pp. 921-932.

[45] Lighthill, J. ,1986, "Fundamentals Concerning Wave Loading on Offshore Structures," Journal of Fluid Mechanics, 173, pp. 667-681, ISSN 8600-1313.

[46] Kwang, H.J., Kuang-An, C., Erick, T.H., 2004, "Two-Dimensional Flow Characteristics of Wave Interactions with a Free-Rolling Rectangular Structure," Ocean Engineering, 32(1), pp. 1-20.

[47] Oshkai, P., Rockwell, D., 1999, "Free Surface Wave Interaction with a Horizontal Cylinder," Journal of fluids and structures, 13(7-8), pp. 935-954, ISSN 1999-0237.

[48] Santiago, I.B. ,2008, "Roll Motion of a Ship and the Roll Stabilising Effect of Bilge Keels," The Journal of Navigation, 61, pp. 667-689, ISSN 0800-4931.

[49] Ray-Qing, L., Weija, K., 2008, "Modelling nonlinear roll damping with a self- consistent, strongly nonlinear ship motion model," Journal of Marine Science and Technology, 13, pp. 127–137, ISSN 00773-007-0262-9.

[50] Korpus, R.A., Falzarano, J.M., 1997, "Prediction of Viscous Ship Roll Damping by Unsteady Navier- Stokes Techniques," Journal of Offshore Mechanics and Arctic Engineering, 119(2), pp. 108-113, ISSN 1.2829050.

[51] El-Bassiniouny, A.F., 2007, "Nonlinear Analysis for a Ship with a General Roll- Damping Model," Physica Scripta, 75, pp. 691-701, ISSN 0031-8949.

[52] Mulk, M.T.U., Falzarano, J., 1994, "Complete Six-Degrees-of-Freedom Nonlinear Ship Rolling Motion," Journal of Offshore Mechanics and Arctic Engineering, 116(4), pp. 191-201.

[53] Bangun, E.P., Utsunomiya, T., 2008, "Evaluation of Viscous Forces Acting on a Moving Body by Navier-Stoke Solver," OCEANS'08 MTS/IEEE Kobe-Techno-Ocean Conference, pp. 1-8, ISSN 978-1-4244-2125-1.

[54] Robert, J.B., Vasta, M., 2000, "Markov Modelling and Stochastic Identification for Nonlinear Ship Rolling in Random Wave," Philosophical Transaction of the Royal Society A: Mathematical, Physical and Engineering Sciences, 358, pp. 1917-1941, ISSN 2000-0621.

[55] Ikeda, Y., 2004, "Prediction Methods of Roll Damping of Ships and Their Application to Determine Optimum Stabilization Devices," Marine Technology, 41, pp. 89-93, ISSN 0025-3316.

[56] Klaka, K., Krokstad, J., Renilson, M.R., 2001, "Prediction of Yacht Roll Motion at Zero Forward Speed," 14th Australasian Fluid Mechanics Conference, Adelaide, Australia, pp. 1-4.

[57] Yuck, R.H., Lee, D.H., Choi, H.S., 2003, "Estimation of roll damping coefficients for non-conventional midship sections," Proceedings of 13th International Offshore and Polar Engineering Conference, Honolulu, Hawaii, 3, pp. 540-543, ISBN 1-880653-60-5.

[58] Inoue, Y., Islam, R., 2001, "Effect of viscous roll damping on drift forces of multi-body floating systems in waves," Proceedings of 11th International Offshore and Polar Engineering Conference, Stavanger, Norway, 1, pp. 279-285.

[59] de Jong, P., van Walree, F., 2008, "Hydrodynamic lift in a time-domain panel method for the seakeeping of fast ships," 6th International Conference on High Performance Marine Vehicles, Naples, Italy.

[60] Ledoux, A., Molin, B., de Joutte, C., Coudray, T., 2004, "FPSO roll damping

prediction from CFD and 2D and 3D model test investigations," Proceedings of 14th International Offshore and Polar Engineering Conference, Toulon, France, 1, pp. 687-695.

[61] Gachet, M., Kherian, J.G., 2008, "Impact of linearization of bilge keel damping on the early assessment of vessel operability," Proceedings of the ASME 27th International Conference on Offshore Mechanics and Arctic Engineering, Estoril, Portugal, OMAE2008-57255.

[62] Rott, N., 1956, "Diffraction of a weak shock with vortex generation," Journal of Fluid Mechanics, 1(01), pp. 111-128.

[63] Brown, C.E., Michael, W.H., 1955, "On Slender Delta Wings with Leading Edge Separation," National Advisory Committee for Aeronautics, Technical Note 3430.

[64] Graham, J.M.R., 1977, "Vortex shedding from sharp edges," Imperial College University, London, Aero report No. 77-06, ISSN 0308-7247.

[65] Al-Hukail, Y.O.I., 1992, "Roll damping due to vortex shedding from slender ship hulls in forward motion," PhD Thesis, Imperial College London (University of London).

[66] Graham, J.M.R., Al-Hukail, Y.O., Bearman, P.W., Zhao, Y.D., Downie, M.J., 1994, "Numerical Prediction of the Effect of Forward Speed on Roll Damping," Proceedings of 20th Symposium on Naval Hydrodynamics, Santa Barbara, USA, pp. 657-668.

[67] Wright, J.H.G., Marshfield, W.B., 1980, "Ship roll response and capsize behaviour in beam seas," Transactions of Royal Institute of Naval Architects, 122, pp. 129-148.

[68] Das, S.K., Das, S.N., 2007, "Modelling of coupled roll and yaw damping of a floating body in waves," Mathematical Problems in Engineering, 2007, Article ID 96373.

[69] Downie, M.J., Bearman, P.W., Graham J.M.R., 1987, "The effect of vortex

shedding on the coupled roll response of bodies in waves," Journal of fluid mechanics, 189, pp. 243-264.

[70] Coznes, P., 1987, "Numerical modelling of the roll damping of ships due to vortex shedding," PhD thesis, Imperial College University, London.

[71] Taylor, R.E., Teng, B., 1993, "The effect of corners on diffraction/radiation forces and wave drift damping," 25th Annual Offshore Technology Conference, Houston, Texas, OTC 7187, ISBN 978-1-61399-089-6.

[72] Graham, J.M.R., Sherwin, S.J., Kendon, T.E., Downie M.J., 2005, "The prediction of the viscous damping of large floating bodies in waves," 20th International Workshop on Water Waves and Floating Bodies, Spitzbergen.

[73] Cardo, A., Francescutto A., Nabergoj, R., 1982, "On damping models in free and forced rolling motion," Ocean Engineering, 9(2), pp. 171–179.

[74] Mathisen, J.B., Price, W.G., 1985, "Estimation of ship roll damping coefficients," Transactions of Royal Institution of Naval Architects, 127, pp. 295–307, ISSN 0035-8967.

[75] Spouge, J.R., 1988, "Nonlinear analysis of large-amplitude rolling experiments," International Shipbuilding Progress, 35(403), pp. 271–320.

[76] Roberts, J.B., 1985, "Estimation of nonlinear ship roll damping from free-decay data," Journal of Ship Research, 29(2), pp. 127–138.

[77] Bass, D.W., Haddara, M.R., 1988, "Nonlinear models of ship roll damping," International Shipbuilding Progress, 35(401), pp. 5–24.

[78] Haddara, M.R., Bennett, P., 1989, "A study of the angle dependence of roll damping moment," Ocean Engineering, 16(4), pp. 411–427.

[79] Haddara, M.R., Bass, D.W., 1990, "On the form of roll damping moment for small fishing vessels," Ocean Engineering, 17(6), pp. 525–539.

[80] Chun, H.H., Chun, S.H., Kim, S.Y., 2001, "Roll damping characteristics of a small fishing vessel with a central wing," Ocean Engineering, 28(12), pp.

1601–1619.

[81] Downie, M.J., Graham J.M.R., Wang, J., 1999, "Effects of porous and solid bilge keels on the response of FPSOs in regular and random waves," Proceedings of 18th International Conference on Offshore Mechanics and Arctic Engineering, St. John´s, Newfoundland, Canada.

[82] Brown, D.T., Eatock Taylor, R., Patel, M.H., 1983, "Barge motions in random seas – a comparison of theory and experiment," Journal of Fluid Mechanics, 129, pp. 385-407.

[83] Borgman, L.E., 1967, "Ocean Wave Simulation for Engineering Design," Hydraulic Engineering Laboratory, College of Engineering, University of California.

[84] Singh, S., 1979, "Forces on bodies in oscillatory flow," PhD Thesis, Imperial College London.

[85] Keulegan, G.H., Carpenter, L.H., 1958, "Forces on cylinders and plates in an oscillating fluid," Journal of Research of the National Bureau of Standards, 60(5), pp. 423-440.

[86] Kaplan, R., 1966, "Lecture notes on nonlinear theory of ship roll motion in a random sea," Proceedings of 11th International Towing Tank Conference, Tokyo, Japan, pp. 393-396.

[87] Bhattacharyya, R., 1978, "Dynamics of marine vehicles," John Willey & Sons, New York, ISBN-13: 978-0471072065.

[88] Nayfeh, A.H., 1981, "Perturbation methods," John Willey & Sons, New York, ISBN-13: 978-0471399179.

[89] Bass, D.W., Haddara, M.R., 1988, "Nonlinear models of ship roll damping," International Shipbuilding Progress, 35, pp. 5-24.

[90] Cardo, A., Ceschia, M., Francescutto, A. and Nabergoj, R., 1980, "Effects of the angle-dependent damping on the rolling motion of ships in regular

beam seas," International Shipbuilding Progress, 27, pp. 135-138.

[91] Cardo, A., Francescutto, A. and Nabergoj, R., 1981, "Ultra-harmonics and sub-harmonics in the rolling motion of a ship: steady-state solution," International Shipbuilding Progress, 28, pp. 234-251.

[92] Cardo, A., Francescutto, A. and Nabergoj, R., 1982, "On damping models in free and forced rolling motion," Ocean Engineering, 9, pp. 171-179.

[93] Cardo, A., Francescutto, A. and Nabergoj, R., 1984, "Nonlinear rolling response in a regular seas," International Shipbuilding Progress, 31, pp. 204-208.

[94] Haddara, M.R., 1973, "On nonlinear rolling of ships in random seas," International Shipbuilding Progress, 20, pp. 377-387.

[95] Journée, J.M.J., Massie, W.W., 2001, "Offshore Hydromechanics," Delft University of Technology.

[96] Havelock, T.H., 1942, "The damping of the heaving and pitching motions of a ship," Philosophical Magazine Series, 33(7), pp. 666-673.

[97] Havelock, T.H., 1955, "Waves due to floating sphere making periodic heaving oscillations," Proceedings of the Royal Society of Mathematical, Physical and Engineering Science, 231(1184), pp. 1-7.

[98] Abramowitz, M., Stegun, I.A., 1964, "Handbook of Mathematical Functions with Formulas, Graphs and Mathematical tables," U.S. Department of Commerce, National Bureau of Standards.

[99] Karlsen, S.H., 2012, "Barge Transportation of heavy objects," Master's Thesis, Norwegian University of Science and Technology.

[100] Bakare, A.A., 2009, "The Influence of Viscous Effects on the Roll Motion of an Offshore Jacket Transport/Launching Barge in Waves," Master's Thesis, Newcastle University, School of Marine Science and Technology.

Appendix A: Preliminary Model Test Data

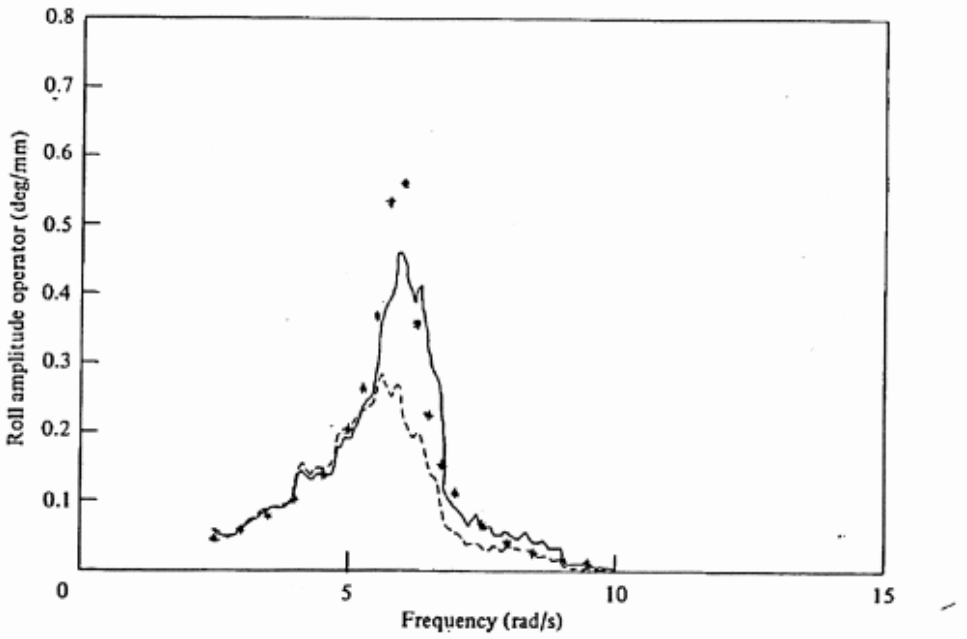

FIGURE 18. Roll transfer function in beam seas for 1:36 scale; full and dotted lines denote data for rounded and sharp keel-edge profiles respectively; asterisks denote theory.

Appendix Figure A- 1: Roll transfer function reported by Brown et al. [82]

Appendix B: Publications

Proceedings of the ASME 2010 29th International Conference on Ocean, Offshore and Arctic Engineering
OMAE2010
June 6-11, 2010, Shanghai, China

OMAE2010-21000

PREDICTION OF ROLL DAMPING IN THE FREQUENCY DOMAIN USING THE DISCRETE VORTEX METHOD

Mohammad Hajiarab
Lloyd's Register EMEA
Aberdeen, United Kingdom

J Michael R Graham
Imperial College London
United Kingdom

Martin Downie
Newcastle University
United Kingdom

ABSTRACT

This paper describes a theoretical approach to predict roll damping for a three-dimensional barge shaped vessel in the frequency domain by matching a simple discrete vortex method (DVM), describing local separated flow, to an inviscid 3-D seakeeping code.

The results are compared with model test experiments to demonstrate validity of the method. A good agreement between the model test RAO and the damped RAO is achieved.

INTRODUCTION

One of the most important subjects in FPSO design is prediction of roll motion. The best known method for predicting the roll motion is to include an equivalent linear viscous roll damping coefficient in the motion equation. Traditionally the roll damping coefficient has been determined by model testing. This is not always practical in the early stages of design and there are difficulties in scaling the results to full scale. Hence, several numerical methods have been developed to predict the roll damping without model testing.

One of these methods makes use of the discrete vortex method which is a technique for analysing two-dimensional separated flows in the time domain. Graham **[1]** implemented a simple discrete vortex analysis for flow about an infinite wedge in oscillatory flows in which the flow in an infinite half-plane, the ς -plane, was transformed to flow about an isolated edge. The method enabled him to calculate a generalised vortex force on the infinite wedge from which he inferred the total force on a finite body with flow separation from its edges. The approach was developed further by Downie et al. **[2, 3]**.

In the present work the same technique is used to model separated flow from a barge shaped vessel to provide input to an inviscid 3-D seakeeping program to calculate its roll RAO, including vortex shedding, in frequency domain.

The roll RAOs predicted by this approach are compared with model test results to assess its validity. The comparison shows a good agreement between the model tests and theoretical calculations.

METHODOLOGY

Downie et al. **[2, 3]** demonstrated that for the 2-D barge as defined in **Figure 1**, rolling about point "O" with an oscillatory angular velocity described by $\dot{a} = \omega \cdot \hat{a} \cdot Sin(\omega t)$ where $\dot{a}$ is the angular velocity and $\hat{a}$ is the angular velocity amplitude, the vortex shedding roll moment F_{v4} can be formulated as:

$$F_{v4} = \frac{1}{2}\rho \cdot c_4 \cdot b^{\frac{4}{3}} \left| \frac{\phi_v - \phi_h}{\Delta\varsigma^*} \right|^2 \Psi(t) \qquad (1)$$

in which ρ is the fluid field density, c_4 is a coefficient representing the lever arm for the vortex roll moment, b is the breadth of the barge, h is the draught of the barge, ϕ_v is the velocity potential at the vertical side of the shedding edge, ϕ_h is the velocity potential at horizontal side of the shedding edge, $\Delta\varsigma^*$ is the distance between points in the ς plane on either side of the edge and $\Psi(t)$ is the dimensionless vortex force coefficient which is pre-calculated using the discrete vortex method **[1]**.

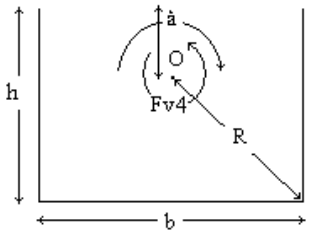

Figure 1: Definition of the cross section of a typical barge

The vortex roll force presented in **Equation (1)** can be transformed in to the frequency domain as:

$$f_{v4} = a_4 + ib_4 = \frac{3^{\frac{5}{3}}}{2^{\frac{4}{3}}} \cdot \frac{(A - iB)}{\pi^2} \cdot \rho \cdot b^2 \cdot \left(\frac{1-\mu^2}{\mu \cdot I_2} \right)^{\frac{1}{3}} \cdot \left(\frac{\mu \cdot b \cdot I_c}{4 I_2} \right) \cdot \left| \frac{q \cdot s^{\frac{1}{3}}}{b^{\frac{1}{3}}} \right| \left(\frac{q_j \cdot s^{\frac{1}{3}}}{b^{\frac{1}{3}}} \right) \cdot x \cdot \frac{H}{2} \quad (2)$$

where a_4 is the vortex induced added mass, b_4 is vortex induced damping coefficient, $(A + iB)$ is the vortex force coefficient calculated with the DVM for an infinite right angle edge and which is equal to 1.566-i0.157, q is the total fluid velocity at the shedding edge calculated for the combined six degree of freedom motion, q_j is the total velocity at the shedding edge calculated in the forced roll motion mode, s is the distance from edge to centre of the facet in which the velocity is calculated, x is width of the facet along the length, H is the wave height and μ is Schwartz-Christoffel ratio which can be calculated by iteration for a given aspect ratio. In this case if the aspect ratio of the cross section of the barge is defined as $AR = \frac{b}{2h}$, then from a Schwartz-Christoffel transformation it can be shown that **[3]**:

$$AR = \frac{I_2}{I_1} = \frac{E(\mu^2) - (1-\mu^2)K(\mu^2)}{E(1-\mu^2) - \mu^2 K(1-\mu^2)}$$

where E and K are elliptic integrals of the first and second kind respectively.

Finally if $\lambda = \frac{1}{\mu}$ then:

$$I_c = \int_1^{\lambda} \left\{ \int_{\sigma}^{\lambda} \left(\frac{\sigma'^2 - 1}{\lambda^2 - \sigma'^2} \right)^{\frac{1}{2}} d\sigma' \right\} \frac{2\sigma \cdot d\sigma}{\left[(\lambda^2 - \sigma^2)(\sigma^2 - 1) \right]^{\frac{1}{2}}} + \int_0^{1} \left\{ \int_{1}^{\sigma} \left(\frac{1 - \sigma'^2}{\sigma'^2 - \lambda^2} \right)^{\frac{1}{2}} d\sigma' \right\} \frac{2\sigma \cdot d\sigma}{\left[(\lambda^2 - \sigma^2)(1 - \sigma^2) \right]^{\frac{1}{2}}} \quad (3)$$

In this case the velocity at the tip of the shedding edge becomes singular in the sharp edged potential flow model. Therefore the velocity of the fluid at the edge for combined motion, (i.e. q), and the forced roll mode, (i.e. q_j) are calculated using weighted averaging of the velocity at the two facets on each side of the vortex shedding edge. Weights are based on the distance between the centre of the facet to the shedding edge (i.e. s).

CASE STUDY

A comparison was conducted between theoretical results and model test data for a sharp keel-edge profile provided by Brown et al. **[4]**.

The main characteristics of the model are presented in **Table 1**. A 3-D diffraction radiation potential hydrodynamic model was used to calculate the required velocities at the shedding edges and the final damped Response Amplitude Operator (RAO). The hydrodynamic model showing the boundary element panel discretisation is presented in **Figure 2**.

Table 1: Main characteristics of the model

Main characteristic	-
Length (m)	2.4
Beam (m)	0.8
Draught(m)	0.105
Mass (kg)	200.8
Longitudinal Centre of Gravity from AP (m)	1.2
Vertical Centre of Gravity from keel (m)	0.111
Roll Radius of Gyration (m)	0.244
Pitch Radius of Gyration (m)	0.688
Yaw Radius of Gyration (m)	0.598

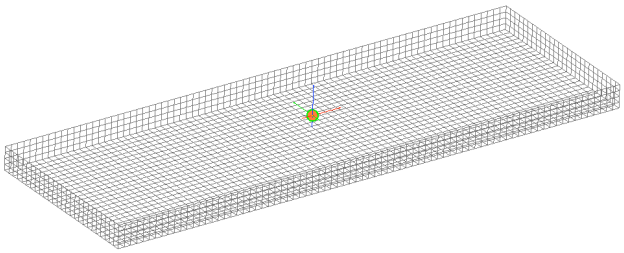

Figure 2: Hydrodynamic model of the barge

Calculation of the final roll RAO with viscous damping consists of the following steps:

1) A potential flow calculation is conducted and the equations of motion solved to calculate the fluid velocity relative to the vessel at the centre of facets along the shedding edge in a six degree of freedom coupled motion.
2) The fluid velocity relative to the vessel at the centre of the facets along the shedding edge in forced roll mode is calculated separately.
3) Based on the velocities calculated in steps 1 and 2, the b_4 (vortex shedding damping) value is calculated from **Equation (2)** for each strip of facets separately on the port and starboard sides.
4) The b_4 values calculated in step 3 are integrated for the full model and the total value is put back in to the hydrodynamic model and motion calculation in steps 1 and 2 above.
5) Steps 1 to 4 are iterated until the difference in the calculated roll amplitude from successive iterations is within acceptable limit. Convergence is then assumed

and the procedure is repeated separately for each frequency.

RESULTS

The results from the calculation are compared with the model test roll RAOs **[4]** and the potential flow roll RAOs in **Figure 3**.

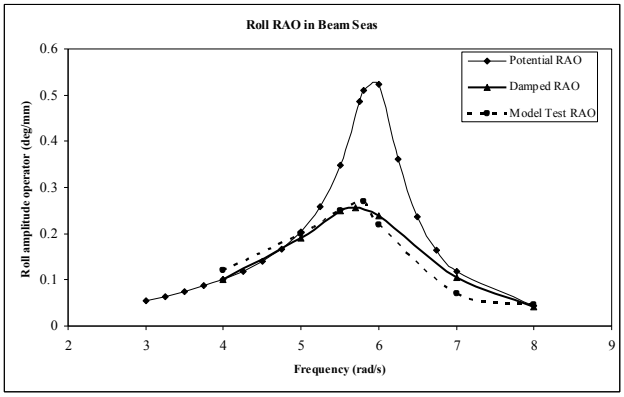

Figure 3: Comparison of Roll RAO in Beam Seas

The model test data shown in **Figure 3** represent the roll RAOs in beam seas for a 1:36 scale model with a sharp keel-edge profile. The reported roll RAO in beam seas in the Brown et al. paper is shown in **Appendix-Figure 1**.

The viscous damping for the damped RAO, which is a function of the wave height since it is non-linear, is calculated here for a 24mm wave height and is converged to an error of 0.1 degree in the roll angle.

DISCUSSIONS AND RECOMMENDATIONS

As demonstrated in **Figure 3**, there is a good agreement between the model test RAO and the damped RAO indicating that the theoretical method provides a good estimate of the viscous damping of the vessel due to vortex shedding from its edges.

Although viscous damping in pitch and heave motions is not as significant as for the roll for a barge, the same methodology can be used to calculate viscous damping for both pitch and heave as well.

As tangential relative fluid velocities are used in this method, the same final velocities can be used to calculate skin friction damping. In this study skin friction damping is considered to be negligible and is ignored in the damped RAO.

Further specific model test studies are taking place in Newcastle University towing tank facilities to measure the roll RAO of a barge shaped vessel for further comparison and validation of the method.

ACKNOWLEDGMENTS

The authors wish to thank Lloyd's Register EMEA and Martec Limited, specially Dr. Graham Stewart, Mr. Richard Bamford, Mr. Richard Nott and Dr. Frank Lin for their support of this work.

The opinions expressed in this paper are those of the authors and are not necessarily those of Lloyd's Register.

REFERENCES

[1] Graham, J.M.R., 1980, "The forces on sharp-edged cylinders in oscillatory flow at low Keulegan-Carpenter number," J. Fluid Mech. (1980), 97(1), pp.331-346.

[2] Downie, M.J., and Graham J.M.R., and Bearman, P.W., 1987, "The effect of vortex shedding on the roll damping of rectangular barge," Fluid Loading Report No. F.L.42, Department of Aeronautics, Imperial College London.

[3] Downie, M.J., and Jillians, W., and Graham J.M.R., 1996, "Theoretical prediction of the viscous damping and response of three-dimensional floating structures," EPSRC Grant Reference GR/J23631 (Newcastle).

[4] Brown, D.T., Eatock Taylor, R., Patel, M.H., 1983, "Barge motions in random seas – a comparison of theory and experiment," . J. Fluid Mech. (1983), 129, pp.385-407.

APPENDIX

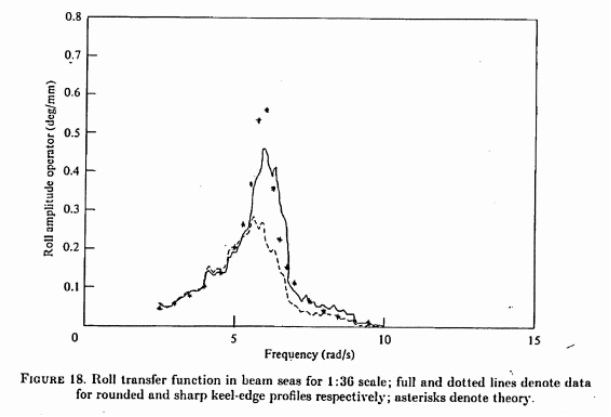

FIGURE 18. Roll transfer function in beam seas for 1:36 scale; full and dotted lines denote data for rounded and sharp keel-edge profiles respectively; asterisks denote theory.

Appendix-Figure 1: Roll transfer function reported by Brown et al. [4]

THE ROYAL INSTITUTION OF NAVAL ARCHITECTS

A study on viscous roll damping of a box-shaped vessel in the frequency domain using the Discrete Vortex Method

M Hajiarab, Lloyd's Register EMEA, UK
M Downie, Newcastle University upon Tyne, UK
M Graham, Imperial College London, UK

SUMMARY

This paper presents a study on viscous roll damping of a floating box-shaped vessel in the frequency domain. The application of the discrete vortex method (DVM) for calculation of the viscous roll damping in regular seas has been validated by model tests. Equivalent roll RAOs associated with a range of regular wave amplitudes are calculated to assess behaviour of the viscous roll damping in relation to incident wave amplitude linearisation. A model test is conducted using the model test facilities of the Marine Hydrodynamics Laboratory at Newcastle University to validate the applicability of the DVM in calculating the roll RAO in regular waves and to study the application of this method to irregular waves. Results of these model tests are presented in this paper.

NOMENCLATURE

μ	Schwartz-Christoffel ratio
ρ	Density of the fluid field
a_4	Vortex induced added mass coefficient
b_4	Vortex induced damping coefficient
b	Breadth of the barge
f_{v4}	Vortex force at shedding edge
$f(t)$	Time series
h	Draught of the barge
q	Coupled motion fluid velocity at shedding edge
q_j	Forced motion fluid velocity at shedding edge
s	Distance of shedding edge to centre of the facet
x	Width of the facet
AR	Aspect ratio of the barge cross section
H	Linearised damping wave height
N	Number of samples in time series
$S(w)$	Power spectrum in frequency domain

1. INTRODUCTION

Prediction of roll damping has been a challenging task for naval architects. Froude [1] studied the effect of wave height and steepness on the rolling of ships and the influence of this phenomenon on the design of ship hull shape.

For floating offshore installations accurate estimate of the roll damping is important as the roll motion governs the transverse loads and this has direct impact on the design of hull, topside structures and process plant on board. Furthermore, noting the calculation limitations and time constraints for conducting motion analysis of a floating vessel in the time domain, frequency domain calculations have become the norm in the industry. Although most vessel responses can be calculated with acceptable accuracy in the frequency domain, this is more difficult for roll response due to the nonlinear behaviour of roll damping.

Theoretically the total roll damping of a floating vessel can be divided into potential and viscous components. The potential component can be predicted accurately since it has a linear characteristic, however the viscous component is non-linear and prediction of this is more problematic.

The challenge is to develop a reliable method for calculating the equivalent linearised roll damping which enables the required response statistics to be calculated in the frequency domain for operational strength and fatigue analysis.

It is a common practice to divide the viscous roll damping into several components such as vortex shedding damping, skin friction damping, eddy damping, etc. [2]. For the case of a rolling box shaped floating vessel, vortex shedding is the dominant roll damping component.

In order to estimate the vortex force on the shedding edge of a box shaped model, Graham [3] implemented a simple discrete vortex analysis for flow about an infinite wedge in oscillatory flow in which the flow in an infinite half-plane, the ς-plane, was transformed to flow about an isolated edge. The method enabled him to calculate a generalised vortex force on the infinite wedge from which he inferred the total force on a finite body with flow separation from its edges. The approach was developed further by Downie et al. [4, 5]. Hajiarab et al. [6] applied the method to a 3-D numerical model for wave diffraction and demonstrated that it produces results that compare well with model test results in regular waves.

In order to eliminate any uncertainty in the model test results used in [6], further model tests were conducted to validate the application of this methodology in regular waves. In this case the roll damping has been linearised

for a given wave amplitude in each frequency. Results of these model tests are presented in this paper.
In line with the Lloyd's Register Response Based Analysis (RBA) methodology [7], the longer term objective of this work is to develop a procedure for linearization of the roll damping to enable spectral analysis of response to be undertaken for given seastates. The progress made towards this is presented in this paper.

2. METHODOLOGY

As outlined in [6], the generated vortex force due to roll at the shedding edge of the box shaped vessel can be formulated as:

$$f_{v4} = a_4 + ib_4 = \frac{3^{\frac{5}{3}}}{2^{\frac{4}{3}}} \cdot \frac{(1.566 - i0.157)}{\pi^2} \cdot \rho \cdot b^2 \cdot \left(\frac{1-\mu^2}{\mu \cdot I_2}\right)^{\frac{1}{3}} \cdot \left(\frac{\mu \cdot b \cdot I_c}{4I_2}\right) \cdot \left|\frac{q \cdot s^{\frac{1}{3}}}{b^{\frac{1}{3}}}\right| \left(\frac{q_j \cdot s^{\frac{1}{3}}}{b^{\frac{1}{3}}}\right) \cdot x \cdot \frac{H}{2}$$

where μ, the Schwartz-Christoffel ratio, can be calculated by iteration for a given barge aspect ratio. In this case if the aspect ratio of the cross section of the barge is defined as:

$$AR = \frac{b}{2h}$$

then from a Schwartz-Christoffel transformation it can be shown [5] that:

$$AR = \frac{I_2}{I_1} = \frac{E(\mu^2) - (1-\mu^2)K(\mu^2)}{E(1-\mu^2) - \mu^2 K(1-\mu^2)}$$

where E and K are elliptic integrals of the first and second kind respectively.

Finally if $\lambda = \frac{1}{\mu}$ then:

$$I_c = \int_1^{\lambda} \left\{ \int_{\sigma}^{\lambda} \left(\frac{\sigma'^2 - 1}{\lambda^2 - \sigma'^2} \right)^{\frac{1}{2}} d\sigma' \right\} \frac{2\sigma \cdot d\sigma}{\left[(\lambda^2 - \sigma^2)(\sigma^2 - 1)\right]^{\frac{1}{2}}} + \int_0^{1} \left\{ \int_{1}^{\sigma} \left(\frac{1 - \sigma'^2}{\sigma'^2 - \lambda^2} \right)^{\frac{1}{2}} d\sigma' \right\} \frac{2\sigma \cdot d\sigma}{\left[(\lambda^2 - \sigma^2)(1 - \sigma^2)\right]^{\frac{1}{2}}}$$

In order to compute the strength of the velocity singularity at the tip of the shedding edge in the sharp edged potential flow model, weighted averaging of the velocity at the two facets on each side of the vortex shedding edge is employed to calculate q and q_j. The weights are based on the distance between the centre of the facet to the shedding edge, s.
The extent of the hydrodynamic panel model of the barge is presented in Figure 1.

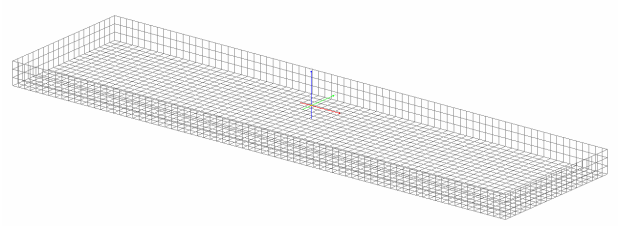

Figure1: Hydrodynamic model of the barge

In this method, for each frequency q and q_j are calculated individually for each strip of panels along the length of the barge and at each iteration. Then by using the weighted averaging approach, the fluid velocity relative to the vessel at the shedding edge is estimated. The estimated relative fluid velocity is then used to calculate the vortex induced damping coefficient for each strip of panels on the port and starboard side of the model. These vortex induced damping coefficients are summed up along the length of the model to calculate the total vortex induced damping coefficient for the frequency under investigation. Finally the total vortex induced damping is inserted back into the hydrodynamic model for the next iteration of calculations. This process is repeated iteratively until the difference in calculated roll RAO in two consecutive iterations is less than 0.1 degrees per meter.

3. CASE STUDY

A box shaped model was used in this study to conduct model tests in the Marine Hydrodynamics Laboratory at Newcastle University. The main characteristics of the model are outlined in Table 1.

Table 1: Main characteristics of the model

Main characteristic	-
Length (m)	1.538
Beam (m)	0.403
Draught(m)	0.064
Mass (kg)	39.67
Longitudinal Centre of Gravity from midship (m)	0.004
Vertical Centre of Gravity from keel (m)	0.032
Roll Radius of Gyration (m)	0.1405
Pitch Radius of Gyration (m)	0.4306
Yaw Radius of Gyration (m)	0.4306

Two separate model tests were conducted to measure the response of the model in regular waves and irregular waves. A wave amplitude probe was situated in the vicinity of the model to measure the incident wave amplitude generated by the wave maker. The motion

response of the model was measured using an optical tracking system.

4. RESULTS

4.1 ROLL RESPONSE IN REGULAR WAVES

The measured regular incident wave amplitudes and the measured motion responses were used to calculate the Model Test RAO for each frequency. Comparison of the measured Model Test RAO and the calculated Damped RAO together with the Potential RAO are presented in Figure 2. The measured incident wave amplitudes at each frequency are presented in Table 2. The measured incident wave amplitudes were used to calculated the Damped RAO.

Table 2: Measured incident wave amplitudes at each frequency

Freq. (rad/s)	5.03	5.34	5.65	5.97	6.28	6.60
Wave Amp. (mm)	10.73	11.59	10.86	9.07	10.09	9.45

Freq. (rad/s)	6.91	7.23	7.54	7.85	8.17	8.80
Wave Amp. (mm)	12.97	11.14	7.27	12.23	14.43	13.98

Freq. (rad/s)	9.42	10.05	12.57
Wave Amp. (mm)	8.66	9.27	4.90

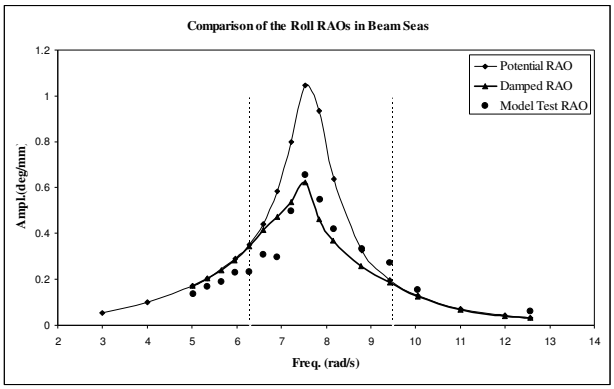

Figure 2: Comparison of Roll RAO in Beam Seas

4.2 ROLL RESPONSE IN IRREGULAR WAVES

Further to the model test in regular waves, an irregular wave train was generated in the wave maker and the time series of the incident irregular wave as well as the roll response were recorded. Using the Fast Fourier Transformation (FFT) technique the incident irregular wave and the associated roll time series were transformed to a power spectrum using:

$$S(w) = \left[\left| FFT\left(f(t)\right) \right| / \frac{N}{2} \right]^2$$

The calculated incident irregular wave and the associated roll response spectra are presented in Figures 3 and 4.

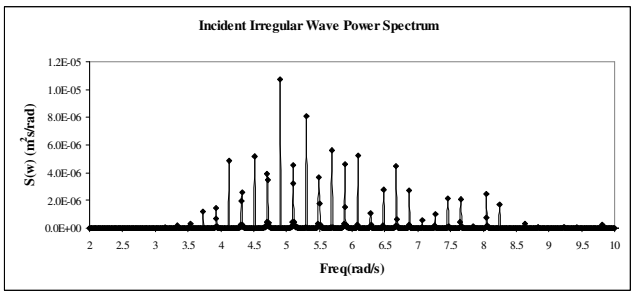

Figure 3: Incident Irregular Wave Power Spectrum

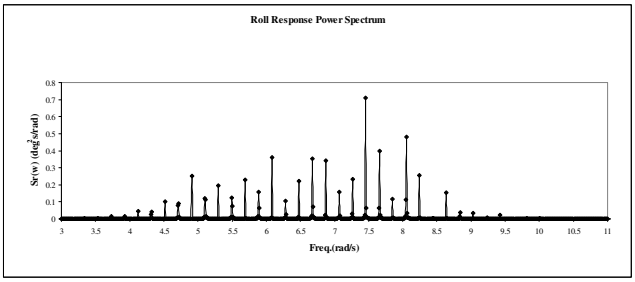

Figure 4: Roll Response Power Spectrum

Assuming a linear system response, the relationship between the incident wave spectrum and the response spectrum may be considered as:

$$S(w)_{response} = RAO_{Equivalent}^{\ 2} \times S(w)_{wave}$$

and the roll RAO associated with the recorded response (i.e. Equivalent RAO) calculated.

Noting the good agreement of the mathematical model in predicting the Damped RAO in Figure 2, a range of Damped RAOs, linearised for regular wave amplitudes of 5mm, 8mm, 10mm, 12mm and 14mm were calculated to assess the effect of linearizing with respect to wave amplitude. These RAOs are illustrated in Figure 5 together with the Equivalent RAO from the model test.

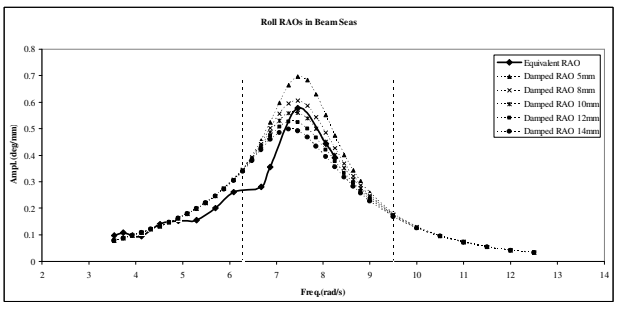

Figure 5: Comparison of Roll RAO database

5. DISCUSSIONS AND CONCLUSIONS

The good agreement between the Model Test RAO and the Damped RAO presented in Figure 2, provides further

evidence of the applicability of the DVM for calculating the viscous roll damping of an oscillating box shaped vessel due to vortex shedding from its edges in regular waves. Although the skin friction damping is considered to be negligible and is ignored in the damped RAO in this study, as tangential relative fluid velocities are used in this method, the same final velocities could be used to calculate skin friction damping.

Investigation of the applicable roll RAO of the box shaped vessel in irregular wave is presented in Figures 5.

Figure 5 demonstrates the effect of roll damping linearisation for a range of constant wave amplitudes. It can be observed that the effect of viscous damping increases with increase in the regular wave amplitudes, especially in the peak region of the RAO. This is an expected relationship between the amplitude of the linearisation wave and the roll RAO. It can be observed from Figure 5 that the amplitude of the roll RAO varies with wave amplitude in a certain frequency band only. The frequency band in this case lies between 6.3 rad/s and 9.5 rad/s. The same frequency band can be observed in Figure 2 between the Potential RAO and the Model Test and Damped RAOs. Therefore it can be concluded that the effect of linearisation of roll damping for a sea state may be focused on a frequency band around the peak of the RAO.

Further study will be undertaken to confirm the validity of assuming a linear systems approach (i.e. $RAO_{Equivalent}$) between the incident wave spectrum (i.e. $S(w)_{wave}$) and the response spectrum (i.e. $S(w)_{response}$) for non-linear behaviour such as roll damping. If such an assumption can be shown to provide the correct roll response statistics then a design methodology can be established for strength and fatigue analyses based on spectral methods.

6. ACKNOWLEDGEMENTS

The authors wish to thank Lloyd's Register, especially Dr. Graham Stewart and Mr. Richard Bamford for their support in this work. Additionally the authors wish to thank Mr. Masih Hajiarabderkani from the University of St Andrews for his professional assistance in software engineering aspects of this work.

The opinions expressed in this paper are those of the authors and are not necessarily those of Lloyd's Register.

7. REFERENCES

1. FROUDE, W., 'The Papers of William Froude M.A. LL.D. F.R.S. 1810-1879', *The Institute of Naval Architects,* 1955.

2. HIMENO, Y., 'Prediction of ship roll damping – State of the art', *The University of Michigan College of Engineering,* 1981.

3. GRAHAM, J.M.R., 'The forces on sharp-edged cylinders in oscillatory flow at low Keulegan-Carpenter number', *J. Fluid Mech. (1980), 97(1), pp.331-346*, 1980.

4. DOWNIE, M.J., and GRAHAM J.M.R., and BEARMAN, P.W., 'The effect of vortex shedding on the roll damping of rectangular barge', *Fluid Loading Report No. F.L.42, Department of Aeronautics, Imperial College London*, 1987.

5. DOWNIE, M.J., and JILLIANS, W., and GRAHAM J.M.R., 'Theoretical prediction of the viscous damping and response of three-dimensional floating structures' *EPSRC Grant Reference GR/J23631 (Newcastle)*, 1996.

6. HAJIARAB, M., and GRAHAM, J.M.R., and DOWNIE, M.J., 'Prediction of roll damping in the frequency domain using the Discrete Vortex Method', *Proceedings of the ASME 2010 29th International Conference on Ocean, Offshore and Arctic Engineering*, 2010.

7. Lloyd's Register, 'ShipRight-FOI, Floating Offshore Installations Assessment of Structure', 2008.

8. AUTHORS BIOGRAPHY

Mohammad Hajiarab holds position of Floating Structures Team Leader at Lloyd's Register EMEA in Aberdeen-UK. He has been researching the application of the Discrete Vortex Method for calculation of the roll damping of floating vessels at Newcastle University upon Tyne since 2005.

Martin Downie is Professor of marine technology at the Newcastle University upon Tyne. He joined Newcastle University as a hydrodynamicist with research interests focussed on numerical modelling and experimentation concerned with the fluid loading and response of fixed and floating vessels in the context of offshore engineering.

Michael Graham is Professor of unsteady aerodynamics at the Imperial College London.